UNIVERSITY OF BIRMINGHAM

Echocardiographic analysis of a murine model with a mutation in the Nav1.5 channel gene Scn5a

By Dr Sosan Andaleeb

Supervisor:

Professor Larissa Fabritz

Co-Supervisor:

Dr Rick Steeds

UNIVERSITY OF BIRMINGHAM | INSTITUTE OF CARDIOVASCULAR SCIENCES

Institute of Cardiovascular Sciences (ICVS)
College of Medical and Dental Sciences (MDS)
School of Biomedical sciences
University of Birmingham
May 2021

Abstract

Cardiomyopathy is defined as a disorder of heart muscle in terms of structure, function or both. It can be defined as dilated, hypertrophic, arrhythmogenic, restrictive or infiltrative all of which contribute significantly to cardiovascular disease burden. The difference in their presentation, prognosis and treatment is dictated by their underlying pathophysiology and changes on a cellular level which manifests itself on cardiovascular imaging using various modalities. Echocardiography is a very useful and convenient tool for heart imaging. Linking cellular changes to phenotype in real time, echocardiographic imaging is a great clinical need which can potentially unlock the understanding and treatment of complex disease processes. Mutations in the cardiac sodium channel Nav1.5 can lead to long QT syndrome, familial AF, Brugada syndrome or cardiomyopathy. In our experiments, a new murine knock-in model M1875T$^{+/-}$ SCN5A was investigated. This causes a gain of function defect in the Nav1.5 channel leading to altered ion transport across the myocyte membrane. This work is primarily based on the echocardiographic assessment of gross cardiac structure and function of this model. This work also describes methods of histological analysis to be applied in mutant (M1875T$^{+/-}$) mice. The Visualsonics Vevo 2100 echo system was used to perform echocardiography in 79 mice from both the SV129 and FVB genetic strain background variants. TThe gross differences in wall thickness and chamber dimensions were analysed for the complete cohort. This did not show any difference between young adults of the two groups. However, mature mice (≥25 up to 40 weeks) with the mutation showed significantly larger LV dimensions and volumes during systole and diatole when compared to the wild-type (M1875T$^{+/+)}$ littermates. Analysis of the left atrium and right ventricle revealed no significant differences between the two groups. Some phenotypic changes of the heart are known to manifest with time and therefore the M1875T$^{+/-}$ gene mutation may be associated with the development of

cardiomyopathy in older mice. This makes a strong case to further study the effect of this gene mutation in a larger and older sample population.

Dedicated to…

All my teachers and mentors, who with their kindness and dedication

widened my horizons, enlightened my path

and guided me when I needed it the most.

ACKNOWLEDGEMENTS

First and foremost, I would like to thank my supervisor, **Prof Larissa Fabritz** whose kind mentorship and unwavering support were essential in the completion of my project. I am truly honoured to have worked under her guidance**.** I also thank my co-supervisor, **Dr Rick Steeds,** for giving me sincere advice whenever I needed it.

I wish to extend a special thanks to **Prof. Paulus Kirchhof** for allowing me to take up the M.Sc by research studentship and taking a keen interest in my research. Without his advice and critique, this thesis would not have been possible. I want to specially mention **Lisa Fortmüller** who guided me in my echo analysis and techniques.

Dr Neena Kalia, my postgraduate research administrator and **Dr Katja Gehmlich**, my external assessor during my annual appraisal deserve a special thanks for giving me valuable advice that was very useful for my upcoming work.

I sincerely thank **Dr Winnie Chua** for helping me settle into the department and and giving me precious advice and support all the time. I am also grateful to my colleagues **Laura, Nashitha, Davor, Chris, Antonia, Jasmeet** whose help and advice has been instrumental to this work. Thank you to **Sophie** for reviewing my thesis and giving me very important suggestions.

Finally, to all those who with their big or small help, their critical appraisal or praise or by a tiny nudge or a big push enabled me to get over the finish line, I say a sincere heart-felt “Thank You”!

LIST OF ABBREVIATIONS

CWD	Continuous wave doppler
C-RAM	c-AMP regulatory element modulator
DCM	Dilated cardiomyopathy
ECG	Electrocardiogram
EF	Ejection fraction
ESC	European society of cardiology
EP	Electrophysiology
FAC	Fractional area change
HCM	Hypertrophic cardiomyopathy
IQR	Inter-quartile Range
KCNQ1	Potassium voltage-gated channel subfamily Q member 1
KNCH2	Potassium voltage-gated Channel subfamily H member 2
LA	Left atrium
LV	Left ventricle
LVOT	Left ventricular outflow tract
LVID(s or d)	Left ventricular internal diameter (systole or diastole)
MRI	Magnetic resonance imaging
OR	Odds ratio
PWD	Pulse wave Doppler
RA	Right atrium
RV	Right ventricle
RVOT	Right ventricular outflow tract
RVID(s or d)	Right ventricular internal diameter (systole or diastole)
SD	Standard deviation
SCN5A	Sodium Channel voltage gated Type V Alpha subunit (Human)
Scn5a	Sodium channel voltage gated Type V alpha subunit (mice)
TAPSE	Tricuspid annular plane systolic excursion

Table of Contents

1. Introduction 1
1.1 Background 1
1.2 Why this work is important 2
1.3 Preliminary histological work 3
2 Literature review 4
2.1 Cardiomyopathies 4
2.2 Cardiac channelopathies 6
2.2.1 Brugada syndrome 7
2.2.2 Long QT syndrome 7
2.2.3 Lone AF 9
2.3 Echocardiography 10
2.3.1 Left Atrial Echocardiography 10
2.3.2 Right ventricular echocardiography 16
2.3.3 Left ventricular echocardiography 20
2.4 Histology 21
2.5 Study aims 22
2.6 Hypotheses 23
3 Methods 24
3.1 Ethical statement 24
3.2 Experimental animals 25
3.3 Experimental echocardiography methods. 26
3.3.1 Echocardiography procedure details 26
3.3.2 Measurements 27
3.4 Histology 48
3.4.1 Tissue Harvesting 48
3.4.2 Method of OCT (Tissue TEK) 49
3.4.3 Slicing and slide preparation 51
3.4.4 Staining 54
3.4.5 Handling histology data 55
3.4.6 Histological imaging 55
3.5 Statistical Methods 56
3.5.1 Inter-observer variability 56
4 Results 57
4.1 Baseline data 57
4.2 Echocardiography Results 59

4.2.1 Echocardiography results for the complete dataset 59
4.2.2 Results for mature mice 64
4.3 Inter-observer variability 77
4.4 Preliminary histological results 78
5 Discussion 80
5.1 Previous work 80
5.2 Significance of echocardiographic findings 81
5.3 Strengths 82
5.3.1 Inter-observer Reproducibility 82
5.3.2 Novelty of work 83
5.4 Limitations 83
5.4.1 Chamber size quantification and histology: 83
5.4.2 Specialised Doppler-echocardiography measurements: 83
5.4.3 Sample size: 84
5.4.4 Effect of disease modifying factors: 84
5.4.5 Differences in physiology of mouse and human heart 85
5.5 Future work 85
5.5.1 Advanced echocardiography techniques 85
5.5.2 Combining echocardiographic findings with histology, molecular analysis and patch clamping 86
5.5.3 Experiments on a single background strain 86
6 References 87

List of Figures

Figure 2-1 ECG features of Long QT syndrome. Long QT1 with braod based T wave pattern, Long QT2 with Bifid T waves and Long QT3 with late onset T waves. 8
Figure 2-2 M1875T protein defect in the Nav 1.5 protein. 9
Figure 2-3 Prolate ellipsoid method of LA volume measurement.[64] 12
Figure 2-4 Biplane area-length method for LA volume measurement.[61] 13
Figure 2-5 Modified biplane Simpson's method.[61] 14
Figure 2-6 3D Echo for assessment of LA volume in a murine model.(Original work) 15
Figure 2-7 Proximal human right ventricular outflow tract on parasternal long axis view 16
Figure 2-8 Proximal human right ventricular outflow tract on the parasternal short-axis view (normal range is 21-35mm). 17
Figure 2-9 Distal right ventricular outflow tract on parasternal short-axis view (normal range 17-27mm). 17
Figure 2-10 Human right ventricular proximal (normal range 25-41mm) and mid-cavity (normal range 19-35mm) mediolateral measurements on apical four-chamber view. 18
Figure 2-11 Human Tricuspid annular plane systolic excursion (TAPSE) measurement on apical four-chamber view. 19
Figure 2-12 Human right ventricular Fractional area change (FAC) measurement on apical four-chamber view. 19
Figure 2-13 Left ventricle on light microscopy 21
Figure 2-14 Right ventricle on light microscopy 22
Figure 3-1M1875T$^{+/-}$construct generation using combination of subsequent PCR reactions .26
Figure 3-2 The chambers and walls orientation on Parasternal long-axis view. (original sketch) 29
Figure 3-3 Parasternal long-axis view in Diastole with measurements of Left ventricular (LV) length, septal (IVSd) and posterior wall thickness (LVPWd) and LV internal diastolic dimension (LVIDd). 30
Figure 3-4 Parasternal long axis view in Systole with measurements of Left ventricular (LV) length, septal (IVSs) and posterior wall thickness (LVPWs) and LV internal systolic dimension (LVIDs). 30
Figure 3-5 M-mode of Parasternal long-axis view, at the aortic root level. 31
Figure 3-6 M-mode of Parasternal long axis view, at papillary muscle level. 31
Figure 3-7 The chamber and wall orientation on parasternal short axis view at aortic root level. (original sketch) 33
Figure 3-8 2D of Parasternal short-axis view, at aortic valve level. 34
Figure 3-9 M-Mode of Parasternal short axis view, at aortic valve level. 34
Figure 3-10 Parasternal short-axis view, at aortic valve level with pulse wave Doppler (PW) of the pulmonary valve. 35
Figure 3-11 The chamber and wall orientation on Parasternal short axis view at papillary muscle level. (original sketch) 35
Figure 3-12 2D of Parasternal short-axis view, at the papillary muscle level. 36
Figure 3-13 M-Mode of parasternal short-axis view, at the papillary muscle level. 36
Figure 3-14 Orientation of cardiac chambers and valves on apical four chamber view. (original sketch) 39
Figure 3-15 Apical 4-chamber view of mouse heart with colour Doppler across mitral and tricuspid valves. 39
Figure 3-16 Apical 4 chamber view, with pulse wave Doppler (PW) of the mitral flow 40
Figure 3-17 Diagram showing the aortic arch on supra-sternal view. (original sketch) 41
Figure 3-18 Figure showing labelled image of aortic arch on supra-sternal view 42

Figure 3-19 Aortic arch view, with pulse wave Doppler (PW) of the aortic flow. 42
Figure 3-20 Aortic arch view, with pulse wave Doppler (PW) of the aortic flow. 43
Figure 3-21 Three-dimensional cube view of the heart (original work).....44
Figure 3-22 Slice view of the three-dimensional echocardiography (original work).....45
Figure 3-23 Surface view of the murine left heart (original work).....46
Figure 3-24 Surface view without data (original work).....47
Figure 3-25 Careful dissection and subsequent weighing on a gravimeter 50
Figure 3-26 (left) OCT solution being poured on the cork; (Right) Tissue placed on the cork with OCT 51
Figure 3-27 Images of the Cryostat used for slicing and slide preparation 53
Figure 4-1(A) Complete dataset. Age in weeks, Median (IQR) (B) Body weight in grams, Mean (SD) for M1875T$^{+/+}$ vs M1875T$^{+/-}$mice (n=79). 34 mice in M1875T+/+ and 45 in M1875T+/- genotype. 58
Figure 4-2 Left Atrial diameter measured in atrial diastole (n=72). For complete dataset 63
Figure 4-3 Comparison between older M1875T+/+ and M1875T+/- mice for Interventricular septum (IVS) thickness in systole (A) and diastole (B). n=20. 65
Figure 4-4 Comparison between older M1875T+/+ and M1875T+/- mice for left ventricular internal dimension in systole (A) and diastole (B). 66
Figure 4-5 Comparison between older M1875T+/+ and M1875T+/- mice for left ventricular posterior wall thickness in systole and diastole. 67
Figure 4-6 Comparison between older M1875T+/+ and M1875T+/- mice for LV endocardial length in systole (A) and diastole (B). 68
Figure 4-7 Comparison between older M1875T+/+ and M1875T+/- mice for aortic annular diameter.....69
Figure 4-8 Comparison between older M1875T+/+ and M1875T+/- mice for left ventricular fractional area change. 70
Figure 4-9 Comparison between older M1875T+/+ and M1875T+/- mice for Left Ventricular Fractional shortening. 71
Figure 4-10 Comparison between older M1875T+/+ and M1875T+/- mice for Left Ventricular systolic (A) and diastolic (B) volume.....72
Figure 4-11 Comparison between older M1875T+/+ and M1875T+/- mice for left ventricular stroke volume.....73
Figure 4-12 Comparison between older M1875T+/+ and M1876T+/- mice for Cardiac Ejection Fraction.....74
Figure 4-13 Comparison between older M1875T+/+ and M1875T+/- mice for cardiac output. 74
Figure 4-14 Comparison between older M1875T$^{+/+}$ and M1875T$^{+/-}$ mice for right ventricular area in systole (A) and diastole (B) on parasternal short axis view.....75
Figure 4-15 Comparison between older M1875T$^{+/+}$ and M1875T$^{+/-}$ mice for left atrial anteroposterior dimension on parasternal long axis view.....76
Figure 4-16 Interobserver variability plot for(A) LV internal diameter in diastole and (B) LV ejection fraction (%). 77
Figure 4-17 Left ventricular gross histology for wild (M1875T$^{+/+)}$ and mutant (M1875T$^{+/-}$) on Masson Trichome stain using light microscope Leica DM6000 under 10x Magnification. (Scalebar =100micron). 78
Figure 4-18 Right ventricular gross histology for wild(M1875T+/+) and mutant M1875T+/- on Masson Trichome stain using light microscope Leica DM6000 under 10x Magnification. (Scalebar =100micron). 79

List of Tables

Table 2-1 Left ventricular measured and derived variables.....20
Table 3-1 Parasternal long-axis view with respective chambers, measurements and calculated parameters.....32
Table 3-2 Parasternal short-axis view with respective chambers, measurements and calculated parameters.....37
Table 3-3 Apical 4 chamber view with respective chambers, measurements and calculated parameters.....40
Table 3-4 Aortic arch parameters.....43
Table 4-1 Baseline data of the complete cohort (n=79).....57
Table 4-2 Results of the camparison of the LV measurements between M1875T$^{+/+}$ and M1875T$^{+/-}$ mice (n=79) for the complete dataset.....60
Table 4-3 Left ventricular calculated values (n=79) for complete dataset.....61
Table 4-4 Right ventricular measured and calculated parameters (n=44) for complete dataset (This variable only available for 44 mice).....62

1. Introduction

1.1 Background

Inherited cardiac conditions are considered as important because of morbidity and mortality, especially in the young, that manifest themselves in a wide spectrum of phenotypic presentations involving the structure, function or electrical conduction of the heart.[1] These inherited cardiac conditions, including channelopathies, are epidemiologically significant, with at least 3% prevalence in the general population.[2] However, studying these diseases in humans is not without its challenges. Many channelopathies manifest as life-threatening arrhythmias or sometimes sudden cardiac death.[3] In the absence of a gross morphological heart defect, identifying such patients can be very difficult. Moreover, studying channelopathies involves not only genetic testing and non-invasive cardiac imaging but frequently involves complex electrophysiological tests and histological assessment of the heart tissue. These extensive investigations are, understandably, not possible in human subjects and hence a suitable animal model is tested with as identical morphology and physiology as can be achieved. For such experimental investigations, murine models are a favoured mammal for research due to their shorter gestation times, lower maintenance costs, ease of handling and manipulation of genes to elicit anatomical and physiological effects.[4, 5] Moreover, there is a significant resemblance between the cardiovascular physiology of mice and humans which makes them a suitable model to study effects of various cardiovascular pathologies through genetic alterations.[6, 7] Nevertheless, there are some physiological differences between human and mice hearts regarding heart rates and actions potentials. For example, the normal heart rate in humans is between 60 to 70

beats per minute while that of mice is 500 to 600 beats per minute.[8] Extensive work has been carried out to for various cardiomyopathies in mouse models.[9-13]

1.2 Why this work is important

Genetic defects like mutations in the SCN5A gene are studied for their link with arrhythmias and cardiomyopathies.[14-18] Genetic variations of the SCN5A gene may affect the structure and/or function of the Nav1.5 protein in the cell membrane of cardiomyocytes.[19] So far, various cardiac channelopathies (Brugada syndrome, long QT syndrome, atrial standstill) and cardiomyopathies (dilated cardiomyopathy, arrhythmogenic right ventricular cardiomyopathy) have been linked to mutations in the SCN5A gene in humans.[19]

Cardiovascular imaging, especially cardiac ultrasound, is an invaluable tool in assessing variations in physiology and anatomy due to genetic modifications.[7, 20] Cardiac ultrasound or echocardiography has evolved as one of the most widely used imaging modalities due to lower costs, live imaging, no risk of radiation and relative ease of imaging.[21] Echocardiography modalities include M-Mode, 2D imaging, colour flow, continuous wave and pulse Doppler assessments.[22-25] For the purpose of this work, the gross morphological assessment of the cardiac chambers in mice, as a starting point remains key in understanding the pathogenesis of Scn5a gene mutation which can be done through aforementioned echocardiography techniques. Some specialised echocardiographic methods like speckle tracking and strain measurements to assess LV systolic and diastolic function have shown good promise.[26, 27] The later methods are, however, quite specialised and require advanced echocardiography equipment with

relevant software modules and expertise on behalf of the operator. Moreover, these are also not routinely used for phenotyping of murine models.

Based on this, transthoracic echocardiography was used to assess any anatomical changes associated with the M1875T$^{+/-}$ gain of function mutation in the Scn5a gene encoding the Nav1.5 sodium channel. This assessment included measurement of wall thickness, chamber dimensions (measured in terms of diameter, length, area and volume) and function measured as fractional shortening, ejection fraction and cardiac output. These are the most commonly measured and clinically relevant parameters in routine echocardiography which enhances the clinical relevance of this work.

1.3 Preliminary histological work

In addition, there is a need to link phenotypic findings observed on cardiac imaging with histological analysis. In preclinical murine experiments, this typically involves tissue sampling and analysis, ideally of the same mice on which echocardiographic analysis has been done to ascertain the disease process on a cellular level. This project principally involved echocardiographic analysis of the effect of the heterozygous M1875T$^{+/-}$ mutation of Scn5a in mouse model. In addition tissue organ harvesting, tissue preservation, slide staining and light mictroscopy were learnt in order to assess tissue changes at a cellular level. These shall be described in the methods section of this manuscript.

2 Literature review

2.1 Cardiomyopathies

Cardiomyopathy, as a term, was first described by Brigden in 1957 as an “uncommon” and “non-coronary” form of cardiac muscle disease.[28] In 1961, Goodwin described cardiomyopathies as a myocardial disease of unknown cause and categorised it as dilated, hypertrophic and restrictive, terms which are still in use to date.[29] With the advent of non-invasive cardiac imaging, including M-Mode and 2D echocardiography, cardiomyopathies were more frequently identified. In 1980, the World Health Organisation (WHO) and International Society and Federation of Cardiology (ISFC) published the broadly endorsed definition by Goodwin.[30]

Over the last 30 years, there has been a significant increase in the understanding of cardiomyopathies and many such conditions are thought to be inherited. This was made possible due to the development of sophisticated gene sequencing techniques.[2] The European Society of Cardiology (ESC) classification adds a further two groups including Arrhythmogenic Right Ventricular Cardiomyopathy (ARVC) and unclassified.[31] Later the ESC added non-dilated hypokinetic cardiomyopathy as well to the previously described phenotypes.[32]

Broadly, cardiomyopathy can be split into the following most notable categories: dilated, hypertrophic, arrhythmogenic and restrictive.[33-36]

Dilated cardiomyopathy:

This is a common type of cardiomyopathy, the main characteristic of which is an increase in cardiac volume. The left ventricular wall is stretched and thus its contractility and cardiac output are compromised.[37] Many factors contribute to the development of dilated cardiomyopathy, including genetic inheritance, alcohol abuse, haemochromatosis, valvular heart disease, chronic anaemia, drugs (Adriamycin) toxicity, peripartum state, sarcoidosis, viral myocarditis etc.[37]

Hypertrophic cardiomyopathy: This is the most common type of cardiomyopathy in which there is usually asymmetric hypertrophy of the myocardium along with interstitial fibrosis, disorganised myocardial architecture and thus impairment of left ventricular performance. The interventricular septum is more predisposed to this condition, but any myocardial segment can be involved including apex, lateral wall, right ventricle or it can be concentric.[38] It is most common hereditary form of cardiomyopathy without any secondary cause.[39] It can develop as a consequence of, septal sarcoma, glycogen storage disease, Fabry's disease and sarcomere gene mutations.

Restrictive cardiomyopathy:

A form of myocardial dysfunction in which the myocardium becomes stiff resulting in the impairment of diastolic function. Systolic function and size of the ventricles can remain normal until the late stages of the disease.[40] Idiopathic restrictive cardiomyopathy with no obvious cause is the most common form and frequently predisposes to arrhythmias and conduction system abnormalities.[41]

Arrhythmogenic cardiomyopathy:

Defined as an inherited disease of the myocardium which is different from the other cardiomyopathies because the arrhythmic symptoms usually develop earlier than the phenotypic changes.[42] This is one of the most common reasons for sudden cardiac death, including in young otherwise healthy individuals. Based on the type of ventricular involvement, it can be classified into subtypes; Isolated RV, Biventricular and Left ventricular arrhythmogenic cardiomyopathy.[43, 44]

2.2 Cardiac channelopathies

Cardiac channelopathies are a type of electrical conduction dysfunction caused by defective ion-gated channels, mostly leading to arrhythmias with occasional changes in the phenotype.[45] Cardiac channelopathies can be genetic or acquired. Long QT syndrome and Brugada's syndrome are classified as genetic cardiac channelopathies, as caused by gene defect in potassium channels (KCNQ1) and sodium channels (SCN5A).[15, 45]

Recently, it has been found that SCN5A gene defects can be related to many cardiac channelopathies and myopathies like long QT syndrome, atrial stand-still, ARVC and dilated cardiomyopathy.[19, 46] Cardiac sodium channel defects were previously considered as purely electrical entities but recently, evidence is accumulating to show the relationship of this channelopathy with cardiac fibrosis, dilation and hypertrophy.[47] A few manifestations of these channelopathies are described below.

2.2.1 Brugada syndrome

Brugada syndrome is a genetically determined, autosomal dominant electrical conduction disorder of the heart which causes life-threatening ventricular arrhythmias or sudden cardiac death.[48] Mutations in the SCN5A gene are responsible for most of the patients with this disease.[14] Loss of function mutations in the SCN5A gene leads to lower expression levels or production of a defective sodium channel protein, causing Brugada syndrome.[46] It is typically characterised by coved ST-segment elevation on the right precordial leads (V1-V3), which is not related to ischemia or any other electrolyte abnormality.[49] This can be seen spontaneously but can become apparent due to a febrile state or exposure to certain drugs like flecainide or ajmaline.[14] Cardiac magnetic resonance imaging (MRI) and Electrophysiology (EP) studies have pointed towards abnormal electrical activity in the epicardial right ventricular outflow tract.[14]

2.2.2 Long QT syndrome

Long QT syndrome is a life-threatening cardiac arrhythmia syndrome characterized by abnormal ventricular repolarization which results in the prolongation of QT interval on ECG.[50] It is one of the leading causes of sudden death in young people.[51] ECG patterns for long QT syndrome are also genotype-specific, for example, long QT1 has broad-based T waves, long QT2 shows low amplitude T waves with a high incidence of notches, while long QT3 carries extended QT segment with narrow peaked T waves on ECG (figure 2-1).[52]

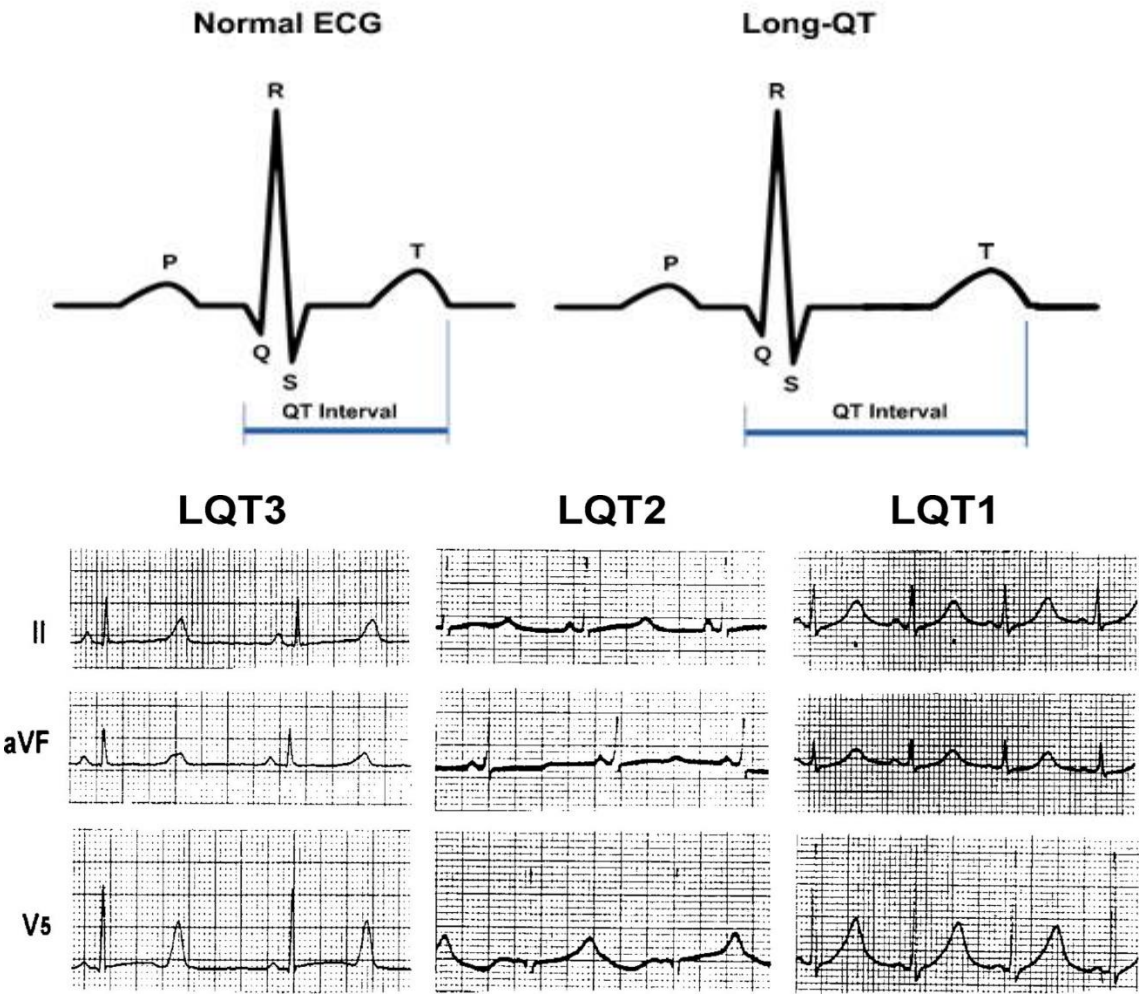

Figure 2-1 ECG features of Long QT syndrome. Long QT1 with braod based T wave pattern, Long QT2 with Bifid T waves and Long QT3 with late onset T waves.

Reproduced from Goldenberg I, Moss AJ. Long QT Syndrome. Journal of the American College of Cardiology. 2008;51(24):2291-300.[53]

Characterization of this syndrome is based on the type of gene mutation involved. Long QT1 and Long QT2 are the outcomes of mutations in the Potassium Voltage-gated Channel subfamily Q member 1 (KCNQ1) and Potassium Voltage-gated Channel subfamily H member 2 (KCNH2) genes respectively.[51] Long QT3 is a predominantly autosomal dominant channelopathy caused by mutation of the SCN5A gene, which encodes the sodium channel protein Nav1.5.[46] This leads to a late sodium current due to the failure of the channel to remain inactivated leading to an abnormal late sodium

current entry during the plateau phase of depolarization.[54] This Nav1.5 mutation is related to long QT3 as well as Familial AF.[55]

2.2.3 Lone AF

In 2008, Makiyama and collegues described the M1875T location mutation leading to a gain of function mutation in the cardiac Nav1.5 channels leading to atrial excitability and familial AF in the absence of long QT syndrome.[55] The M1875T point mutation of the SCN5A gene affects the alpha subunit of the voltage-gated sodium channel.[55] This is shown in Figure 2.2. Moreover, in this phenotype, despite the same gene being involved, had distinctive features, separating this from Long QT3 syndrome type 3. The generation technique for the scn5a M1875T$^{+/-}$ model used in this research is given in the methods section.

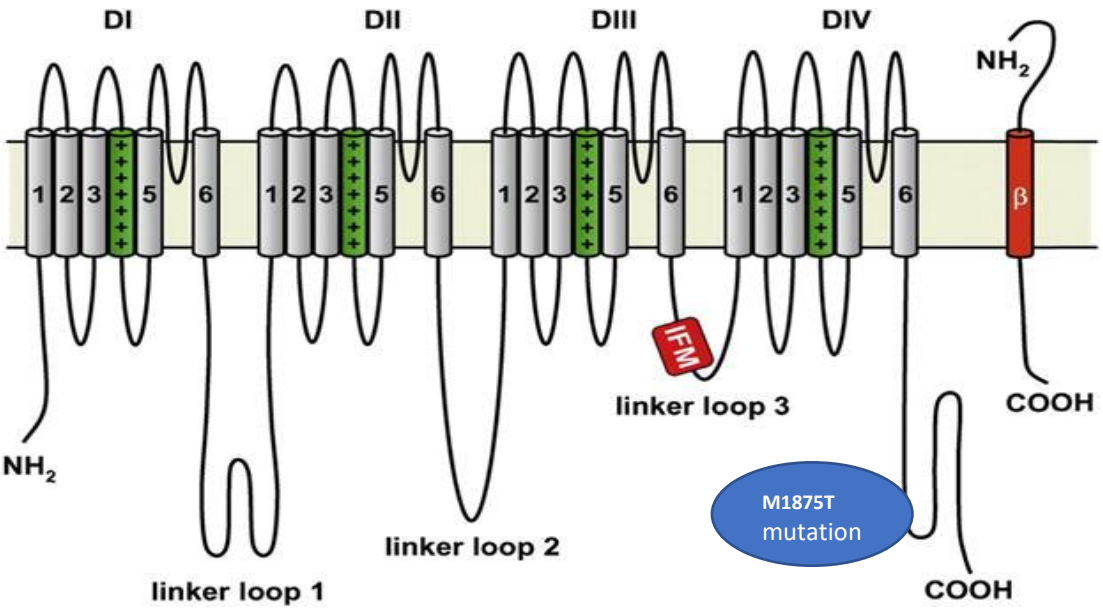

Figure 2-2 M1875T protein defect in the Nav 1.5 protein.

Adapted from and modified from: DeMarco, K.R. and C.E. Clancy, *Cardiac Na Channels: Structure to Function.* Curr Top Membr, 2016. **78**: p. 287-311.

2.3 Echocardiography

Echocardiography is one of the most commonly used non-invasive diagnostic modality for assessing cardiac phenotype in humans.[56] Moreover, with some adaptations, it has become the standard non-invasive technique for investigating cardiac malformations in genetically modified mice.[57, 58]

The basic echocardiographic modalities are; two dimensional (2D), M mode, colour Doppler, continuous wave (CWD) and pulse wave Doppler (PWD), 3-Dimensional (3D)echocardiography. The standard acoustic windows for assessing the chamber dimensions and valvular functions are; parasternal long-axis view (PLAX), parasternal short axis view (PSAX), apical four-chamber view, apical five-chamber view, subcostal view and aortic arch view.[56, 59, 60]

2.3.1 Left Atrial Echocardiography

The left atrium (LA) plays an important role by acting as a barometer for diastolic function. There is strong evidence that LA enlargement, as determined by echocardiography, is a robust predictor of cardiovascular outcomes such as stroke, heart failure and atrial fibrillation in cardiomyopathy and many other cardiovascular diseases.[61]

Recently, it has been shown that LA volume is a more reliable measure of LA size than conventional linear measurement as it takes account of both short and long axis expansion of the chamber, and can also account for asymmetric remodelling of LA chamber.[61, 62] Both 2D and 3D echocardiography can be used to determine LA volume.

Two-dimensional echo for LA volume:

There are three suggested methods for LA volume measurement using 2D echocardiography. These may also be used for assessment of right atrial (RA) size. These are

- Prolate ellipsoid method
- Biplane area-length method
- Modified biplane Simpson's method [56]

Prolate ellipsoid method:

This requires the parasternal long-axis and apical 4-chamber views. The anteroposterior dimension is measured in the PSAX view at the aortic root level. The maximum dimension is achieved at ventricular systole.[63] By measuring mediolateral (D_1), longitudinal (D_2) and anteroposterior (D_3) dimensions as indicated in Figure 2-3, Equation 1 can be used to calculate LA volume.

$$LA\ Volume = \frac{4}{3}\pi\left(\frac{D_1}{2} \times \frac{D_2}{2} \times \frac{D_3}{2}\right) = 0.53 \times D_1 \times D_2 \times D_3$$

Equation 1 shows prolate ellipsoid method of LA volume assessment

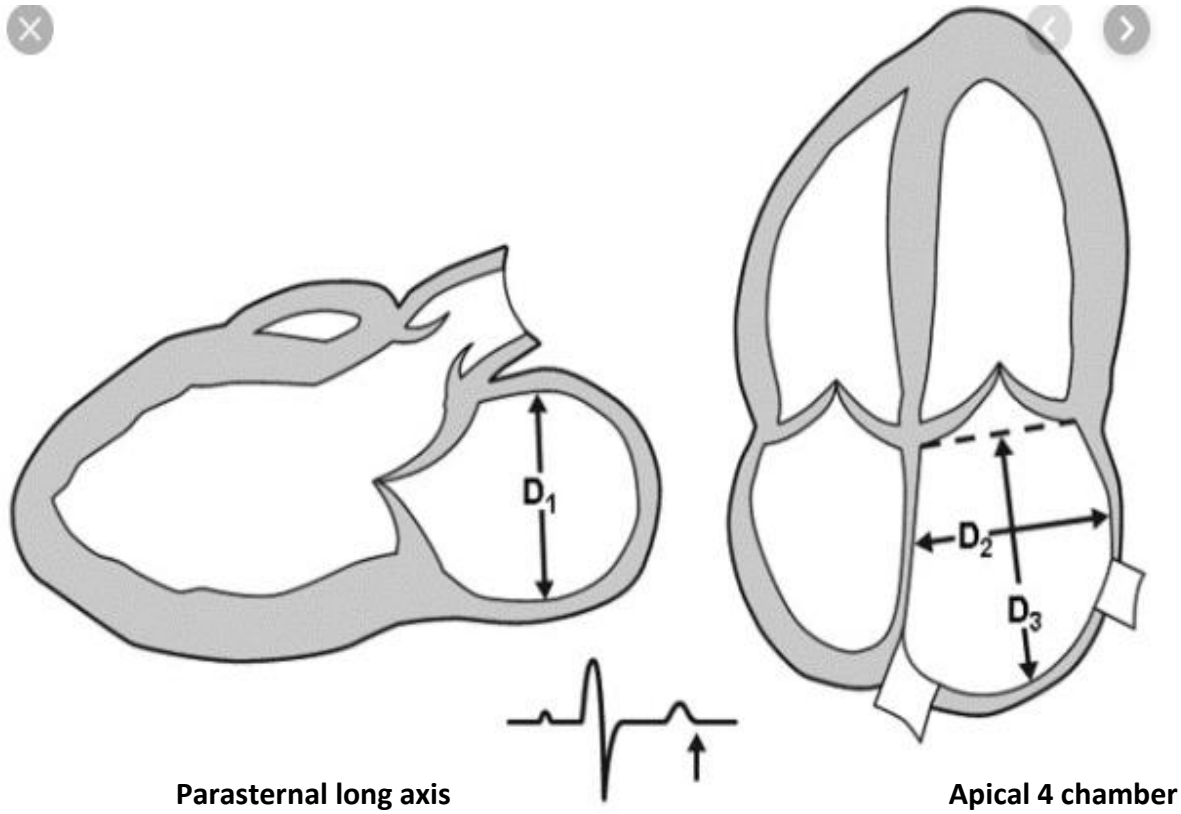

Figure 2-3 Prolate ellipsoid method of LA volume measurement.[64]

Adapted from Ujino, K., et al., *Two-dimensional echocardiographic methods for assessment of left atrial volume.* Am J Cardiol, 2006. **98**(9): p. 1185-8.

Biplane area length method:

This requires apical 2-chamber (2CH) and 4-chamber (4CH) views (Figure 2-4). It makes use of LA area (A) and length (L) measured from mitral annular plane to the posterior wall of LA. Using Equation 2, LA volume can be calculated as given in Figure 2-4.

$$LA\ Volume = \frac{0.85 \times A_{4CH} \times A_{2CH}}{L}$$

$$Where\ \ L = Average\ of\ L_{4CH} + L_{2CH}$$

Equation 2 ; Biplane method to assess LA volume

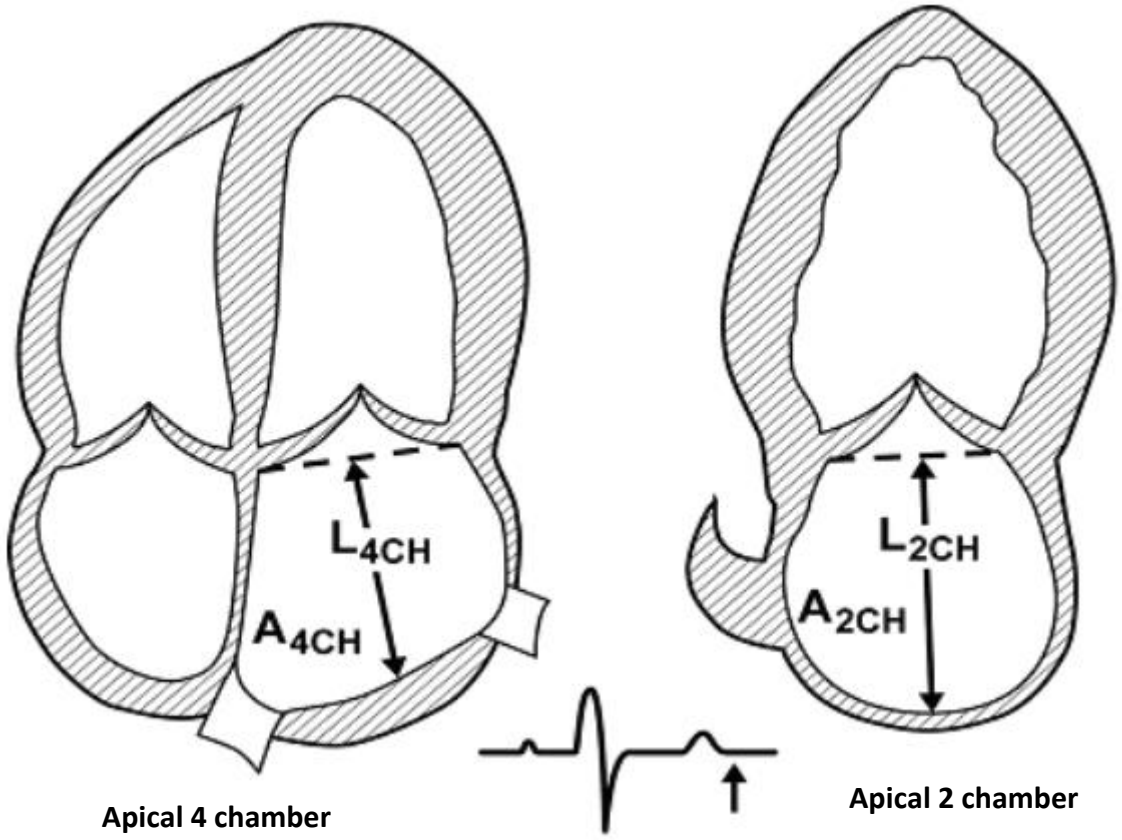

Figure 2-4 Biplane area-length method for LA volume measurement.[61]

Adapted from Abhayaratna, W.P., et al., *Left atrial size: physiologic determinants and clinical applications.* J Am Coll Cardiol, 2006. **47**(12): p. 2357-63.

Modified Biplane Simpson's method:

The modified biplane Simpson's method uses the assumption that the LA cavity is made up of a series of stacked discs. Apical 2CH and 4CH measurements are taken which require both the area as well as the longitudinal length of the LA (Figure2-5).

$$\boldsymbol{LA\ Volume} = \frac{\boldsymbol{\pi}}{\boldsymbol{4}}\ (\boldsymbol{h}) \sum \boldsymbol{D_{4CH}} \times \boldsymbol{D_{2CH}}$$

h= height of discs
D=diameter

Equation 3; Simpson's method to assess LA volume

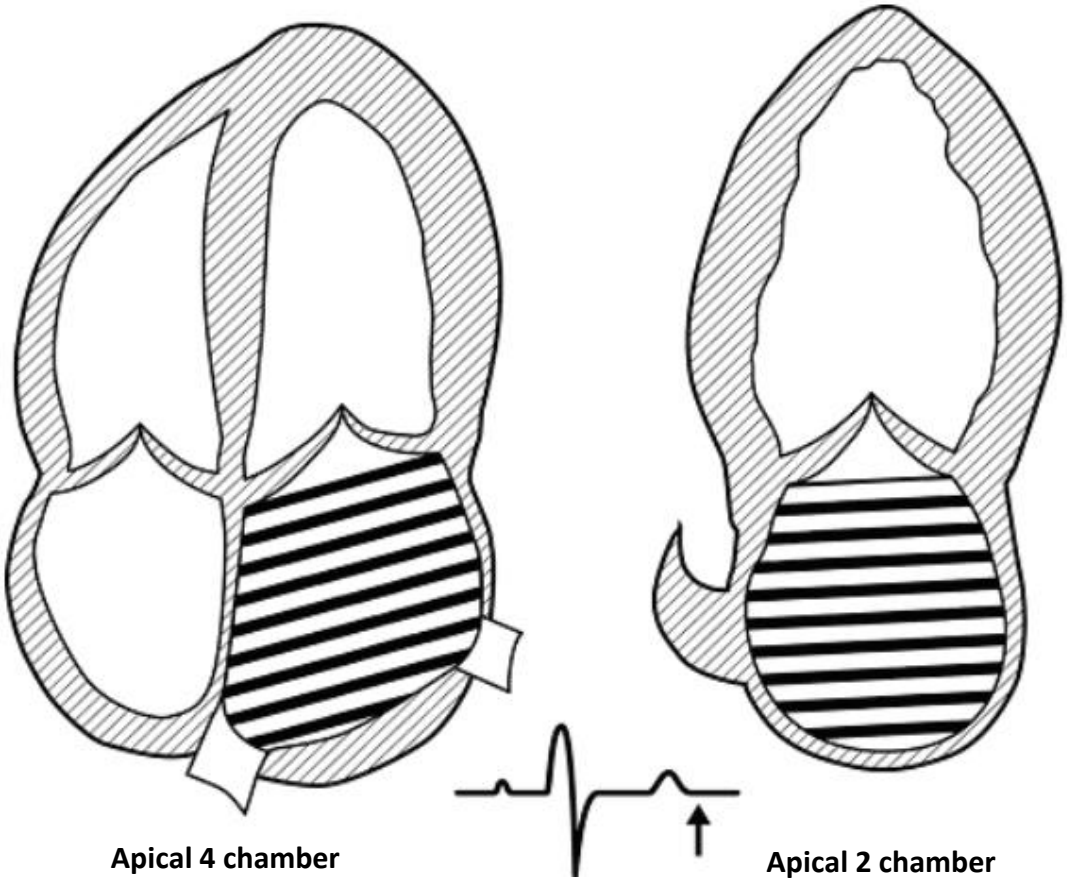

Figure 2-5 Modified biplane Simpson's method.[61]

Adapted from Abhayaratna, W.P., et al., *Left atrial size: physiologic determinants and clinical applications.* J Am Coll Cardiol, 2006. **47**(12): p. 2357-63.

Three-dimensional echocardiography:

Two-dimensional echocardiography can sometimes be incorrect and less reproducible due to atrial foreshortening, geometric assumptions and inconsistencies in volume measurement. These can be overcome by real-time 3D echocardiography, which is a novel methodology in murine models, but in humans is shown to accurately and reproducibly estimate left atrial volume when compared to Cardiac MRI.[65] On the other hand 3D echo relies on the good quality 2D measurements with endocardial border definition. In the absence of this the calculated 3D volumes may not be representative of the true LA size.

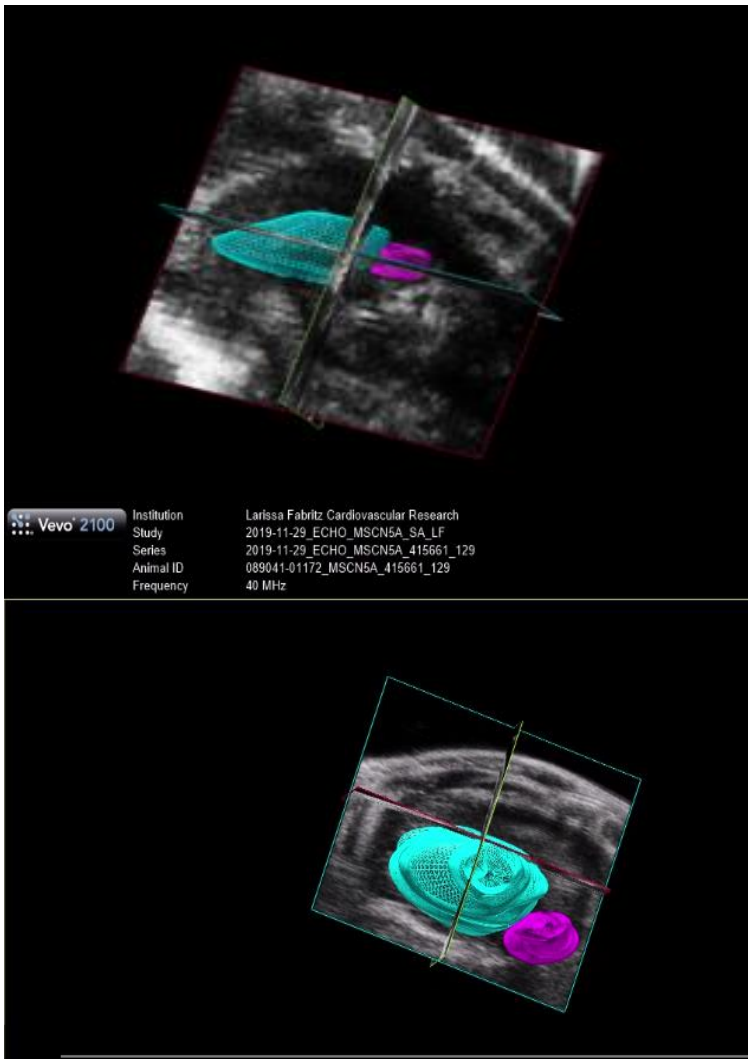

Figure 2-6 3D Echo for assessment of LA volume in a murine model.(Original work)

2.3.2 Right ventricular echocardiography

The right ventricle (RV) is a crescent-shaped structure, wrapping around the LV, and can be difficult to evaluate by echocardiography because of its complex shape and shadowing behind the sternum.[59] Therefore, dimensions must be acquired from multiple views, including PLAX, PSAX and $A4_{CH}$ to structurally and functionally quantify the RV.[56]

Assessment of right ventricular size:

The proximal right ventricular outflow tract (RVOT) can be measured by PLAX, PSAX and $A4_{CH}$ views (Figure 2-7 to 2-10) while the distal RVOT can be measured by PSAX view.[66] Apical four-chamber view is used for structural as well as a functional assessment of right ventricle.[66]

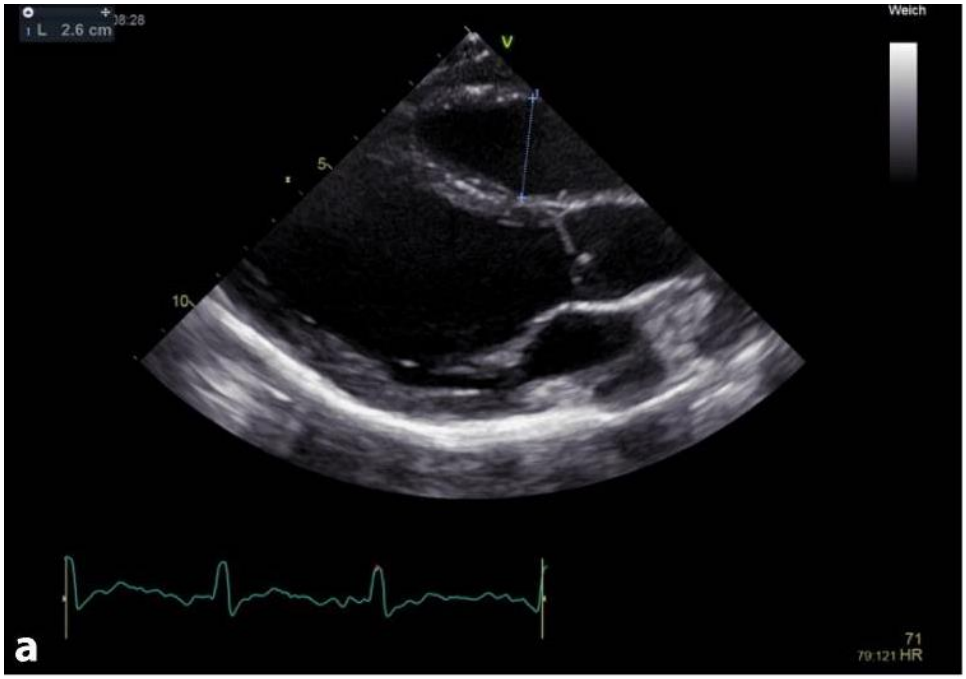

Figure 2-7 Proximal human right ventricular outflow tract on parasternal long axis view

Image adapted from Schneider M, Binder T. Echocardiographic evaluation of the right heart. Wien Klin Wochenschr. 2018;130(13-14):413-20

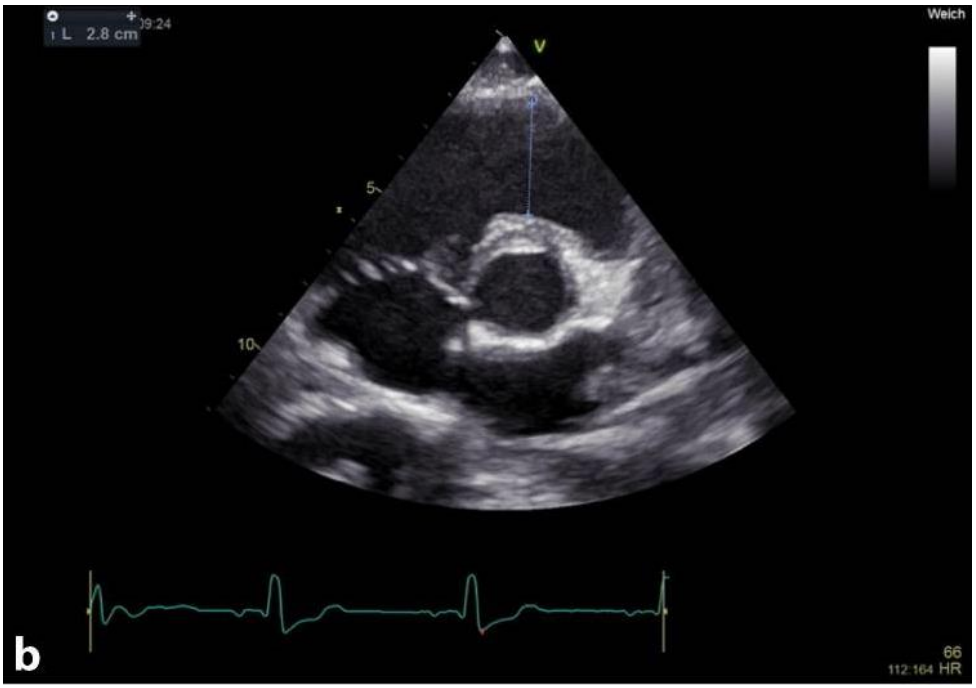

Figure 2-8 Proximal human right ventricular outflow tract on the parasternal short-axis view (normal range is 21-35mm).

Image adapted from Schneider M, Binder T. Echocardiographic evaluation of the right heart. Wien Klin Wochenschr. 2018;130(13-14):413-20

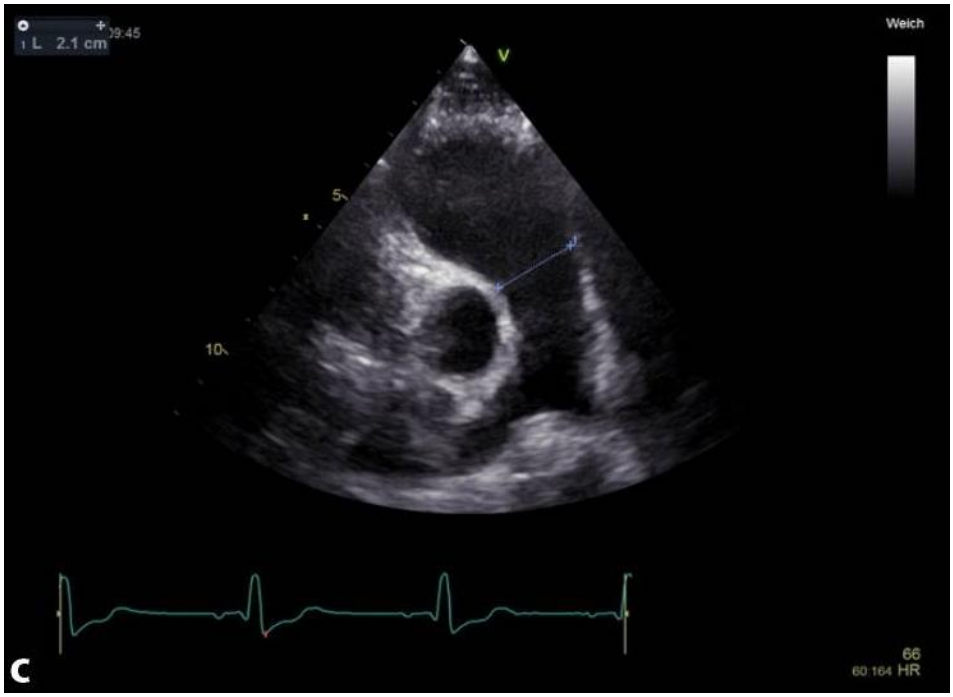

Figure 2-9 Distal right ventricular outflow tract on parasternal short-axis view (normal range 17-27mm).

Image adapted from Schneider M, Binder T. Echocardiographic evaluation of the right heart. Wien Klin Wochenschr. 2018;130(13-14):413-20

Figure 2-10 Human right ventricular proximal (normal range 25-41mm) and mid-cavity (normal range 19-35mm) mediolateral measurements on apical four-chamber view.

Image adapted from Schneider M, Binder T. Echocardiographic evaluation of the right heart. Wien Klin Wochenschr. 2018;130(13-14):413-20

Evaluation of right ventricular function:

Visual examination of RV function can prove to be inaccurate as it has many pitfalls.[66, 67] Measurement of tricuspid annular plane systolic excursion (TAPSE) is a common parameter used for RV functional assessment.[66] In $A4_{CH}$ view, M mode is used to measure annular systolic excursion of the lateral wall of the tricuspid valve (Figure 2-11).[66] M-Mode is preferred as it gives an accurate assessment in pulmonary hypertensive patients, a low TAPSE value depicts poor prognosis.[68] As this only measures longitudinal contraction, it reflects only one aspect of global RV dysfunction, so ignores radial and 'bellow' functions of the RV.[66] Fractional area change (FAC) is an alternative , which is a ratio of the change in the systolic area during the cardiac cycle with the diastolic area (Figure 2-12).

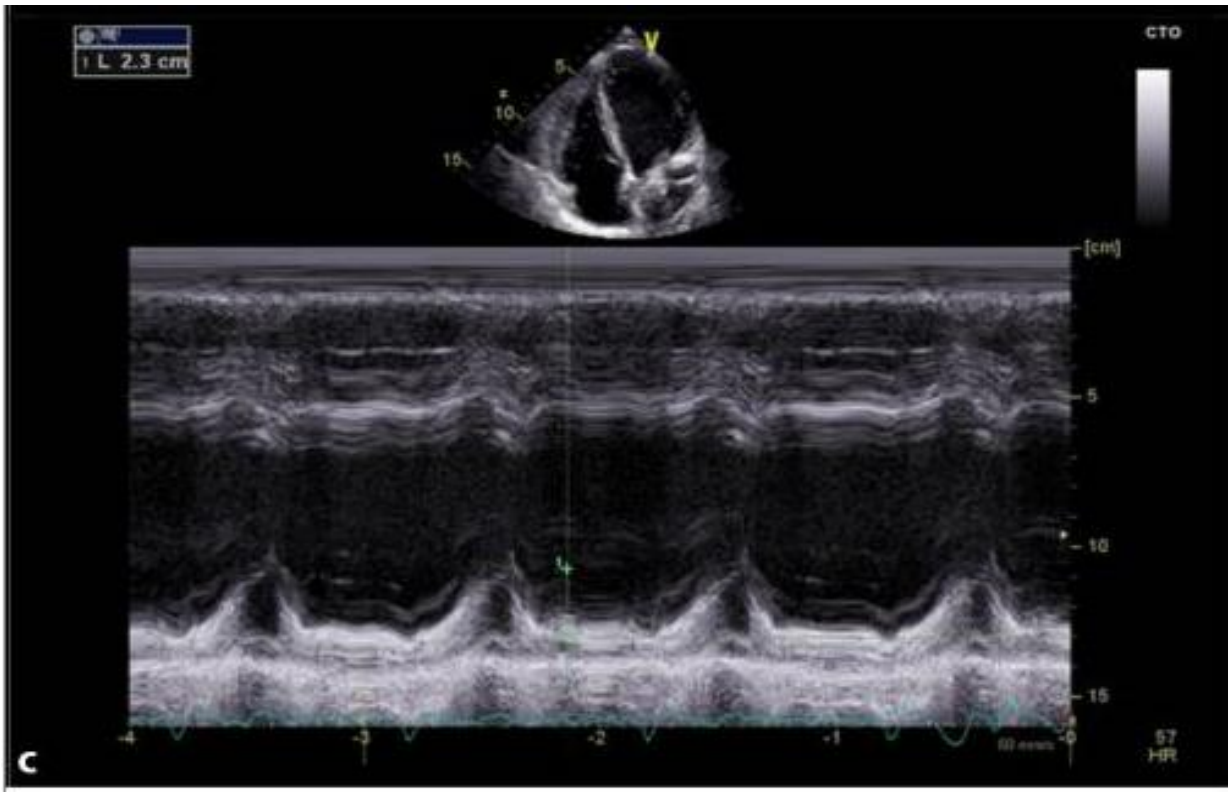

Figure 2-11 Human Tricuspid annular plane systolic excursion (TAPSE) measurement on apical four-chamber view.

Image adapted from Schneider M, Binder T. Echocardiographic evaluation of the right heart. Wien Klin Wochenschr. 2018;130(13-14):413-20

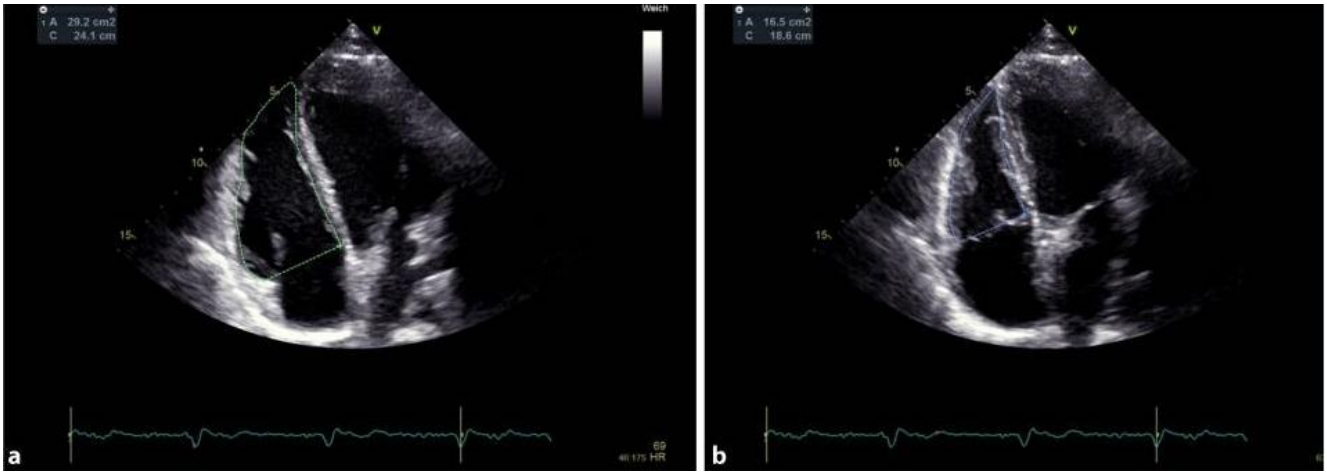

Diastole **Systole**

Figure 2-12 Human right ventricular Fractional area change (FAC) measurement on apical four-chamber view.

Image adapted from Schneider M, Binder T. Echocardiographic evaluation of the right heart. Wien Klin Wochenschr. 2018;130(13-14):413-20

2.3.3 Left ventricular echocardiography

Measurements such as that of wall thickness, chamber diameter, length and area of the left ventricle (LV) are usually performed on 2D, as well as M-mode of the PLAX view rather than the $A4_{CH}$ view. This is due to the alignment of the murine heart not being optimal for such measurements unlike human hearts.

The details of LV measured values and derived values are given in the Table 2-1.

Table 2-1 Left ventricular measured and derived variables

Left Ventricular measured variables	**Left ventricle derived variables**
LVIDd and LVIDs	Fractional shortening (FS) **(LVIDd-LVIDs)/LVIDd x 100**
IVSd and IVSs	
LV Length in diastole (LVLd)	**LV Volumes** 1. Simpson's biplane method 2. Cylinderical Hemi-ellipsoid method **(**Volume = 5/6AL) 3. Area-length method **Stroke Volume = LV volume diastole - LV volume systole** **Ejection fraction= (Stroke Volume/End diastole volume)x100** **Cardiac output = Stroke Volume x Heart rate**
LV Length in systole (LVLs)	
LV area in diastole	
LV area in systole	
Aortic annulus diameter LVOT diameter	

LVID: Left Ventricular Internal Diameter, s: Systole, d: Diastole, IVS: Inter ventricular Septum, LVL: Left ventricular Length, LVOT: Left ventricular Outflow Tract.

2.4 Histology

Microscopic and histological analysis is a good modality for diagnosis of cardiomyopathies.[69] In hypertrophic cardiomyopathy, cardiomyocytes are bigger in size and display bizarre forms of distribution with a disorganised architecture. Replacement myocardial fibrosis, as well as interstitial fibrosis, may also be seen.[70] Moreover, in dilated cardiomyopathy, cardiomyocytes are thin with extensive loss of myofibrils and fibrosis can be seen in the interstitium.[71]

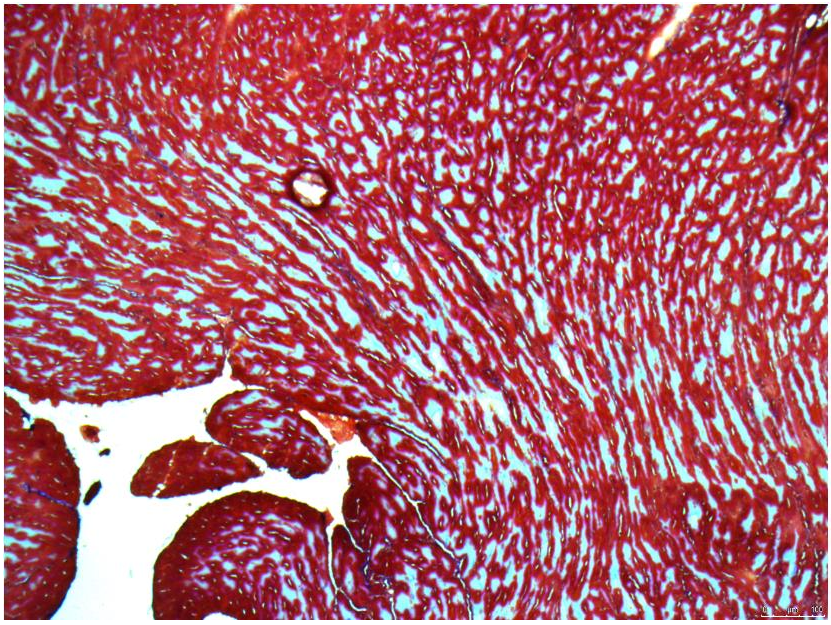

Figure 2-13 Left ventricle on light microscopy

Masson-Trichome stain with 10x magnification. Muscle is stained red with the blue stain of collagen and dark blue nuclei.
(Image from own experiment taken from Leica DM6000 Light microscope)

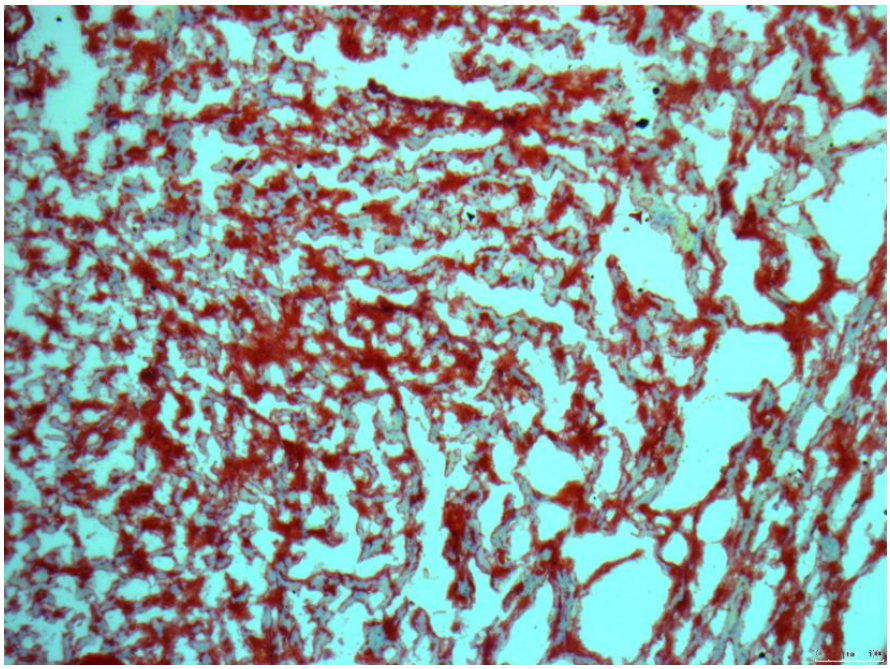

Figure 2-14 Right ventricle on light microscopy

Masson-Trichome stain with 10x magnification. Muscle is stained red with the blue stain of collagen and dark blue nuclei.
(Image from own experiment taken from Leica DM6000 Light microscope)

2.5 Study aims

The main aim of this work is to provide a overview of the work done during the study period for the M.Sc by research. This includes,

- Describe the setup of experiment to perform echocardiography in mice.
- Description of organ harvesting and setup of histological techniques to perform lght microscopy.
- Assess the structure and function for the M1875T+/- Scn5 gene defect in newly designed murine model.

2.6 Hypotheses

For transthoracic echocardiography in older mice (≥ 25 weeks), for heterozygous ($M1875T^{+/-}$) as compared to wild-type ($M1875T^{+/+}$), there is a:

a. Difference in left ventricular wall thickness, dimensions and/or volume

b. Difference in left atrial dimension

c. Difference in right ventricular size

3 Methods

Echocardiography will be used to investigate the impact of the M1875T mutation in the Scn5a gene in a murine mouse model. Mice heterozygous ($M1875T^{+/-}$) for this mutation will be compared to wild-type ($M1875T^{+/+}$) littermates. The presence of this mutation appears to be embryonic lethal due to the absence of any homozygous littermates. Histological analysis was also performed to complement echocardiographical measurements and to generate preliminary data for this mouse model.

This work was undertaken following a departmental laboratory induction and completing Home Office licence modules A-C in safe animal handling, anaesthesia and specialised procedures like echocardiography. All the echos were performed by atleast two operators, with one performing echo and the other colleague controlling anaesthesia with respect to the required heart rate for different views The echo experiments were performed by LF, SA, SNK and LS. The histological experiments were performed by SA, SNK and LS.

3.1 Ethical statement

All animal work was performed in the Biomedical Research Unit (BMSU), University of Birmingham. All the procedures were performed according to the rules and regulations for animal research and welfare by licenced researchers under the Home Office, UK. All procedures were conducted in accordance with rules and regulations for experiments with animals and approved by the UK Home Office (PPL number 30/2967) and by the institutional review board of University of Birmingham. The personal home office licence number for this experiment was IDCAD9AB2.

3.2 Experimental animals

Heterozygous *Scn5a*-M1875T$^{+/-}$ mice were generated by T-C point-mutating exon 28 of the cardiac sodium channel *Scn5a* gene through a CRISPR/Cas9 system in murine embryonic stem (ES) cells. Mutation-harboring ES cells were injected into blastocysts using well established techniques,[72, 73] Figure 3-1.

The mouse line was established by breeding male with female C57Bl/6J mice to produce heterozygous mice. After birth the pups were weaned at 19 to 23 days and the females were kept separately from males. The mice were housed at the Biomedical Services Unit (BMSU) at the University of Birmingham in well-ventilated cages, with sex-matched littermates (2–5 mice/cage). This was done under controlled standard conditions: 12 hours light/dark circle, 22°C and 55% humidity. Food and water were given *ad libitum*. General health checks were performed regularly in order to ensure that any findings were not the result of deteriorating physical conditions of the animals.

A total number of 89 mice, from both the genetic strain backgrounds SV129 and FVB were used in this study. They were grouped into young (8-24 weeks) and mature (≥ 25 weeks up to 40 weeks) mice.

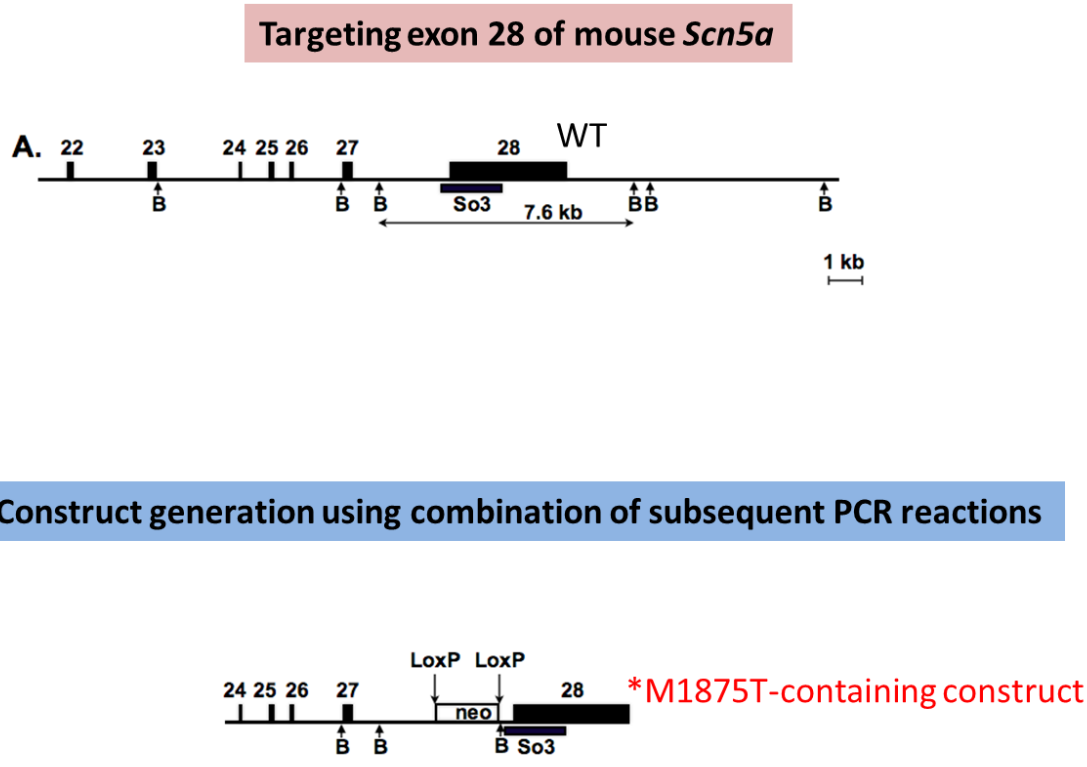

Figure 3-1M1875T$^{+/-}$construct generation using combination of subsequent PCR reactions

3.3 Experimental echocardiography methods.

Online training modules with Fujifilm Visual Sonics^{TM} for the basic understanding of setup, performing and analysis of mouse echocardiography were completed prior to live scans. Training and sign off for safe mouse handling, anaesthesia and mouse echocardiography was completed before starting the experiments.

3.3.1 Echocardiography procedure details

Preperation of mice for echocardiography:

The body weight of each mouse was recorded before the procedure. Mice were kept under light anaesthesia throughout the procedure. 3-4% of isoflurane mixed with 1 L/min of O_2 was used for the induction of anaesthesia and 1-1.5% for the maintenance dose. During anaesthesia, the mice were immobilized in a supine position on a heating

pad to maintain a core body temperature of 36-37^{o}C. Heart rates and respiratory physiology were continuously monitored by ECG electrodes integrated in the heating pad. Mice chests were first shaved and then a hair removing cream was applied to remove surplus hair. Warmed ultrasound gel was then applied to the area of interest.

Performing transthoracic echocardiography:

Transthoracic echocardiography was performed using the Vevo 2100 system (by VisualSonics^{TM}) with a 50 MHz transducer. A rig and rail system was used to hold the transducer throughout the procedure. This technique is preferred over hand-held to maintain stability in focus. All the echocardiographic images were captured as cine loops and saved in the software on the machine as well as on a secure server at the University of Birmingham. These images were later analysed offline through Vevo lab 3.1.1 and a Microsoft Excel file was generated which was then used to populate the database.

Mouse recovery:

The mice recovered from the anaesthesia in a prewarmed cage and observation was continued until they were fully awake and mobile.

3.3.2 Measurements

Echocardiographic measurements performed from mice with heart rate range between 370-520 beats per minute was taken into consideration. This led to an exclusion of 10 mice and 79 mice were used for the final analysis. Anaesthesia adjustment was only made according to the heart rate and also for corresponding echo modality studied. For example heart rate was kept at lower end of range for the 2D measurements in A4C.

The mice were further split into young adult (8-24 weeks) and mature mice (≥25 up to 40 weeks). The split in age was made to assess for any age-related differences as it is known that some phenotypic difference will become apparent in older animals.[74] Measurements were validated by a second, blinded expert in mouse echocardiography using the coefficient of variance testing. The schematics from standard British Society of Echocardiography (BSE) and the European Association of Cardiovascular Imaging (EACVI) guidelines were adapted and modified for mouse echocardiography.[75, 76] Murine specific guidelines were studied as previously published.[77, 78] Finally, specific to our available equipment and set-up, the echocardiography protocols used in previous studies from our group were also considered.[11, 12]

The steps of the experiment are as follows:

- ID, strain, date of birth, weight, other parameters are recorded
- Adequate anaesthesia is administered under temperature control
- ECG and respiration are recorded

Mouse echocardiography is performed as per a set protocol which involved certain measurements required for the experiment. This includes the 2D and M-Mode measurements to assess relevant cardiac chamber sizes, wall thickness and Doppler echocardiography to assess flow dynamics. A summary of step-wise echo analysis is as follows:

Parasternal long-axis view (PLAX):

The heart is first imaged in parasternal long axis (PLAX) by placing the ultrasound probe parallel to the long axis of the heart, to examine the left ventricle, aortic root, right ventricular outflow tract (RVOT) and left atrium (Figure 3-2, 3-3). It is considered one of the most important initial acoustic windows of the heart, as based on the right orientation of PLAX, the other views can also be appropriately achieved. M-Mode measurements are also obtained (Figure 3-4, 3-5) and used to assess wall thickness and internal diameter during systole and diastole. Table 3.1 shows measurements obtained using PLAX.

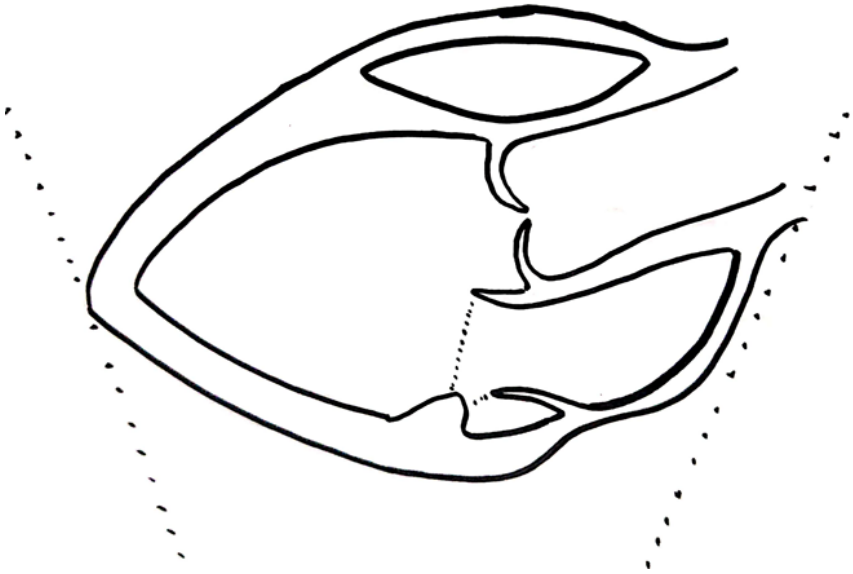

Figure 3-2 The chambers and walls orientation on Parasternal long-axis view. (original sketch)

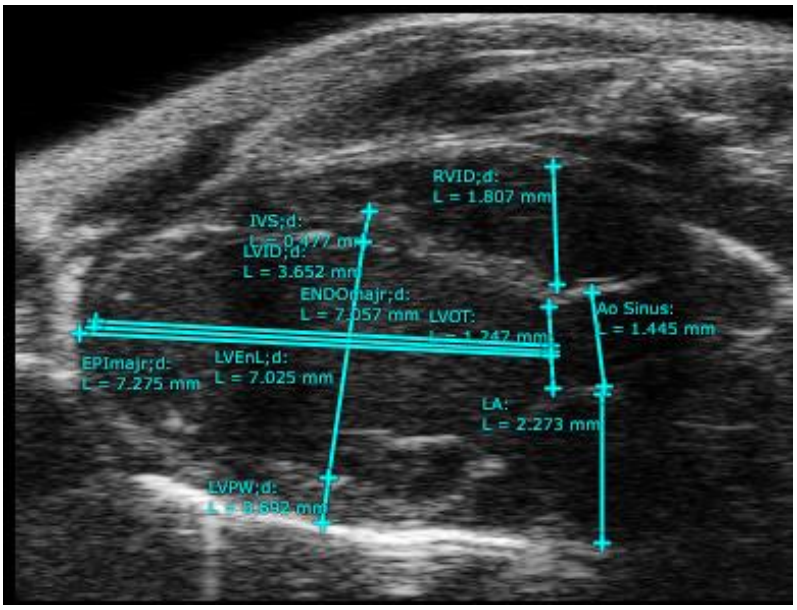

Figure 3-3 Parasternal long-axis view in Diastole with measurements of Left ventricular (LV) length, septal (IVSd) and posterior wall thickness (LVPWd) and LV internal diastolic dimension (LVIDd).

Maximal diastolic Right ventricular Internal dimension (RVIDd) is given. Aortic root dimensions are also measured in diastole.

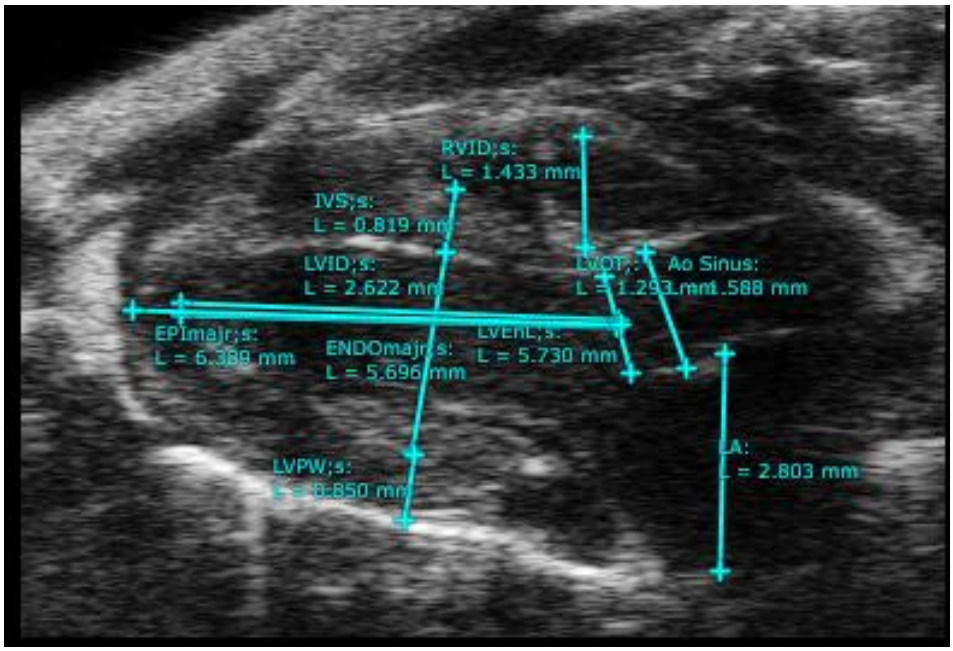

Figure 3-4 Parasternal long axis view in Systole with measurements of Left ventricular (LV) length, septal (IVSs) and posterior wall thickness (LVPWs) and LV internal systolic dimension (LVIDs).

Systolic Right ventricular Internal Dimension (RVIDs) is given. Left atrial (LA) dimension (L) and area (A) are also measured in systole.

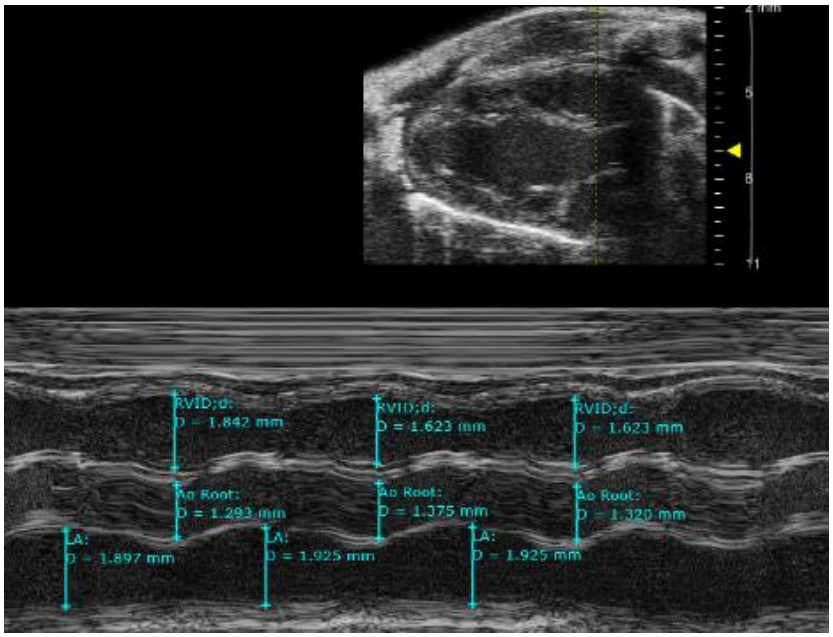

Figure 3-5 M-mode of Parasternal long-axis view, at the aortic root level.

Right ventricular internal dimensions (RVIDs and RVIDd) in systole and diastole, aortic root and left atrium (LA) are measured at three consecutive cardiac cycles.

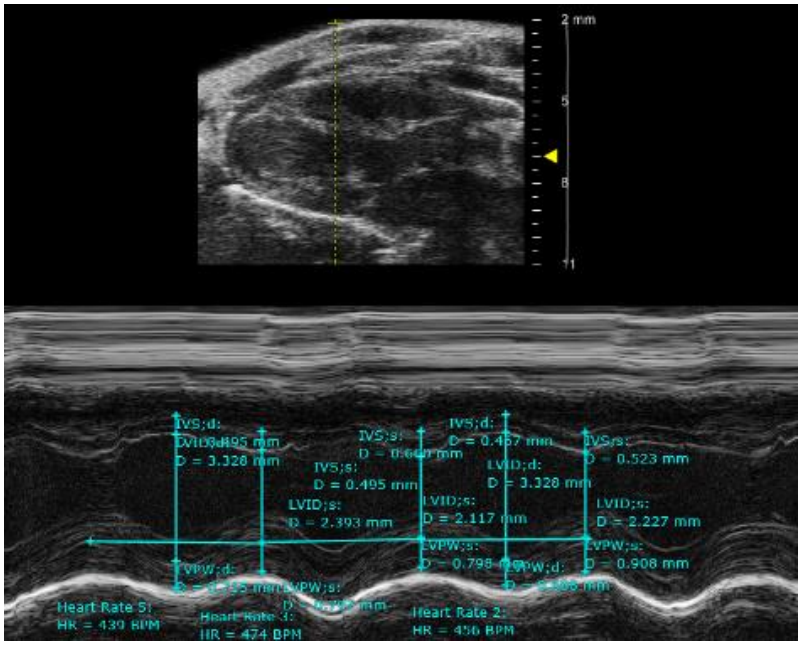

Figure 3-6 M-mode of Parasternal long axis view, at papillary muscle level.

Wall thickness of interventricular septum (IVSs), left ventricular posterior wall (LVPWs) and left ventricular internal diameter (LVIDs) are measured in systole. Heart rate (HR) is also calculated by selecting three consecutive cardiac cycles.

Table 3-1 Parasternal long-axis view with respective chambers, measurements and calculated parameters			
Echocardiographic window	Chamber	Parameters measured	Calculated Parameters
Parasternal long axis (PLAX)	Left ventricle (LV)	a. Wall thicknesses and internal diameters in both systole and diastole b. M-mode for chamber dimensions c. LVOT and AoR dimensions	Fractional shortening Cardiac output
	Right ventricular outflow tract (RVOT)	a. RVOT anteroposterior diameter b. RVOT area	Fractional area change
	Left Atrium (LA)	a. LA anteroposterior dimension b. LA area	LA Volume

Parasternal short-axis view (PSAX):

This view was achieved by rotating the probe 90 degrees clockwise from the previous position of PLAX. The images are acquired at various levels by tilting the probe from cephalad to the caudal position. In ideal cases the acquired sections are as follows:

a. Aortic root level

b. Mitral valve level

c. Papillary muscle level

d. Apical level

A summary of the measurements and calculations attained from PSAX is given in the Figure 3-7 to Figure 3-13 and .

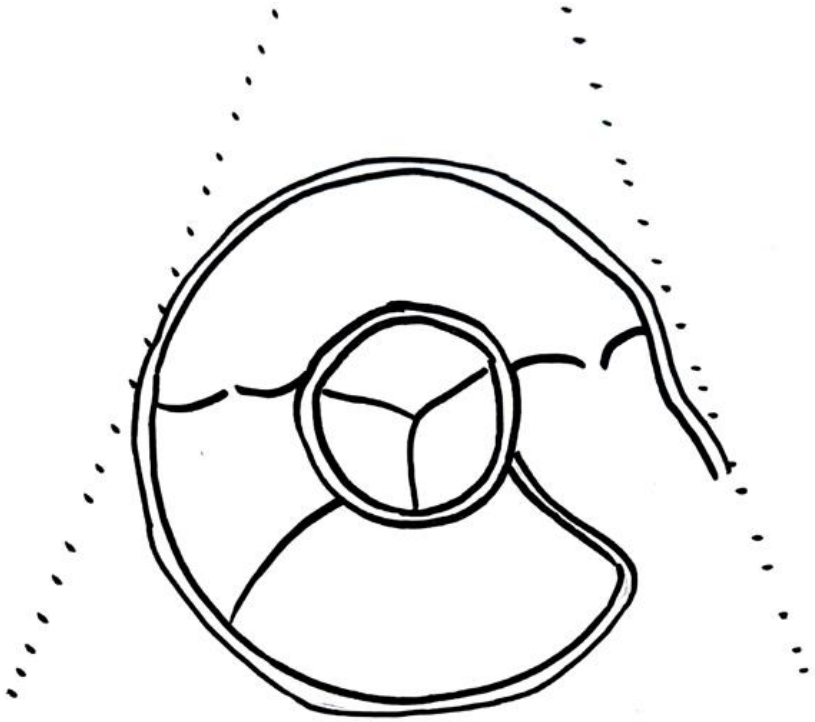

Figure 3-7 The chamber and wall orientation on parasternal short axis view at aortic root level. (original sketch)

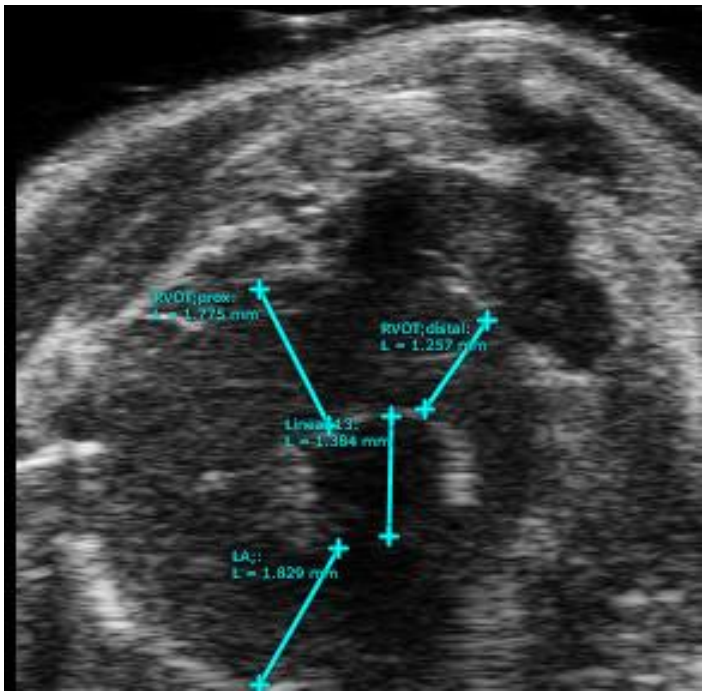

Figure 3-8 2D of Parasternal short-axis view, at aortic valve level.

Aortic root (AoR), Proximal and distal Right ventricular Internal dimension (RVID) and Left Atrial (LA) dimensions are measured.

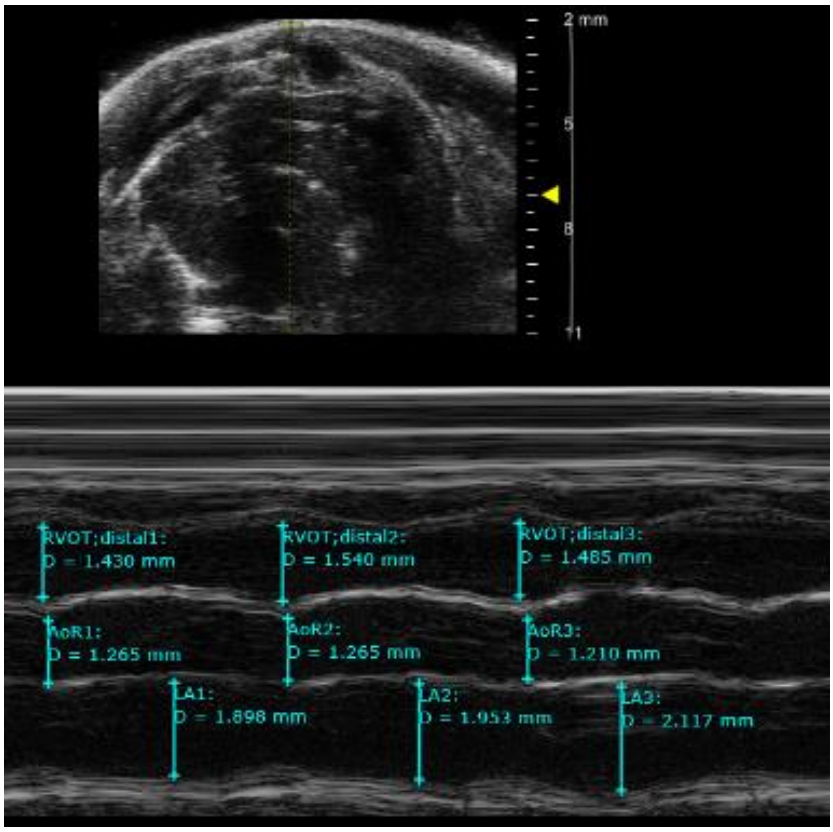

Figure 3-9 M-Mode of Parasternal short axis view, at aortic valve level.

Aortic root (AoR), distal right ventricular outflow tract (RVID distal) and left atrial (LA) dimensions are measured.

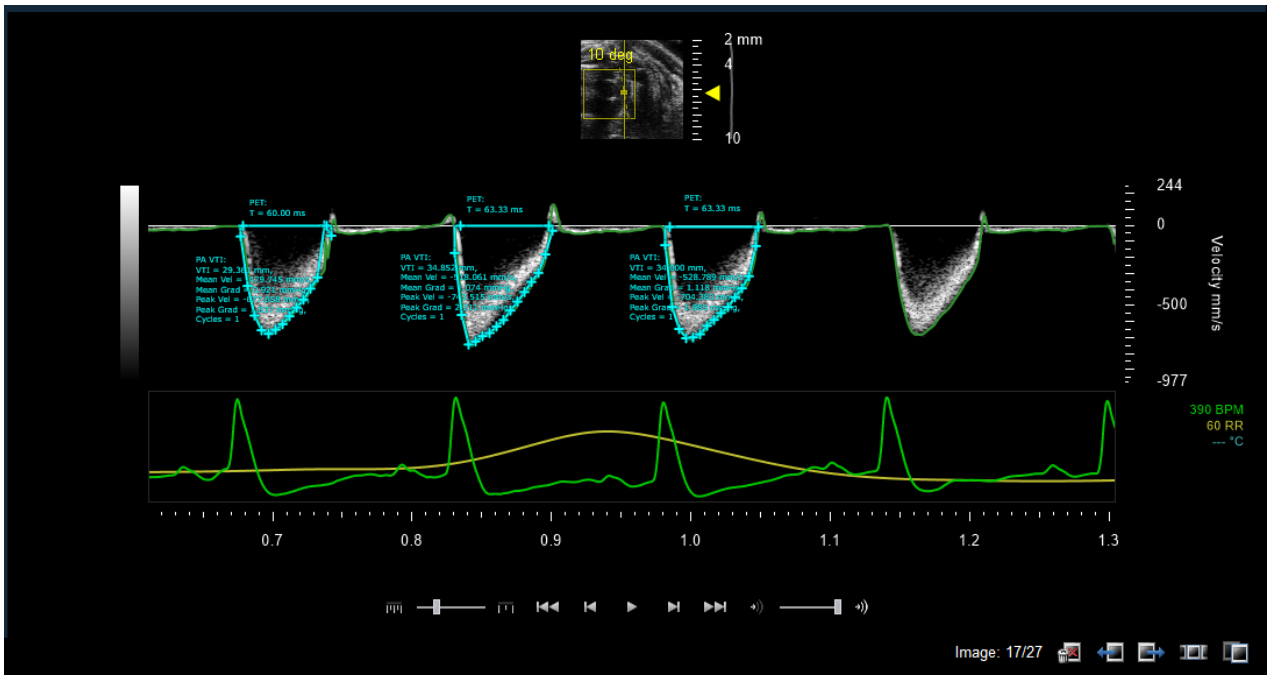

***Figure 3-10* Parasternal short-axis view, at aortic valve level with pulse wave Doppler (PW) of the pulmonary valve.**

Measurements indicate pulmonary valve velocity-time integer (PV VTI) alongside mean and peak velocities, pulmonary acceleration time (PAT), pulmonary ejection time (PET)

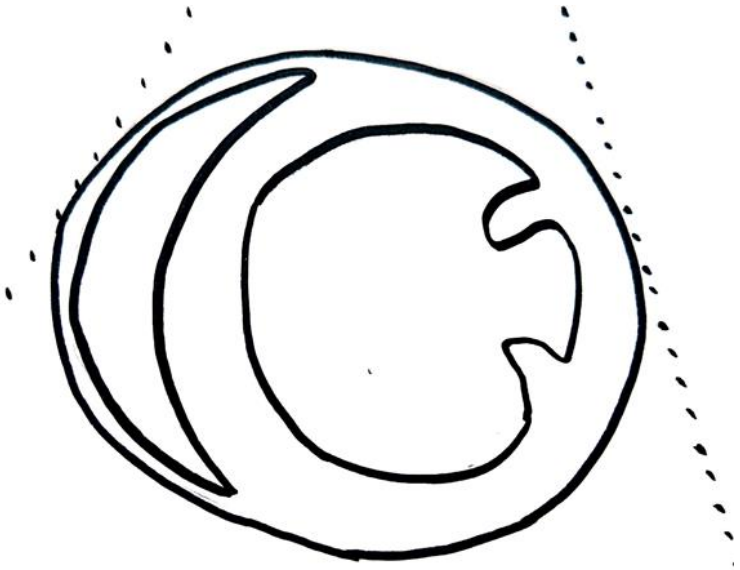

Figure 3-11 The chamber and wall orientation on Parasternal short axis view at papillary muscle level. (original sketch)

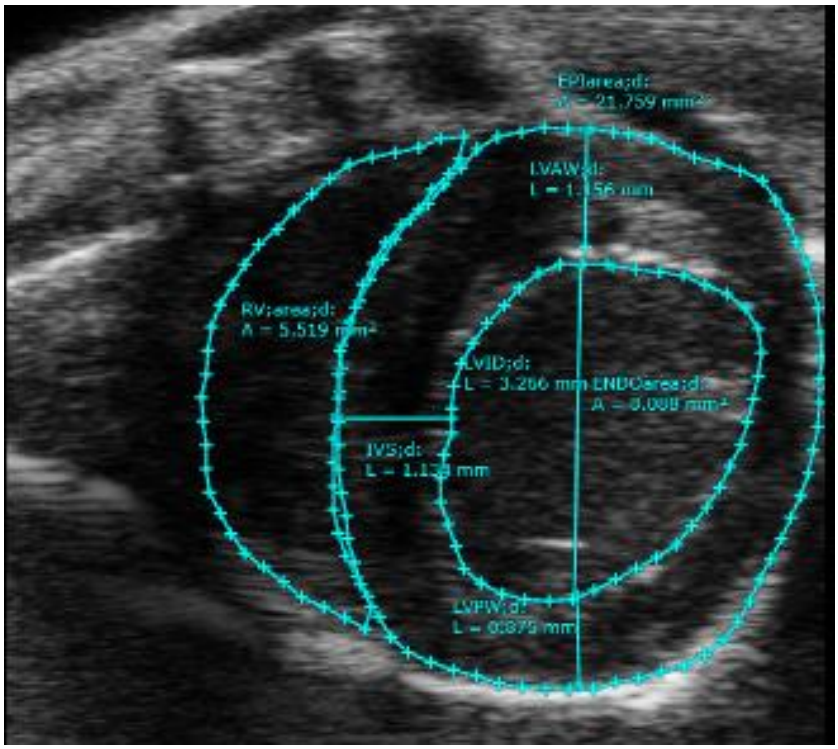

Figure 3-12 ***2D of Parasternal short-axis view, at the papillary muscle level.***

Aortic root (AoR), Proximal and distal right ventricular internal dimension (RVID) and left atrial (LA) dimensions are measured.

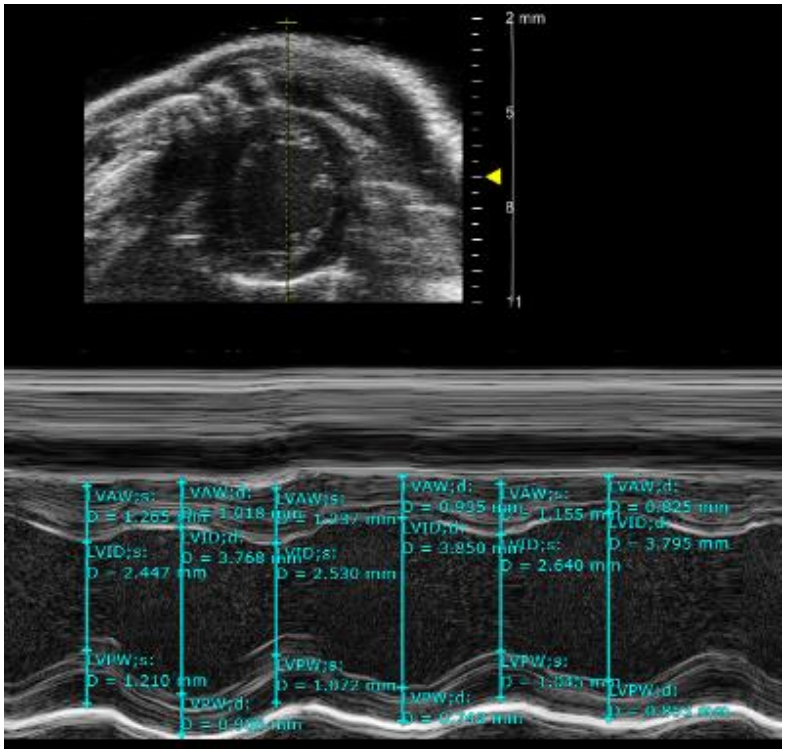

Figure 3-13 M-Mode of parasternal short-axis view, at the papillary muscle level.

Left ventricular anterior (LVAW) and posterior wall (LVPW) in systole and diastole). Left ventricular internal dimensions (LVID) in systole and diastole are also measured

Table 3-2 Parasternal short-axis view with respective chambers, measurements and calculated parameters			
Echocardiographic window	Level	Parameters measured	Calculations
Parasternal short axis (PSAX)	Base (AoR) level	a. RVOT proximal and distal dimensions in diastole b. Tricuspid and Pulmonary forward and backward flow can be measured, provided the jets are parallel to Doppler signal.	Pulmonary and tricuspid valve forward flow and regurgitant velocities alongside pulmonary ejection time (PET)
	Mitral valve level	a. The shape of the right ventricle and anterior, inferior and lateral walls	
	Papillary muscle	a. LV endocardial and epicardial area b. M-Mode for LV wall thickness and internal diameter c. Valuable for initial assessment of RV size but not for RV systolic function because of the asymmetric nature of RV contraction d. Septal flattening from RV volume or pressure overload is well appreciated in diastole and systole.	

Apical four and five-chamber views:

These views were achieved by placing the ultrasound probe along the apex of the heart, looking at the cross-section of the chambers through the apex. It is important for measuring sizes of the four chambers and valvular velocities for tricuspid and mitral valve. It must be noted that it is more difficult to achieve good endocardial border definition in this view compared to the parasternal view due to sub-optimal echo windows in mice because of their small and curved rib cage. However, acquisition of the trans-valvular velocities and TAPSE is still possible. Figure 3-14 shows the schematic of the apical 4-chamber view. Figure 3-15 shows colour flow Doppler of the mitral inflow while Figure 3-16 shows the mitral inflow velocities in the apical 4 chamber view. Table 3-3 summarises the parameters measured through these views.

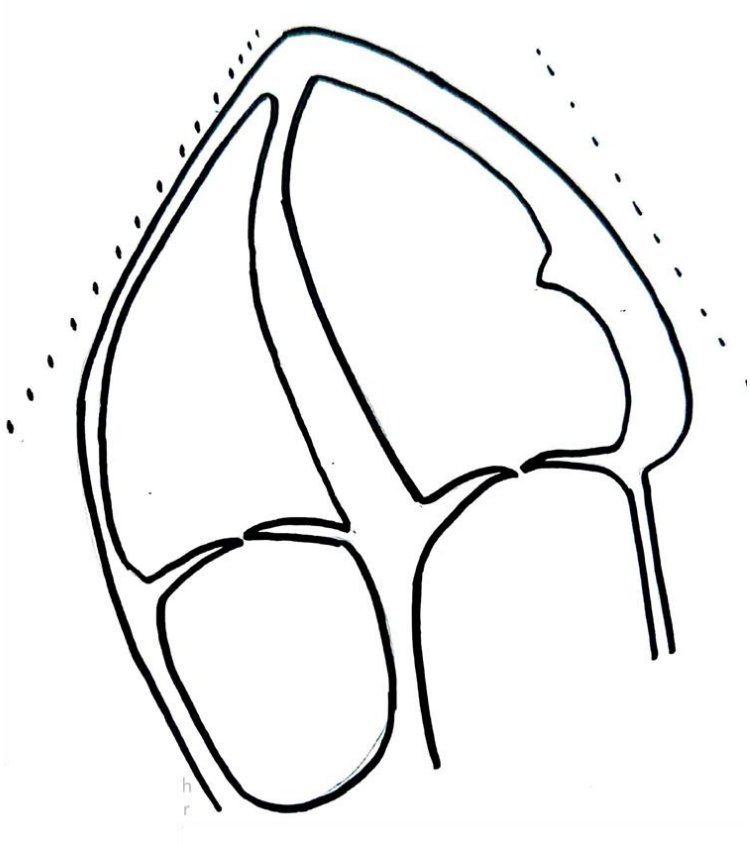

Figure 3-14 Orientation of cardiac chambers and valves on apical four chamber view. (original sketch)

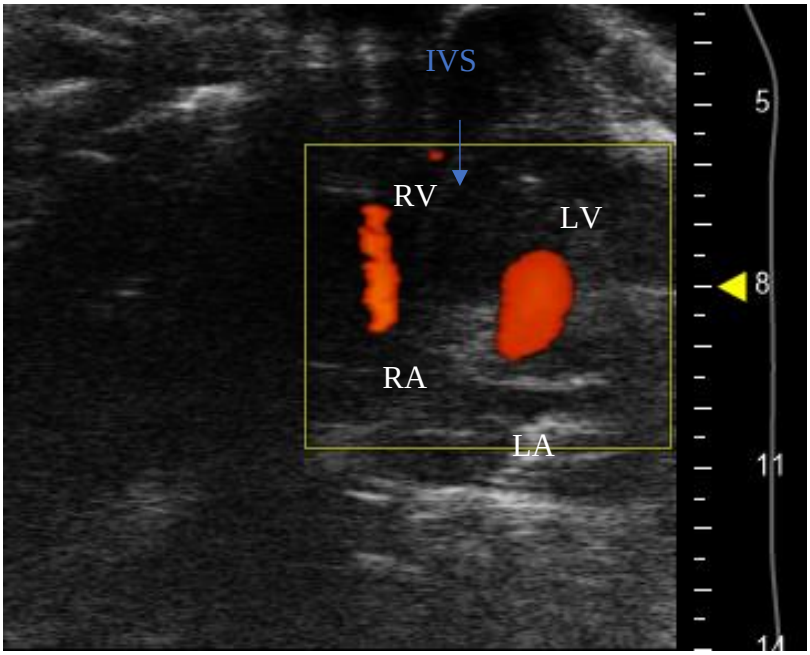

Figure 3-15 Apical 4-chamber view of mouse heart with colour Doppler across mitral and tricuspid valves.

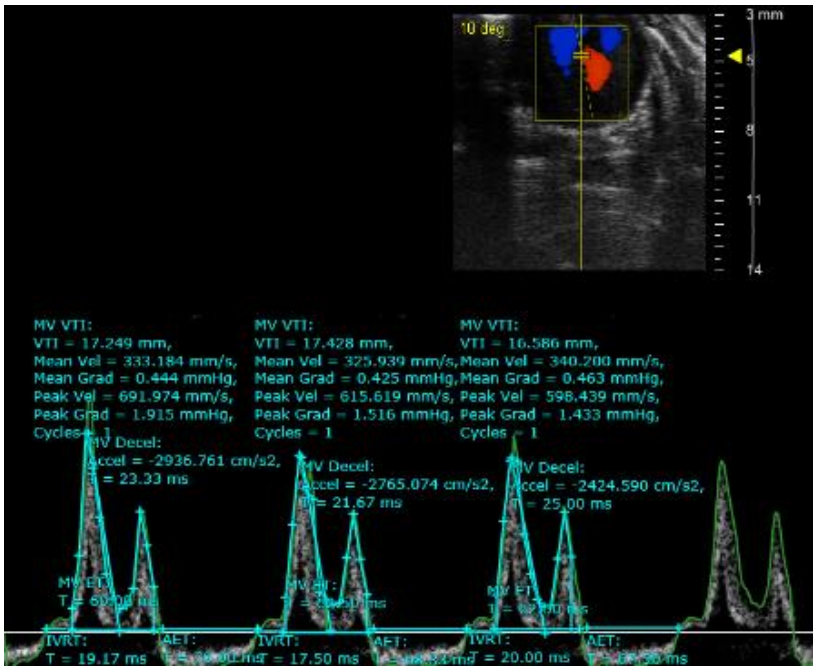

Figure 3-16 Apical 4 chamber view, with pulse wave Doppler (PW) of the mitral flow.

Measurements indicate mitral valve velocity-time integer (MV VTI) alongside mean and peak velocities, mitral deceleration time (MV-Decel), mitral ejection time (MET) and isovolumetric relaxation time (IVRT)

Table 3-3 Apical 4 chamber view with respective chambers, measurements and calculated parameters

Echocardiographic window	Chamber	Parameters measured	Calculations
Apical Four chamber view	Left and Right Ventricle	a. LV systolic and diastolic area and lengths b. RV maximal long-axis distances, minor distances at both base and mid-level. RV area fractional area change. c. Tricuspid annular plane systolic excursion (TAPSE) for RV longitudinal function	LV Ejection fraction (Simpson's method) RV function
	Left (and right) atrium	Left (and right) atrial longitudinal and mediolateral dimensions LA Area	LA and RA volume

Aortic Arch view:

The aortic arch view is valuable in assessing forward velocities in the descending aorta. This view was acquired by placing the ultrasound probe suprasternal, to view the aortic arch. Colour and pulse wave Doppler was performed at the ascending and descending aortic level. Figure 3-17 to Figure 3-20 show the appearance of ascending and descending aorta as well as their forward flow velocities.

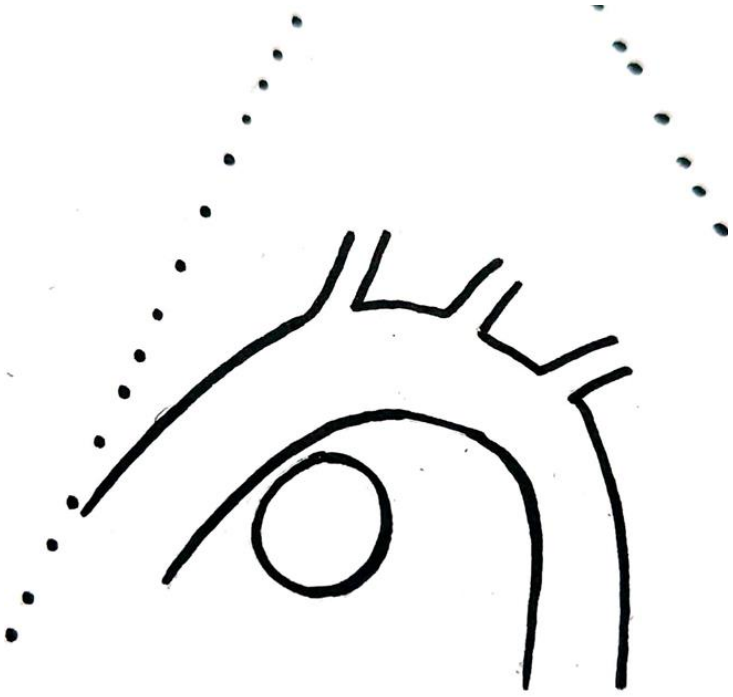

Figure 3-17 Diagram showing the aortic arch on supra-sternal view. (original sketch)

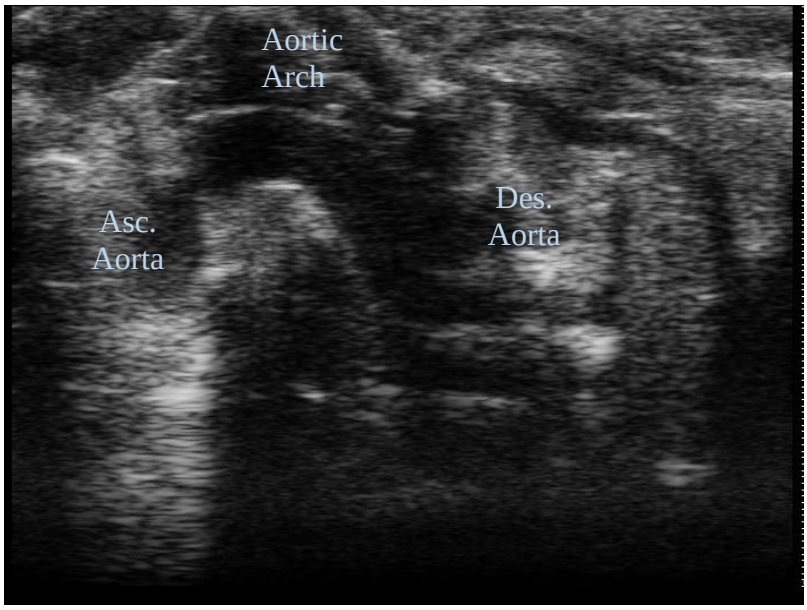

Figure 3-18 Figure showing labelled image of aortic arch on supra-sternal view.

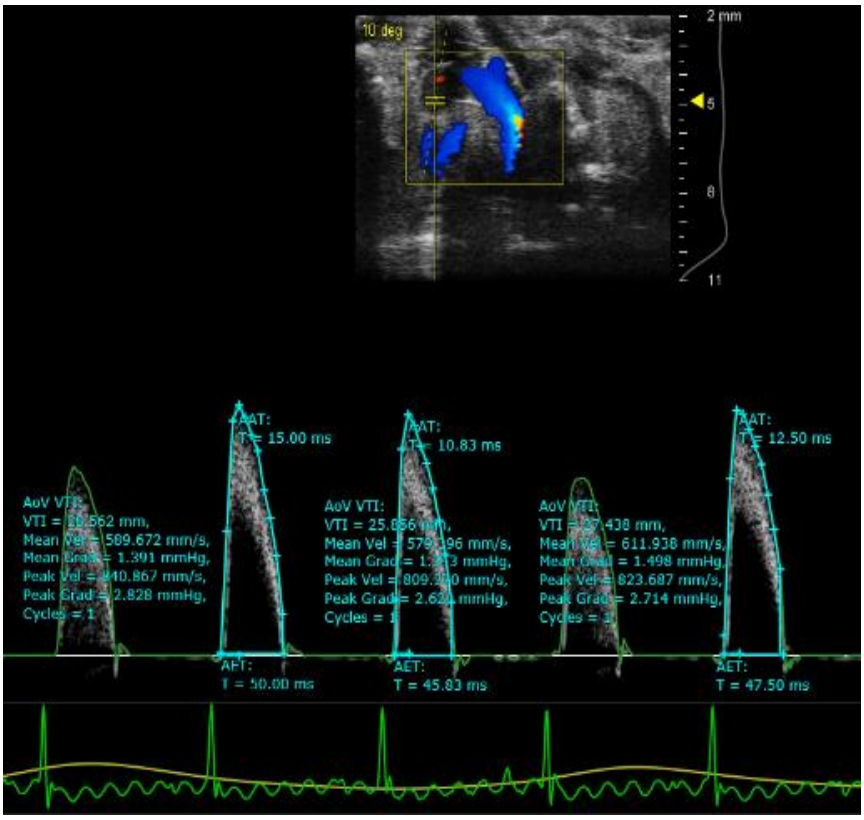

Figure 3-19 Aortic arch view, with pulse wave Doppler (PW) of the aortic flow.

Measurements show ascending aortic velocity-time integral (Ao VTI) alongside mean and peak velocities and aortic ejection time (AET)

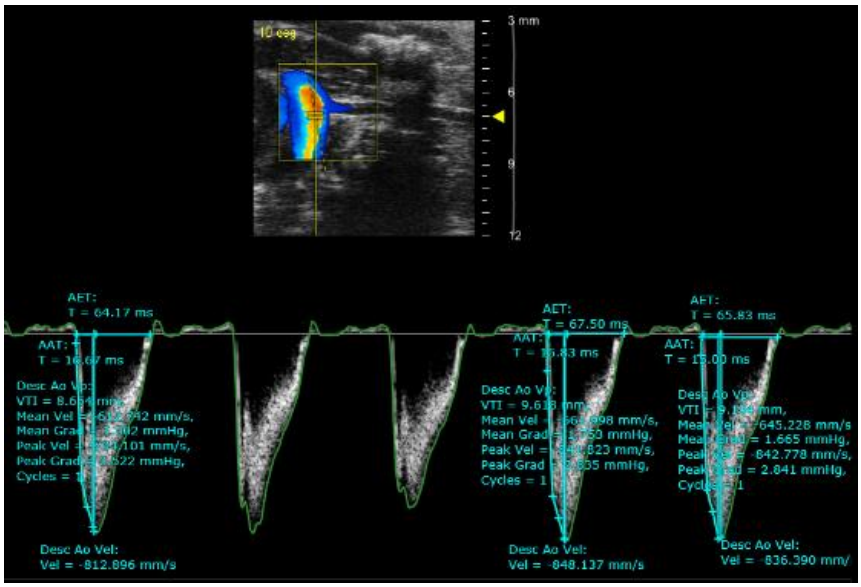

Figure 3-20 Aortic arch view, with pulse wave Doppler (PW) of the aortic flow.

Measurements show Descending aortic velocity-time integer (Ao VTI) alongside mean and peak velocities and aortic ejection time (AET)

Table 3-4 Aortic arch parameters

Echocardiographic window	Chamber	Parameters measured	Calculations
Aortic Arch View	Ascending aorta, arch and descending aorta	Measurement of the descending aortic flow	Forward flow velocities

Three-dimensional (3D) echocardiography:

Three-dimensional echocardiography is potentially a reliable parameter for assessing volumes of different chambers. It is performed by aligning the ultrasound probe along the short axis or long axis of the mouse heart. Measurements are hitherto mainly taken for the LV as it is technically more challenging for other chambers.

We trigger the software for systole and attain the images. The machine then triggers again for diastole to attain another set of images. They are then reconstructed by the software and reproduced as 3D images in different views such as cube view, longitudinal view, transverse view, slice view, surface view with and without data. Figure 3-21 to Figure 3-24 show different views of murine 3-D echocardiography.

Cube view: The below figure shows the cube view of the heart, which can be moved three dimensionally to see different cuts of the organ.

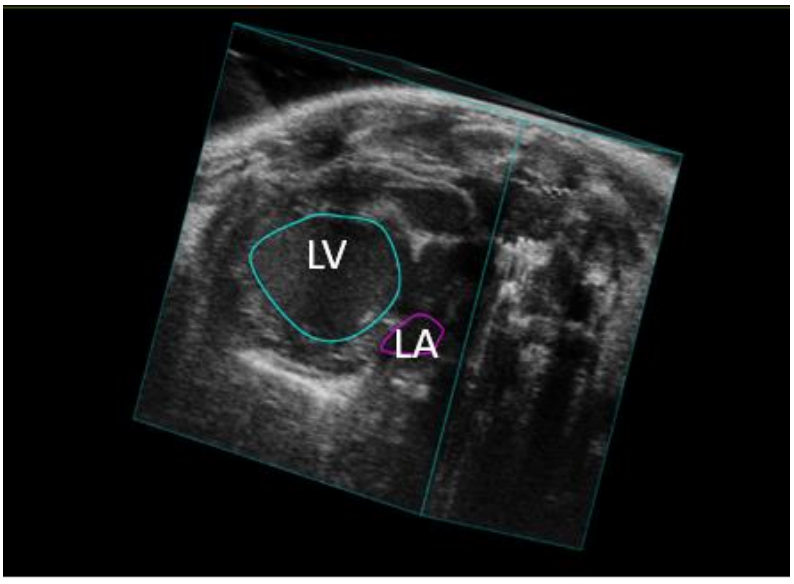

Figure 3-21 Three-dimensional cube view of the heart (original work).

Slice view: This view is used for offline data analysis. The respective chamber outline is traced at different levels, in multiple slices, which are then reconstructed to form the volume of the chamber. Figure 3-22 shows the chambers traced along their endocardial borders.

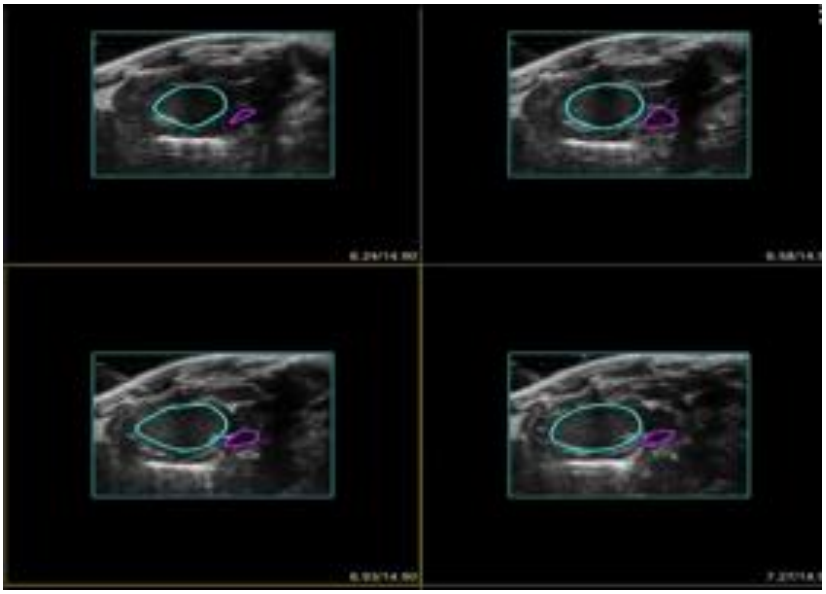

Figure 3-22 Slice view of the three-dimensional echocardiography (original work)

Surface View: The below figure shows the complete surface outline of the left ventricle and left atrium, which is reproduced at the end of the offline analysis. This can be rotated three-dimensionally.

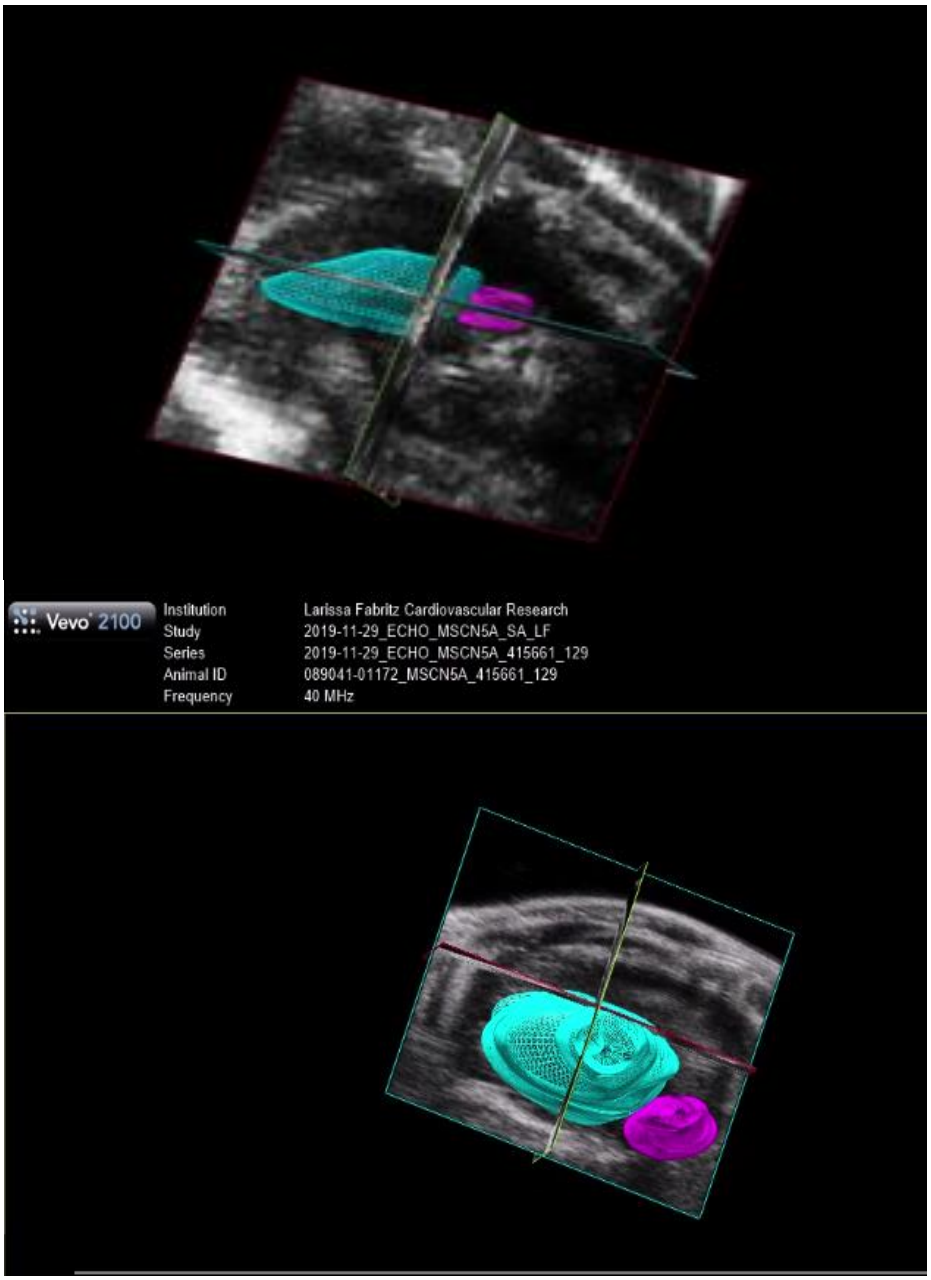

Figure 3-23 Surface view of the murine left heart (original work)

Surface view without data: The below figure is used for a better look at the reconstructed chambers from different angles.

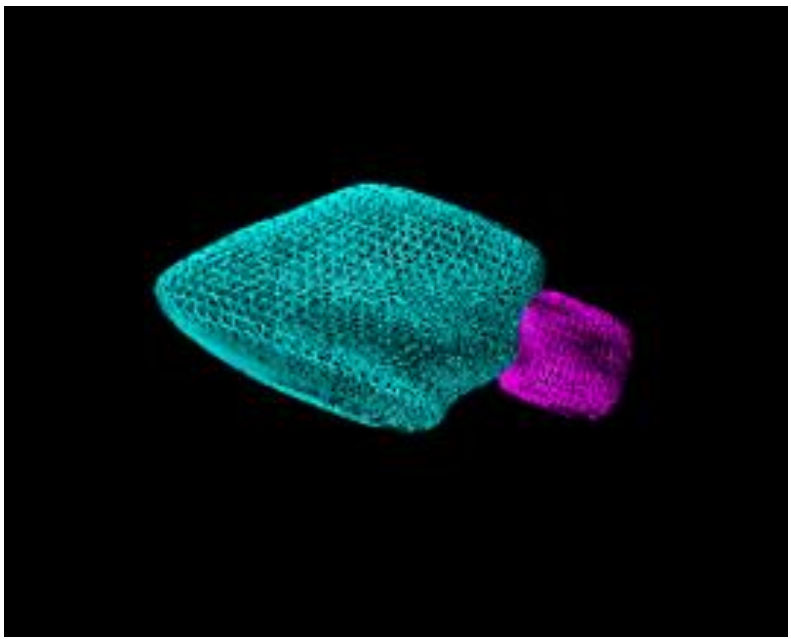

Figure 3-24 Surface view without data (original work)

Advantages and disadvantages of 3D Echo – 3D echo is useful in gaining a more accurate volumetric assessment of the cardiac chambers. Moreover it provides better anatomical definition of cardiac structures. On the other hand, 3D echocardiography requires more technical expertise as compared to 2D echo and the echo analysis module depending on provider can be expensive. The echo analysis quality is dependant on the mouse heart rate. There is a requirement to manually trace endocardiac borders and the calculations are done based on assumptions requiring complicated analysis software.

3.4 Histology

3.4.1 Tissue Harvesting

Terminal experiments for organ harvesting were performed at the Biomedical services unit (BMSU), University of Birmingham. Care was taken to perform all of the procedure while the animal was deeply anaesthetized to prevent suffering. Moreover, tissue harvest was done under general anaesthesia because most of the atria were first used for optical mapping before preservation. Mice were euthanized under the effect of 4-5% Isoflurane. After confirming deep terminal anaesthesia and a negative pedal reflex, the animal was put in a supine position with all four limbs restrained. A subdiaphragmatic incision was taken and extended laterally, cutting through the ribs and diaphragm to expose the heart. While holding the main vessels with thin curved forceps, the heart was extracted by cutting the vessels with curved scissors. The excised heart was immediately transferred to a petri dish, containing Kreb's solution with a few drops of heparin. The animal's death was confirmed by immediately performing another Schedule 1 procedure of cervical dislocation. The heart was then flushed with heparinized Kreb's solution to remove blood. It was then quickly dried by gentle dab on a tissue cloth. After weighing the heart, the four chambers and interventricular septum were separated and preserved for histology.

Organ harvesting was done by OCT (TISSUE TEK) technique. The following materials were required for the procedure.

1. Small plastic beaker or other suitable containable that can withstand extreme cold temperature.

2. Isopentane/2-methyl butane.
3. Stirrer.
4. Cork discs
5. Fine waterproof marker.
6. Dressmakers' pins.
7. OCT/TISSUE TEK.
8. Forceps
9. Liquid nitrogen
10. Weight scale/gravimeter
11. Small trays

3.4.2 Method of OCT (Tissue TEK)

According to the standard protocol, the following steps were performed.

The organs were carefully dissected and placed on white fabric. All the organs were weighed individually and their weights recorded. Cork discs were labelled with the mouse number, type, tissue type and date. Isopentane was poured in the beaker, ensuring the liquid was at least 40mm deep. The beaker was placed in liquid nitrogen to cool the isopentane, by frequently stirring. Two pins were inserted into the unlabelled side of the cork disc, to support the tissue. Optimal cutting temperature (OCT) solution was poured along with the pin, on the cork disc. The tissue was placed on the cork disc and the cork disc was used to prop the tissue in the desired, orientation. This allows optimal cross sectioning of the heart tissue later. Some more OCT solution was poured to cover the tissue, as well as, removing all the bubbles. The sample was quickly dropped

into cooled Isopentane and kept for about 30 seconds until the OCT solution solidified and turned white.

The sample was then removed from isopentane with forceps and put into liquid nitrogen for a few hours or until the end of the experiment. After a few hours, the tissues were preserved in a labelled box at -80^{o}C . The same steps were repeated for all the chambers of the heart and other organs such as liver, kidneys, spleen, muscle.

The Figure 3-25 and Figure 3-26 highlight some of these steps.

Figure 3-25 Careful dissection and subsequent weighing on a gravimeter

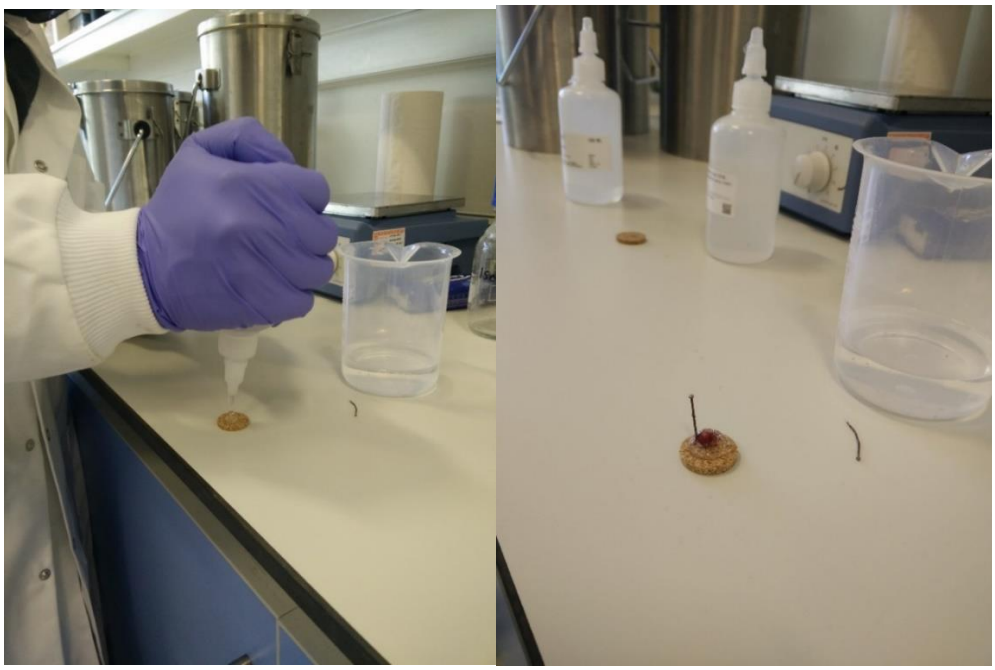

Figure 3-26 (left) OCT solution being poured on the cork; (Right) Tissue placed on the cork with OCT

3.4.3 Slicing and slide preparation

The following materials were required for this procedure.

1. Cryostat
2. Frozen sample (brought in dry ice)
3. OCT (Tissue-Tek)
4. Cryostat knife (kept at -20 ^{o}C in the freezer)
5. Microscope slides
6. Pencil for labelling slides
7. Soft, clean paintbrush for wiping away the OCT flakes from the blade

Methods for slide preparation:

The knife was fixed on the cryostat holder. The plastic anti-roll plate was aligned over the knife so that it was in line and at the same angle as the knife. The sample was stuck

onto the metal mounting disc with OCT and allowed to freeze in the cryostat chamber at -20 ^{o}C. The disc was fixed with tissue sample on the object holder. The initial slice thickness was sustained at 20-30 microns to remove excess OCT and reach the tissue sample. After reaching the sample, the slicing thickness was decreased to 6µm and secured with the anti-roll plate. The sample was slowly rolled and the desired slices were carefully mounted by placing the microscope slide on the top of the sliced sample.

Two or three slices were collected on one slide. The cryostat and blade were cleaned with acetone/alcohol. After lodging the tissue on the slides, it was left at room temperature for 30mins to dry. This time did not exceed one hour.

Figure 3-27 Images of the Cryostat used for slicing and slide preparation

Slide fixation:

Slides were dipped in acetone at -20^{o}C in a rectangular glass jar with the slide holder/comb for 20mins. The slides were removed from acetone and left to air-dry in a fume hood for 5-10 mins. The slides were kept at -20^{o}C in the freezer in a labelled slide container, until staining.

3.4.4 Staining

Trichome Stain Kit (Modified Massons's connective tissue stain, Abcam AB150686), was used according to the manufacturers instructions.

The Bouin's Fluid was preheated in a water bath to 56-64 °C in a fume hood. The slides were then placed in the preheated Bouin's fluid for 60 minutes, followed by a ten minute cooling period. The slides were rinsed in plain water until the section was completely clear and then rinsed with distilled water. Equal parts of Weigert's (A) and Weigert's (B) were mixed to create working Weigert's Iron Hematoxylin and used to stain the slides for 5 minutes. After this, the slides were rinsed in running tap water for two minutes. The slides were dipped in Biebrich Scarlet / Acid Fuchsin Solution for 15 minutes before being rinsed with distilled water. The slides were differentiated in Phosphomolybdic/ Phosphotungstic acid solution for 10-15 minutes or until collagen was not red. Without rinsing, Aniline Blue Solution was applied to slides for 5-10 minutes.

The slides were again rinsed with distilled water. We then applied Acetic acid (1%) to slides for 3-5 minutes. The slides were dehydrated quickly in two changes of 95% alcohol, followed by two changes of Absolute ethyl alcohol in the hood. The alcohol was left in the hood to evaporate. The slides were cleared with Xylene and mounted in synthetic resin.

Some of the solutions were photosenstive and covered with foil. These included: Weigert's (A), Weigert's (B), Weigert's Iron Hematoxylin, Biebrich, Scarlet/Acid Fuchsin solution, Phosphomolybdic acid and Aniline blue. Collagen was stained blue, muscle fibres were stained red and nuclei were stained black/blue.

3.4.5 Handling histology data

Depending upon the staining method, several histopathological parameters such as myocyte atrophy, vascular degeneration, myocytolysis, lipofuscin accumulation, interstitial fibrosis, lipomatosis and inflammatory infiltrate can be assessed. The actual assessment on the slides for this experiment was for fibroblast and cardiomyocyte ratio in the slide section.

3.4.6 Histological imaging

The slides fixed with Masson Trichome stain were viewed by light microscope, Leica DM 6000 under X10 magnification. Image-J software was used for histological analysis. This was developed by the NIH for low-level processing of digital images. It also has the capability of analysing fibrosis by using an algorithm which was developed by the Shapiro lab group.[79]

3.5 Statistical Methods

Descriptive statistics were performed to determine statistical differences in measurments between M1875T$^{+/+}$ and M1875T$^{+/-}$ mice which included mean and standard deviation (SD) for normally distributed variables and median and interquartile range (IQR) for non-normal distribution pattern. The normal or non-normal distribution was assessed by observing the distribution histogram and also performing the Kolmogorov-Smirnov test. Fot this a p-vale of <0.05 was statistically significant and indicated non-normal distribution pattern. A separate sub-group analysis to assess the effect of SCN5A mutation on the older mice only (age ≥ 24 weeks) was also performed.

For all analysis, the categorical variables were compared using the Chi-square test and continuous variables with Student T test for normally distributed variables and Mann-Whitney U test for non-normally distributed variables. All the statistical analysis was performed using IBM SPSS v25 and the graphs were generated using Graphpad Prism 9.0.0(121).

3.5.1 Inter-observer variability

Random sample IDs for various variables were checked against expert measurements to assess for inter-observer variability. Selected variables like LV internal dimension and LA dimension were observed against another operator and the variability was assessed using Spearman correlation. The variability coefficient or coefficient of determination (r^2) was calculated with a value of 1 meaning perfect linear correlations between the two observations. The observations were graphically represented through a Bland-Altmann's plot.

4 Results

4.1 Baseline data

Age in weeks was measured. In the complete sample 45 (57%) were heterozygous mutants (M1875T$^{+/-}$) and 34 (43%) were wild-type (M1875T$^{+/+}$). M1875T$^{+/+}$ and M1875T$^{+/-}$ mice were weighed before being subjected to the echo protocol. This revealed no significant differences between genotypes. Other subjective parameters were used to assess the general health of the mice that included alertness, mobility, unruffled appearance with smooth fur, no discharge from the eyes and non-humped appearance of the back. The presence of the mutation did not appear to alter the normal growth and general health of the mice when compared to their M1875T$^{+/+}$ littermates. There was no difference in baseline heart rates between the genotypes. Of the total, 48 (61%) were of the FVB background. The baseline analysis for the complete dataset is given in table 4-1.

Table 4-1 Baseline data of the complete cohort (n=79)

Variable	Genotype		P value
	M1875T+/+ (n=34)	M1875T+/- (n=45)	
Age, weeks, median (IQR)	16.5 (14.4-18.2)	16.5 (13.3-33.4)	0.982
Weight, grams, mean (SD)	30.0 (6.1)	30.5 (5.9)	0.747
Heart rate, bpm, mean (SD)	431.1 (40.7)	431.0 (33.5)	0.914
RR Interval, ms, mean (SD)	139 (27.1)	142 (17.9)	0.281
P duration, ms, mean (SD)	15.9 (2.6)	15.2 (3.1)	0.793
PR duration, ms, mean (SD)	38.4 (6.8)	38.1 (8.9)	0.892
QRS duration, ms, mean (SD)	15.4 (2.7)	15.6 (2.9)	0.781

P valiue <0.05 is taken as statistically significant. Mann Whitney U test - Age and Student T test - rest of variables

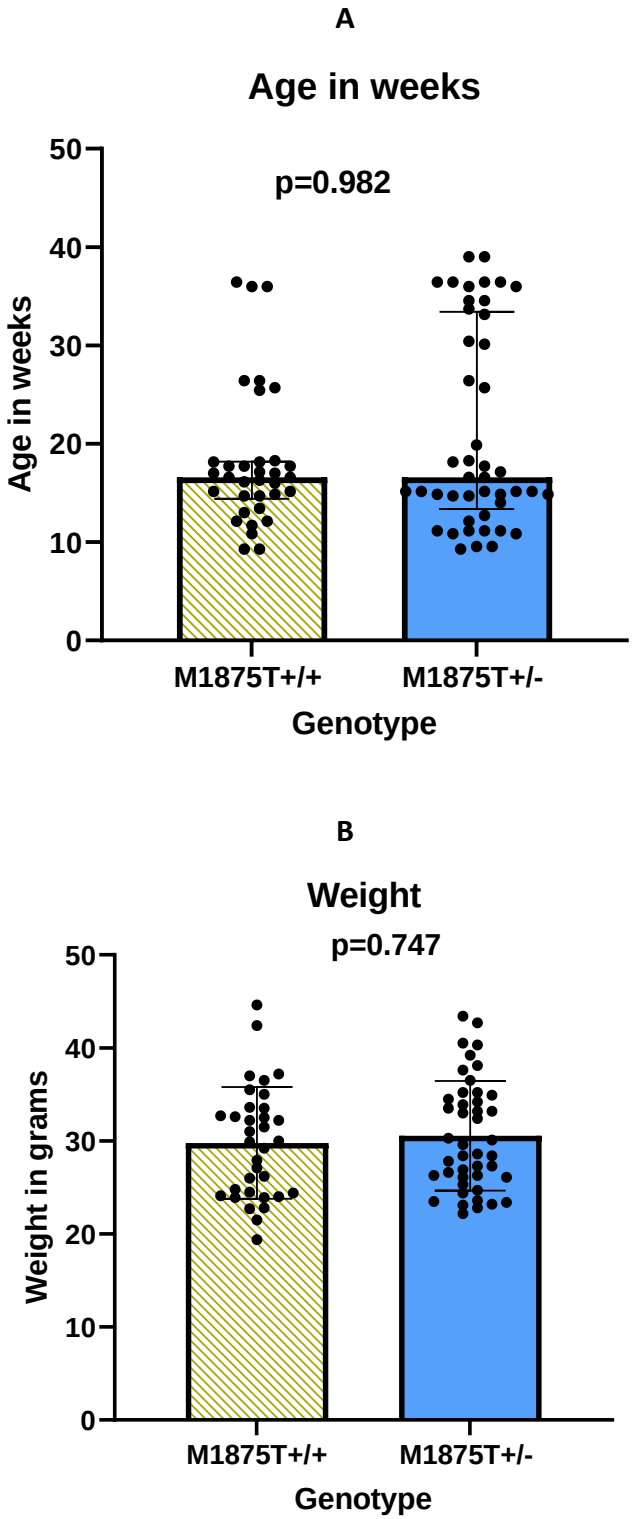

Figure 4-1(A) Complete dataset. Age in weeks, Median (IQR) (B) Body weight in grams, Mean (SD) for M1875T$^{+/+}$ vs M1875T$^{+/-}$ mice (n=79). 34 mice in M1875T+/+ and 45 in M1875T+/- genotype.

Mann-Whitney test is applied for age and Student T test for Weight.

4.2 Echocardiography Results

The results are given in order of representative chambers. In order to assess any changes associated with the M1875T mutation, echocardiography was carried out blinded to genotype cage-wise on M1875T$^{+/+}$ and M1875T$^{+/-}$ mice littermates. This is described for the whole dataset of 79 mice split into the two cohorts. Further statistical analysis was applied to subsets of the data based on age. Mice aged 25 weeks and older were separated from the original dataset and compared to their age-matched counterparts for the respective chambers and calculated values. As mentioned in methods, the split in age was made to assess for any difference manifested as the animal matures.

4.2.1 Echocardiography results for the complete dataset

4.2.1.1 Left ventricular measurements

The table below describes the comparison between left ventricular measured variables for the M1875T$^{+/-}$ and the M1875T$^{+/+}$ mice groups. In general, there were no significant differences in the thickness of the interventricular septum (IVS), left ventricular posterior wall (LVPW), or in terms of the left ventricular internal dimensions (LVID), length and area in systole and diastole.

Table 4-2 Results of the camparison of the LV measurements between M1875T$^{+/+}$ and M1875T$^{+/-}$ mice (n=79) for the complete dataset

Variable	Genotype		P value
	M1875T+/+ (n=34)	M1875T+/- (n=45)	
IVSd, mm, median (IQR)	0.86 (0.72-0.99)	0.91 (0.83-0.99)	0.749
IVSs, mm, median (IQR)	1.10 (1.05-1.38)	1.31 (1.02.1.37)	0.991
LVPWd, mm, median (IQR)	1.00 (0.84-1.11)	0.85 (0.76-1.06)	0.758
LVPWs, mm, median (IQR)	1.37 (1.07-1.54)	1.09 (0.95-1.25)	0.982
LVIDd, mm, median (IQR)	4.10 (3.51-4.37)	4.04 (3.78-4.23)	0.964
LVIDs, mm, median (IQR)	2.93 (2.08-3.41)	2.92 (2.79-3.22)	0.468
LVLd, mm, median (IQR)	6.96 (6.82-7.11)	7.12 (6.98-7.56)	0.109
LVLs, mm, median (IQR)	5.90 (5.49-6.43)	6.13 (6.02-6.36)	0.377
LVAd, mm^2, median (IQR)	22.52 (20.84-24.13)	22.12 (21.81-23.19)	0.945
LVAs, mm^2, median (IQR)	14.93(12.42-16.55)	15.04 (14.26-15.56)	0.549
LVOT diameter, mm, median (IQR)	1.44 (1.36-1.55)	1.45 (1.40-1.50)	0.690

(**IVSd** Interventricular septum in diastole, **LVIDd** Left ventricular internal dimension in diastole, **LVPWd** Left ventricular posterior wall in diastole, **IVSs** Interventricular septum in systole, **LVIDs** Left ventricular internal dimension in systole, **LVPWs** Left ventricular posterior wall in systole, **LVOT** Left V ventricular outflow tract, **LVLd** Left ventricular length in diastole, **LVLs** Left ventricular length in systole, **LVAd** Left ventricular area in diastole, **LVAs** Left ventricular area in systole)
Mann Whitney U test is applied.

4.2.1.2 Left ventricular calculated values

The LV volume was calculated as an objective assessment of LV cavity size using the cylinderal-hemi ellipsoid method formula. The details of formula are described in the introduction section. These measurements were acquired using 2D echocardiography. The table below describes the comparison between left ventricular calculated variables for M1875T$^{+/-}$ and M1875T$^{+/+}$ littermates. There was no difference in the LV cavity volume, stroke volume, ejection fraction or cardiac output.

Table 4-3 Left ventricular calculated values (n=79) for complete dataset

Variable	Genotype		P value
	M1875T+/+ (n=34)	M1875T+/- (n=45)	
LV volume diastole (LVVd), mm^3, median (IQR)	66.74 (58.47-77.39)	69.89(57.94-76.79)	0.964
LV Volume systole (LVVs), mm^3, median (IQR)	30.91 (25.76-43.29)	36.92(26.69-43.60)	0.475
LV Stroke Volume (LVSV), mm^3, median (IQR)	34.99 (27.48-39.21)	32.95(29.09-37.89)	0.465
LV Ejection fraction (LVEF), %, median (IQR)	48.93(44.34-59.72)	48.03(41.90-55.70)	0.392
Cardiac Output (CO), ml/min, median (IQR)	15.18 (11.50-17.77)	14.12(11.91-16.70)	0.648

(**LVVd** Left ventricular volume in diastole, **LVVs** Left ventricular volume in systole, **LVSV** Left ventricular stroke volume, **LVEF** Left ventricular ejection fraction, **CO** Cardiac output) Mann Whitney U test is applied.

4.2.1.3 Right ventricular measurements

Analysable RV views were available for 44 mice. This is this variable was not consistently and reliably recorded for all the mice. Moreover, in some mice the echocardiographic windows did not allow for accurate measurement of this data. The RV area and RVOT diameter were measured to look for any RV dilation associated with this gene defect. RV area was measured in systole and diastole using the PSAX view. The RVOT diameter was measured in the PLAX view. The RV area in systole and diastole was then used to calculate the RV fractional area change.

Interestingly, the data shows a trend towards increased RV diastolic area in M1875T$^{+/+}$ littermates and also fractional area change was slightly reduced in this group. This difference was, however, not statistically significant. This lack of statistical significance may be due to mice number in this analysis.

Table 4-4 Right ventricular measured and calculated parameters (n=44) for complete dataset (This variable only available for 44 mice)

Variable	Genotype		P-value
	M1875T+/+ (n=19)	M1875T +/-(n=25)	
RV area in diastole (RVAd), mm^2, mean (SD)	7.18 (4.50-8.27)	6.45 (5.15-7.33)	0.320
RV area in systole (RVAs), mm^2,mean (SD)	4.10 (3.34-5.01)	4.17 (3.58-5.13)	0.722
RV Outflow Tract diameter in diastole, mm, mean (SD)	1.70- (1.52-1.94)	1.65 (1.50-1.87)	0.594
RVOT diameter in systole, mm, mean (SD)	1.37 (1.27-1.48)	1.42 (1.31-1.51)	0.653
RV fractional area change	38.73 (34.06-42.17)	31.79 (27.91-38.97)	0.112

(**RV** Right ventricle, RVOT Right Ventricular outflow tract)
Student Test is used in comparing variables

4.2.1.4 Left atrial measurements

The left atrial AP dimension was measured in the parasternal view. The LA was significantly foreshortened in the apical views hence this view was not taken for further measurements. There was no significant difference between LA measurements (LA AP dimension) between M1875T$^{+/+}$ and M1875T$^{+/-}$ subgroups.

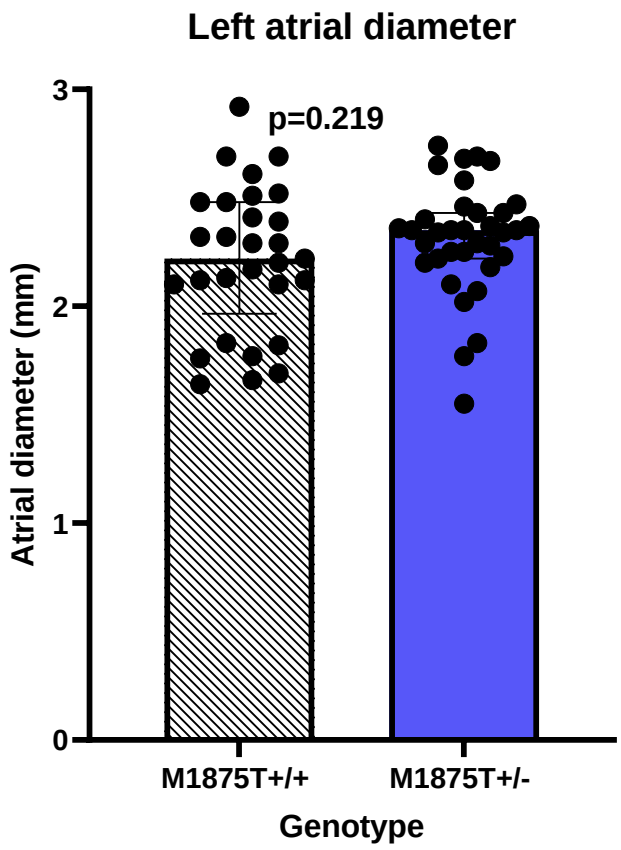

Figure 4-2 Left Atrial diameter measured in atrial diastole (n=72). For complete dataset

31 mice in M1875T+/+ and 41 in M1875T+/- genotype.
Mann-Whitney U Test for non-parametric variables is applied.The bars represent Median (IQR).

4.2.2 Results for mature mice

Subgroup analysis for 23 mice ≥25 weeks up to 40 weeks was performed using LV, RV and LA parameters. As explained above, we carried out this analysis to look for any phenotypic changes that would manifest themselves in slightly older mature mice, while the overall analysis included young adults.

4.2.2.1 Left Ventricular Measurements and Calculations:

The individual values and differences between the mature M1875T$^{+/+}$ and M1875T$^{+/-}$ mice is given in Figure 4-3 to 4-6.

The systolic and diastolic measurements of the IVS, LVID and LVPW, LVOT and aortic annular diameter are described. Moreover, calculated variables like fractional shortening, fractional area change, LV systolic and diastolic volumes, stroke volume, cardiac output and ejection fraction are also included.

Interventricular septum:

There was no statistically signicant difference in IVS measurements for systole and diastole between the M1875T$^{+/-}$ and M1875T$^{+/+}$ groups.

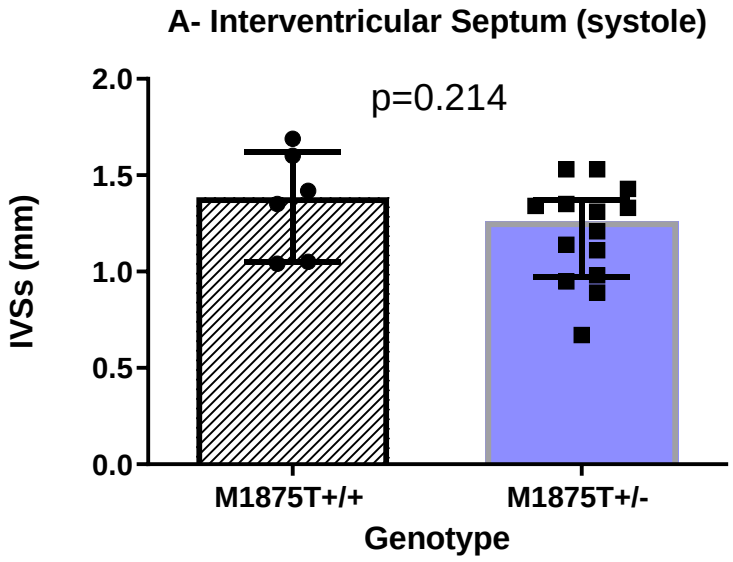

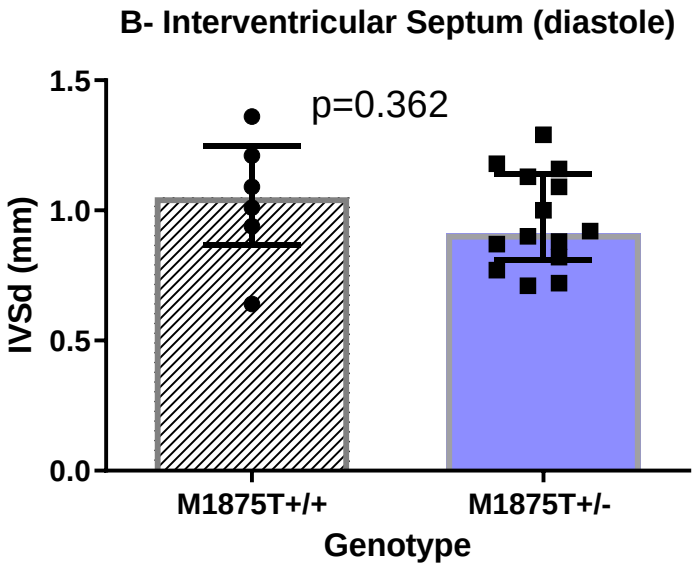

Figure 4-3 Comparison between <u>older</u> M1875T+/+ and M1875T+/- mice for Interventricular septum (IVS) thickness in systole (A) and diastole (B). n=20.

6 mice in M1875T+/+ and 14 in M1875T+/- genotype.

Mann-Whitney Test for non-parametric variables is applied.The bars represent Median (IQR)

Left ventricular internal dimension:

The median (95% CI) for LV internal diameter in systole for M1875T$^{+/+}$ and M1875T$^{+/-}$ was 2.75 (2.62-2.96) and 3.37 (3.31-3.90), p=0.006 and for diastole this 3.85 (3.57-4.75) 4.16 (4.03-4.60) p= 0.012. This indicated larger LV dimensions for the mutant mice .

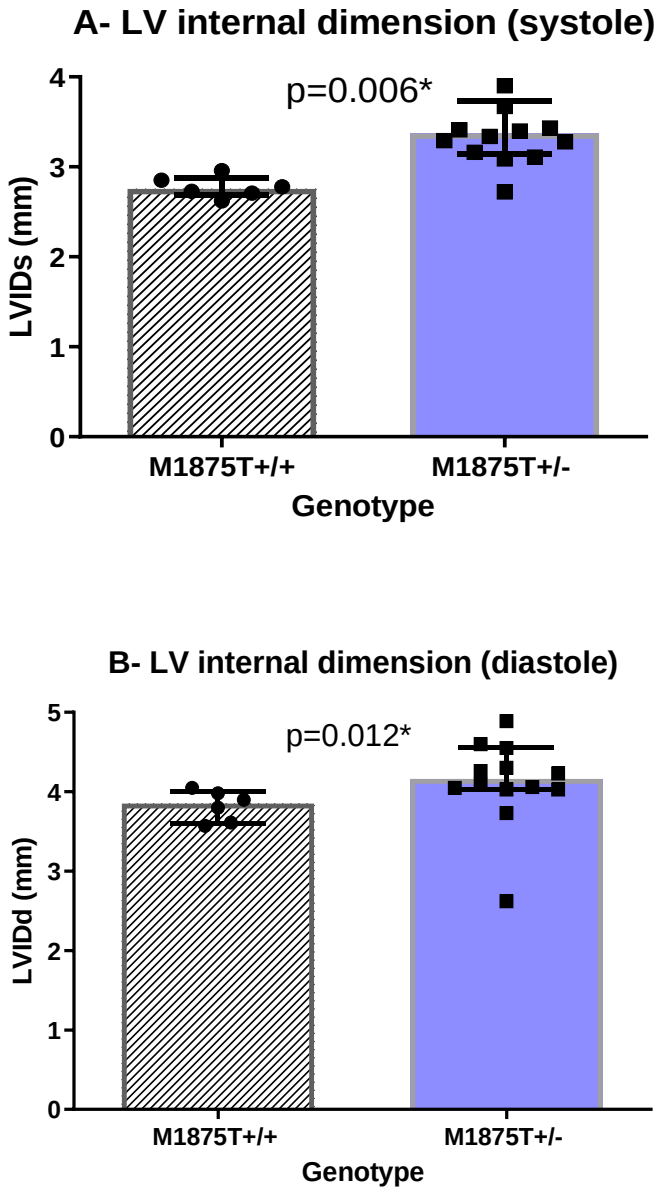

*Figure 4-4 **Comparison between older M1875T+/+ and M1875T+/- mice for left ventricular internal dimension in systole (A) and diastole (B).***

n=18. 6 mice in M1875T+/+ and 12 in M1875T+/- genotype.
The difference is statistically significant with cut off for p value <0.05.

Mann-Whitney Test for non-parametric variables is applied.The bars represent Median (IQR)

Left ventricular posterior wall thickness:

There was no difference in the LV posterior wall thickness for the M1875T$^{+/+}$ and M1875T$^{+/-}$ mice.

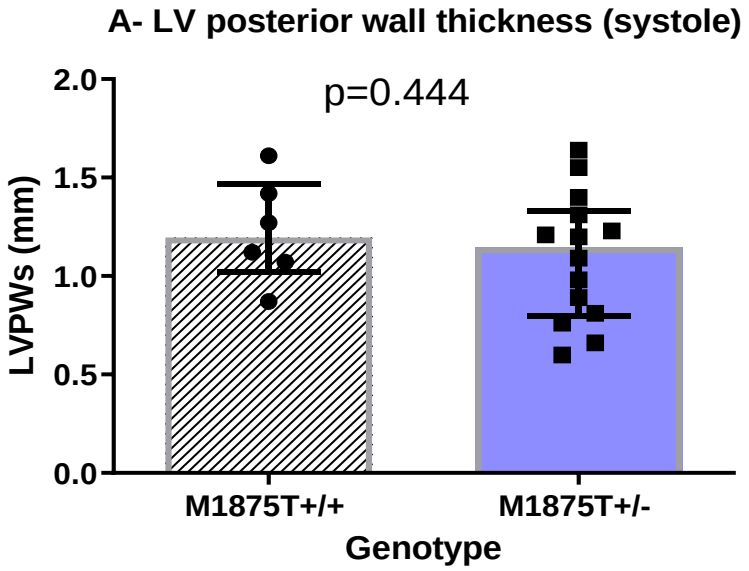

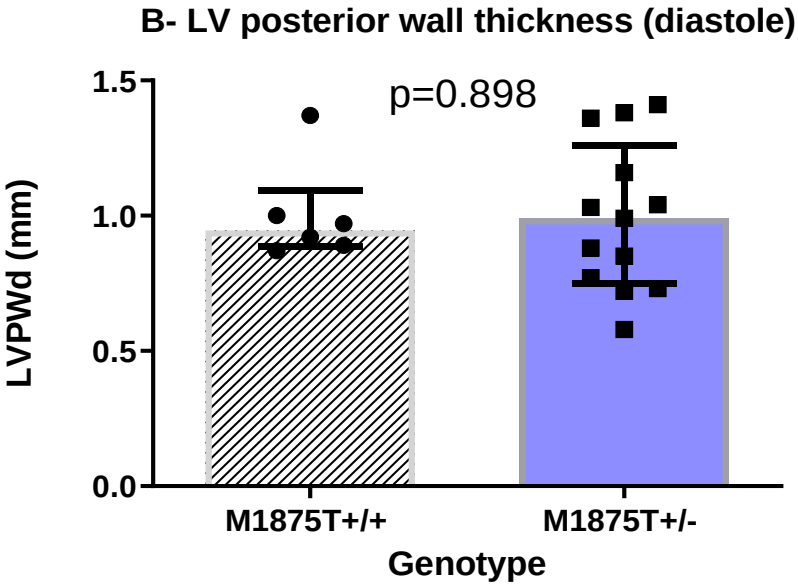

Figure 4-5 Comparison between older M1875T+/+ and M1875T+/- mice for left ventricular posterior wall thickness in systole and diastole.

n=19. 6 mice in M1875T+/+ and 13 in M1875T+/- genotype.
Mann-Whitney Test for non-parametric variables is applied. The bars represent Median (IQR)

Left ventricular endocardial length:

The endocardial length is taken from the mitral valve level to the LV apex. There was no signficant difference in the LV endocardial length for the M1875T$^{+/+}$ and M1875T$^{+/-}$mice in systole or diastole median.

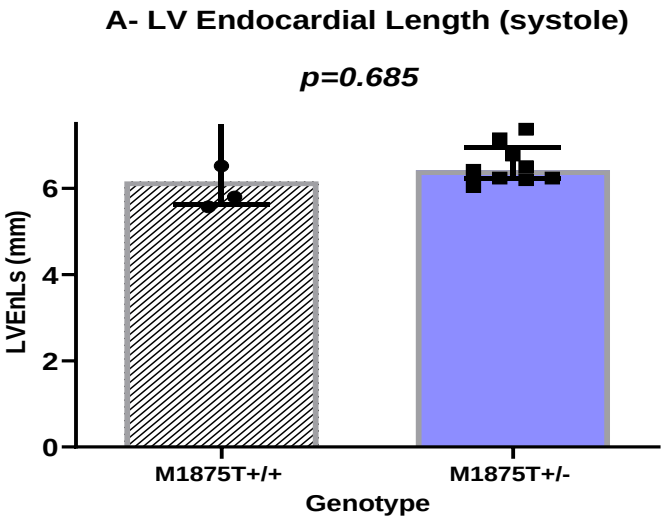

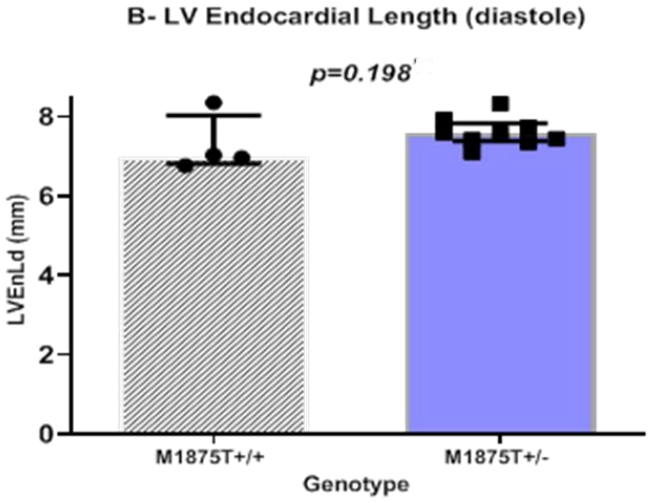

Figure 4-6 Comparison between <u>older</u> M1875T+/+ and M1875T+/- mice for LV endocardial length in systole (A) and diastole (B).

n=18. 5 mice in M1875T+/+ and 13 in M1875T+/- genotype.
Mann-Whitney Test for non-parametric variables is applied. The bars represent Median (IQR)

Aortic Annular diameter:

There was no difference in the aortic annular diameter for the M1875T$^{+/+}$ and M1875T$^{+/-}$ mice.

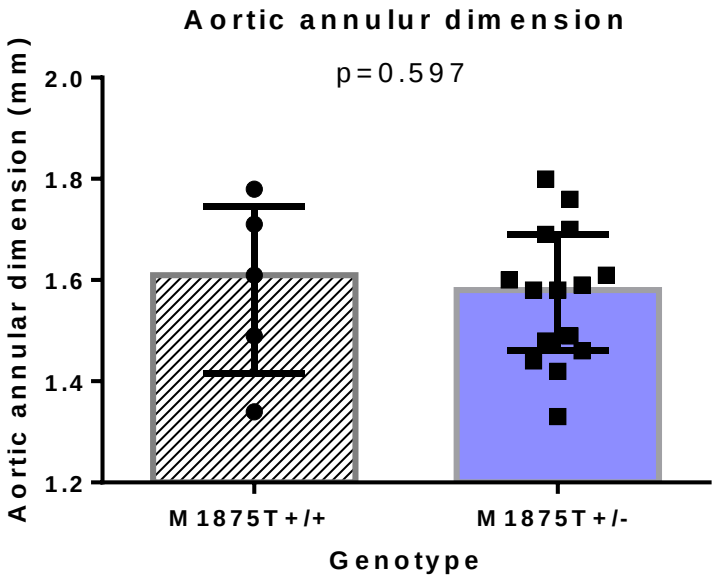

Figure 4-7 Comparison between older M1875T+/+ and M1875T+/- mice for aortic annular diameter.

n=18. 5 mice in M1875T+/+ and 13 in M1875T+/- genotype.
Mann-Whitney Test for non-parametric variables is applied. The bars represent Median (IQR)

LEFT VENTRICULAR CALCULATED PARAMETERS:

The following left ventricular calculated variables were looked at:

1. LV fractional area change
2. LV fractional shortening
3. Left ventricular volumes (in diastole and systole and stroke volumes)
4. LV ejection fraction and cardiac output

LV fractional area change

There was no difference between mature M1875T$^{+/+}$ and M1875T$^{+/-}$ mice for LV fractional area change (figure 4-8).

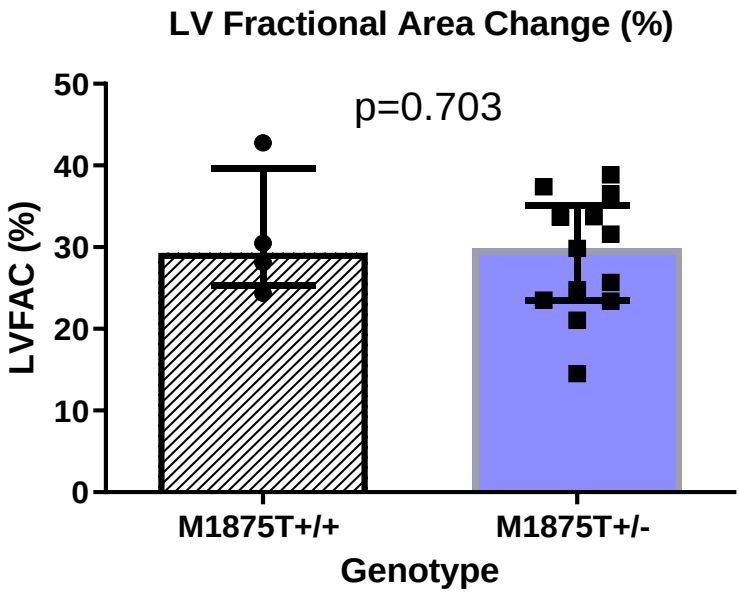

Figure 4-8 Comparison between <u>older</u> M1875T+/+ and M1875T+/- mice for left ventricular fractional area change.

n=18. 4 mice in M1875T+/+ and 14 in M1875T+/- genotype.
Mann-Whitney Test for non-parametric variables is applied. The bars represent Median (IQR)

LV fractional shortening

LV fractional shortnening depends on the LV internal dimension. This was significantly lower in mutant mice with the median (95% CI) for LV fractional shortening in systole for M1875T$^{+/+}$ 26.89 (25.45-27.39) and for M1875T$^{+/-}$ 22.78 (18.84-24.98), p<0.001. This is shown in Figure 4-9.

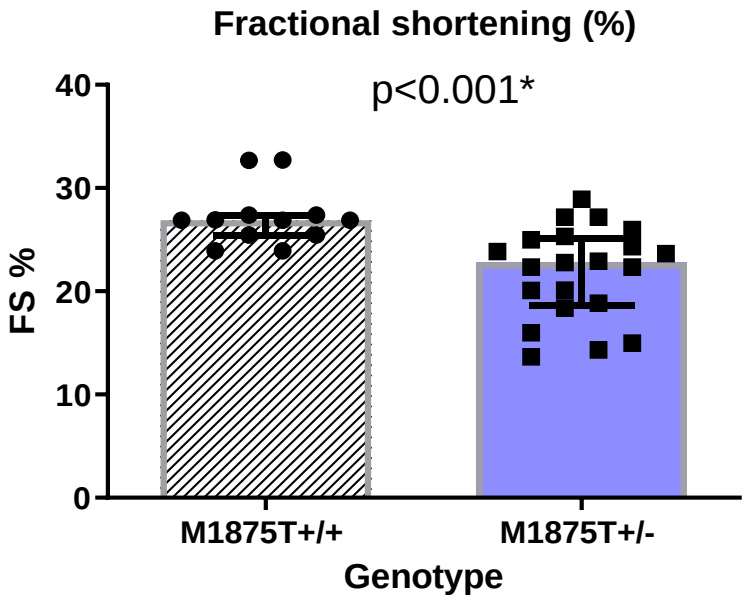

Figure 4-9 Comparison between older M1875T+/+ and M1875T+/- mice for Left Ventricular Fractional shortening.

n=23. 12 mice in M1875T+/+ and 13 in M1875T+/- genotype.
Mann-Whitney Test for non-parametric variables is applied.The bars represent Median (IQR)

LV Volumes

The LV volumes were significantly higher for systole and diastole in the older mutant mice. For systole the median (95% CI) for LV volumes for M1875T$^{+/+}$ and M1875T$^{+/-}$ was 28.30 (25.06-23.97) and 46.38 (38.21-65.74) respectively, p=0.006 (Figure 4-10). For diastole this was 63.89 (53.16-72.05) vs 77.40 (71.42-97.16) respectively, p= 0.002.

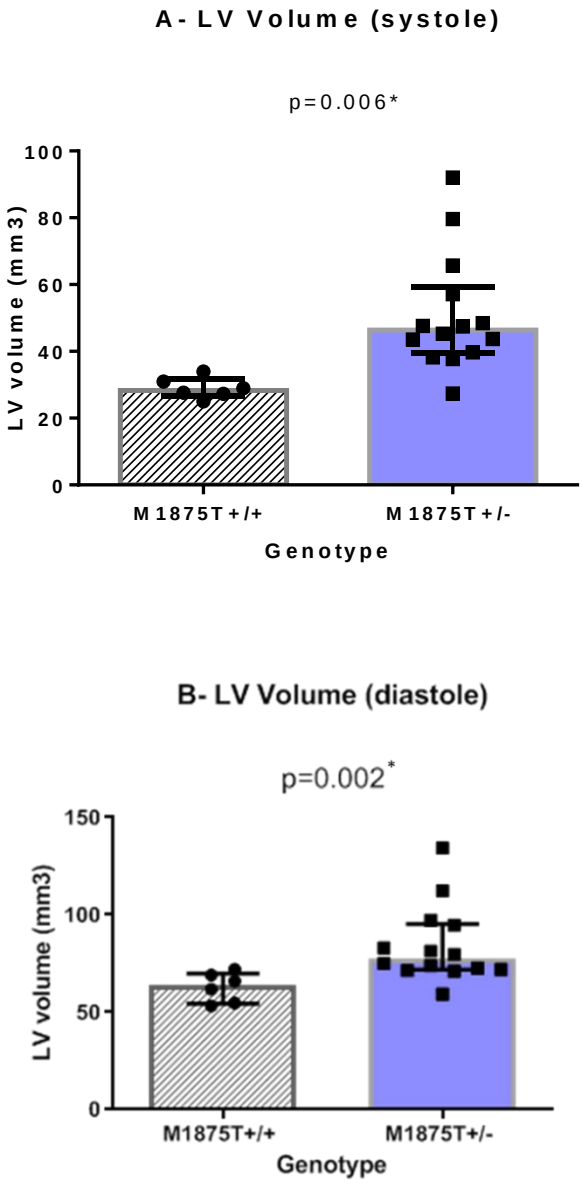

Figure 4-10 Comparison between older M1875T+/+ and M1875T+/- mice for Left Ventricular systolic (A) and diastolic (B) volume.

n=20. 6 mice in M1875T+/+ and 14 in M1875T+/- genotype.
Mann-Whitney Test for non-parametric variables is applied.The bars represent Median (IQR)

There was no difference between the two groups in the LV stroke volumes.

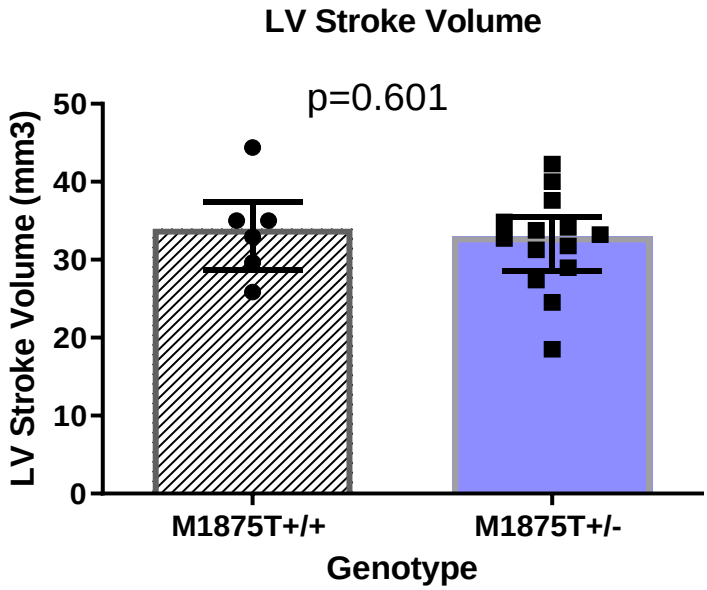

Figure 4-11 Comparison between <u>older</u> M1875T+/+ and M1875T+/- mice for left ventricular stroke volume.

n=20. 6 mice in M1875T+/+ and 14 in M1875T+/- genotype.
Mann-Whitney Test for non-parametric variables is applied.The bars represent Median (IQR)

LV ejection fraction and cardiac output

LV ejection fraction was significantly lower in older mutant mice with the median (95% CI) for LV ejection fraction for $M1875T^{+/+}$ 53% (49-64) and for $M1875T^{+/-}$ 41% (31-48), p=0.006

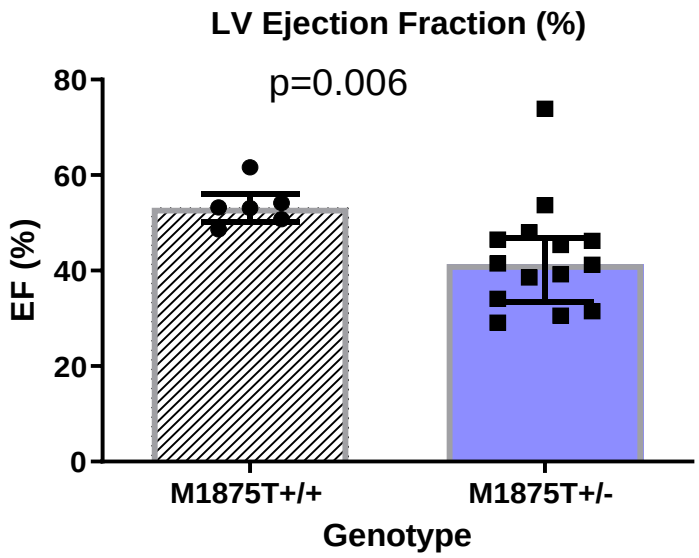

Figure 4-12 Comparison between older M1875T+/+ and M1876T+/- mice for Cardiac Ejection Fraction.

n=20. 6 mice in M1875T+/+ and 14 in M1875T+/- genotype.
Mann-Whitney Test for non-parametric variables is applied.The bars represent Median (IQR)

There was no difference between the two groups for the cardiac output.

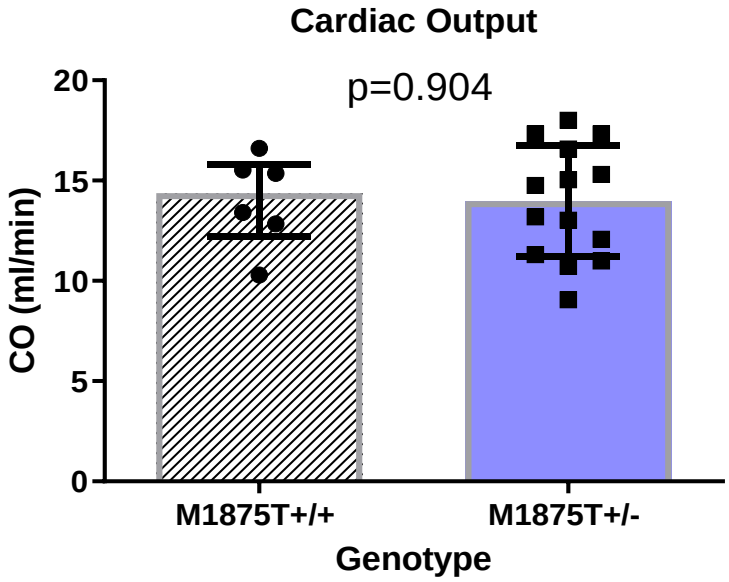

Figure 4-13 Comparison between older M1875T+/+ and M1875T+/- mice for cardiac output.

n=20. 6 mice in M1875T+/+ and 14 in M1875T+/- genotype.
Mann-Whitney Test for non-parametric variables is applied.The bars represent Median (IQR)

4.2.2.2 *Right ventricular and left atrial variables*

Figure 4-14 shows the comparison for right ventricular area between M1875T$^{+/+}$ and M1875T$^{+/-}$ subgroups for mature mice with no significant difference between the two groups.

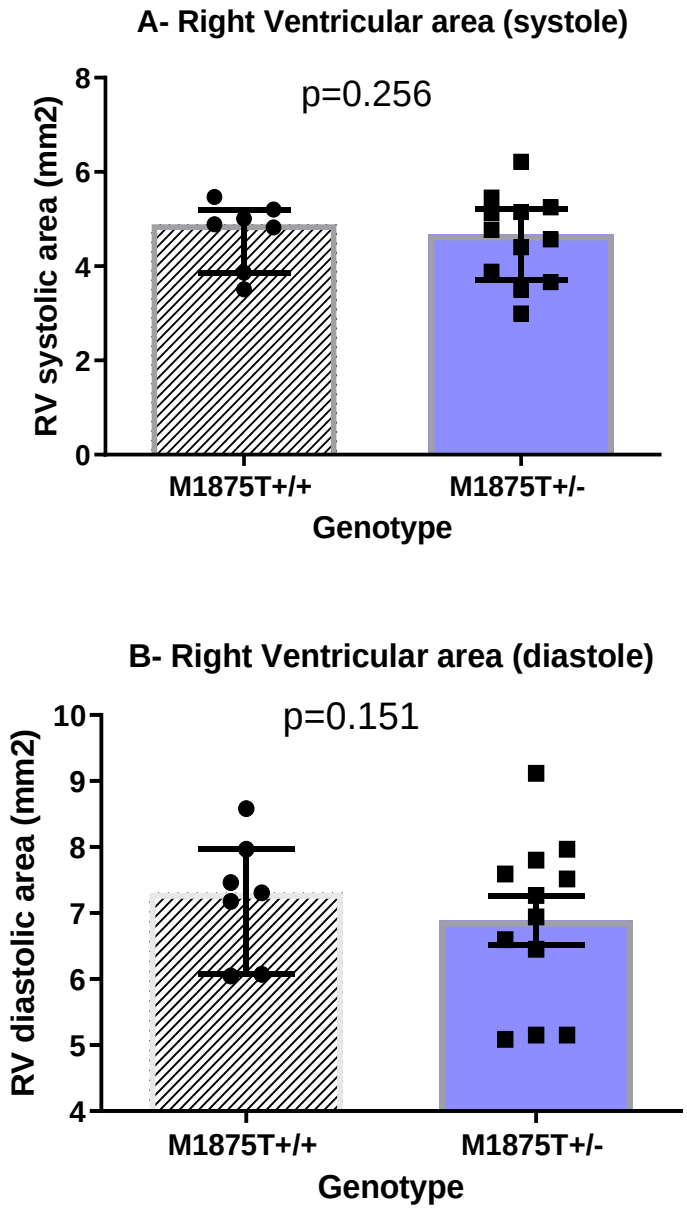

Figure 4-14 Comparison between <u>older</u> M1875T$^{+/+}$ and M1875T$^{+/-}$ mice for right ventricular area in systole (A) and diastole (B) on parasternal short axis view.

Mann-Whitney Test for non-parametric variables is applied.The bars represent Median (IQR)

Left Atrial diameter

There was no significant difference between the older, M1875T$^{+/+}$ and M1875T$^{+/-}$ mice for the LA diameter .

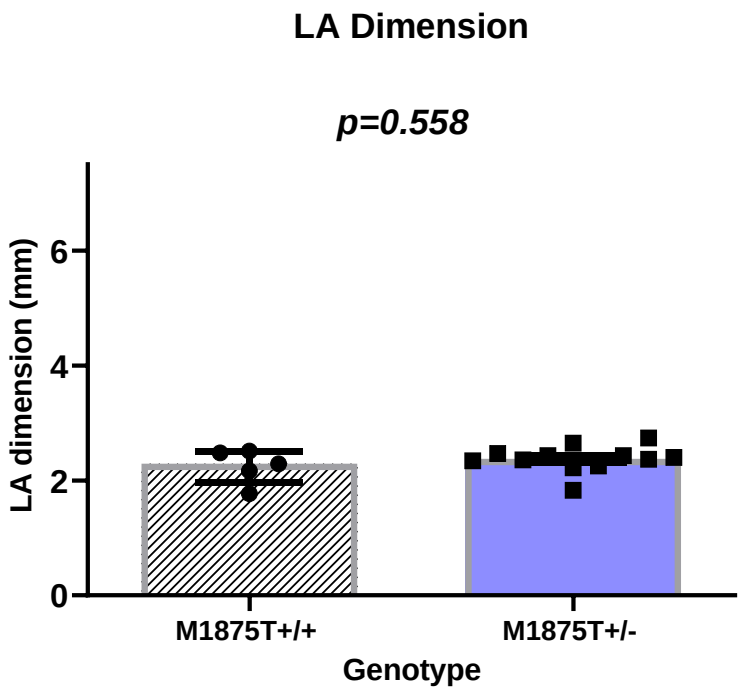

Figure 4-15 Comparison between <u>older</u> M1875T$^{+/+}$ and M1875T$^{+/-}$ mice for left atrial anteroposterior dimension on parasternal long axis view.

Mann-Whitney Test for non-parametric variables is applied.The bars represent Median (IQR)

4.3 Inter-observer variability

There was good correlation between the observed values compared with experts' analysis of the same parameter with r^2 of >70 for all measured parameters.

Figure 3-28 shows the correlation for left ventricular internal diameter in diastole and LV ejection fraction.

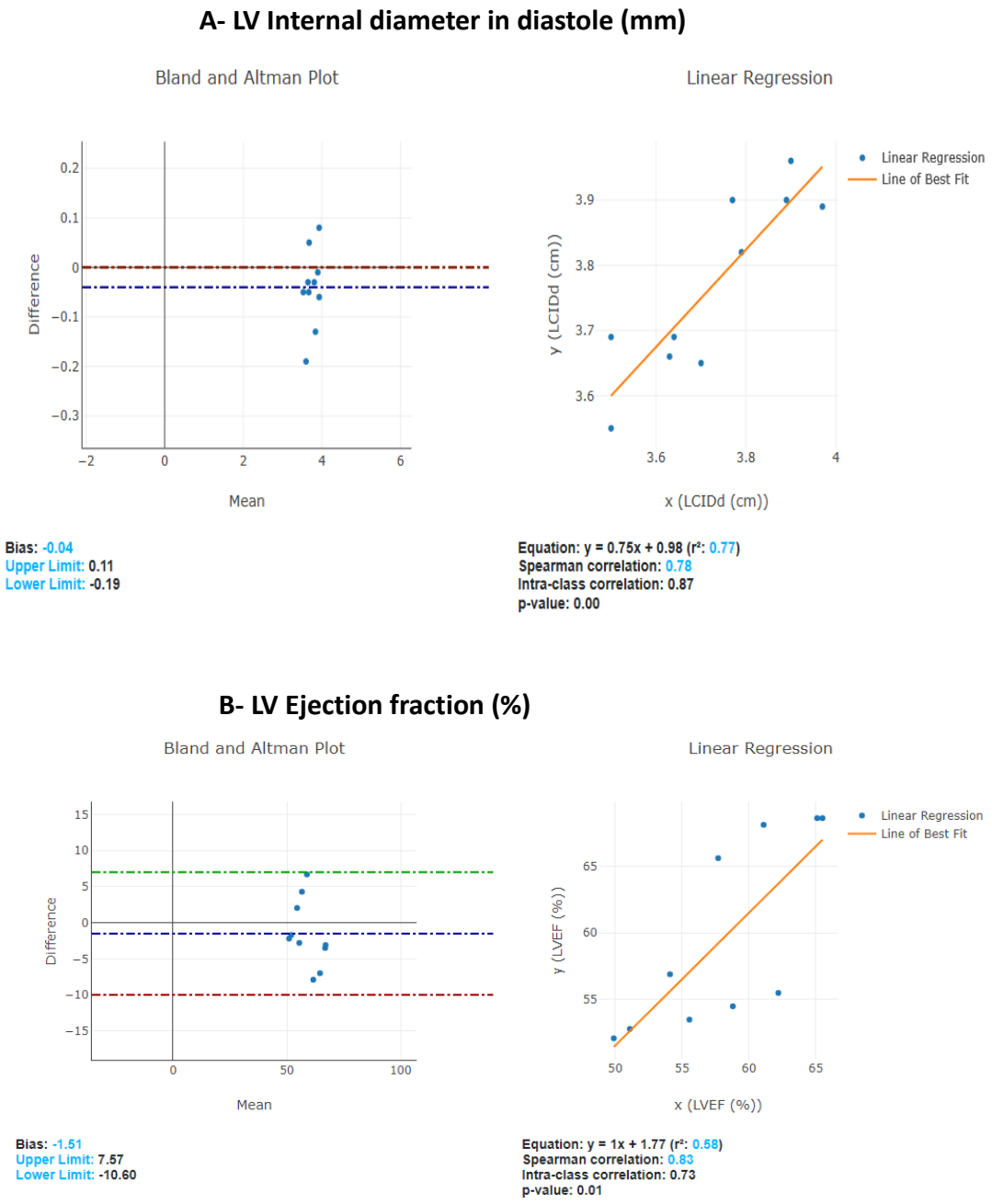

Figure 4-16 Interobserver variability plot for(A) LV internal diameter in diastole and (B) LV ejection fraction (%).

4.4 Preliminary histological results

A complete histological analysis with quantitative analysis was not performed for the complete cohort of mice. However, the histological methods were learnt and light microscopy was performed for a representative sample.

Figure 4-17 and 4-18 show representative left and right ventricles isolated from SCN5A mutants ($M1875T^{+/-}$) and wild-type mice ($M1875T^{+/+}$). These slides are prepared using Masson Trichome stain and the light microscopy was performed at 10x magnification using Leica DM 6000.

Left Ventricle

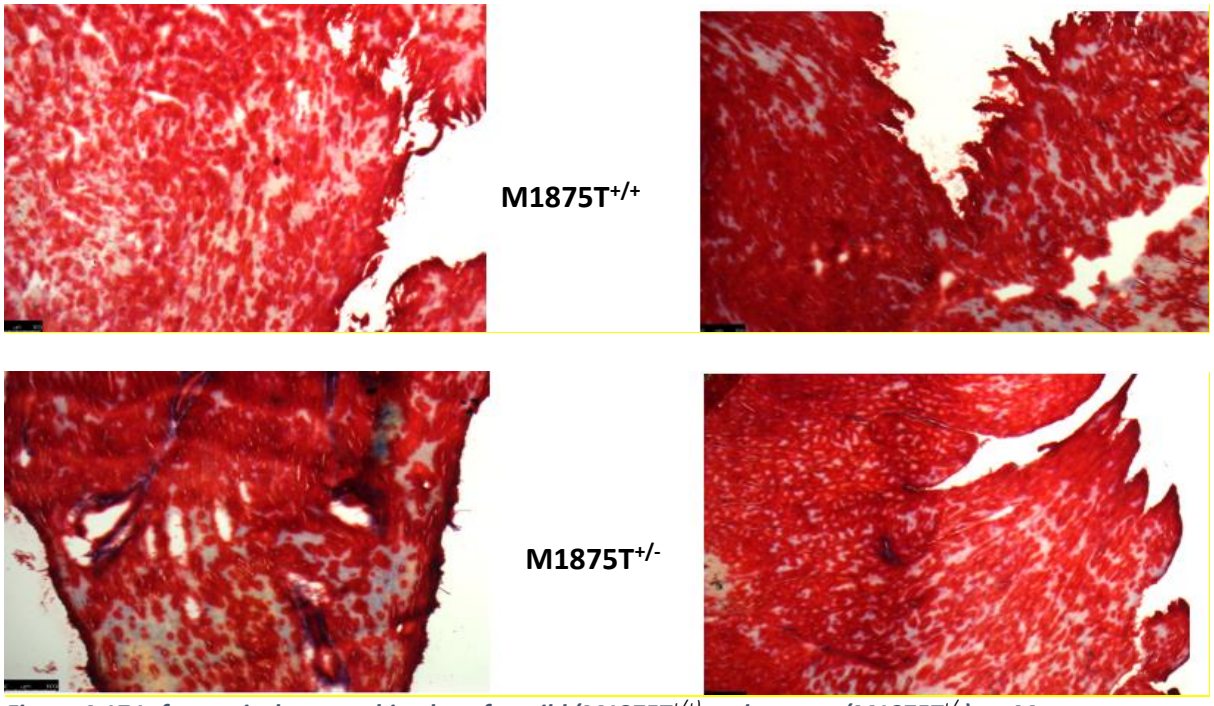

Figure 4-17 Left ventricular gross histology for wild ($M1875T^{+/+}$) and mutant ($M1875T^{+/-}$) on Masson Trichome stain using light microscope Leica DM6000 under 10x Magnification. (Scalebar =100micron).

$M1875T^{+/+}$ Mouse ID 398758(L), 402135(R) ; $M1875T^{+/-}$ ID 402126(L), 402120(R)

Right Ventricle:

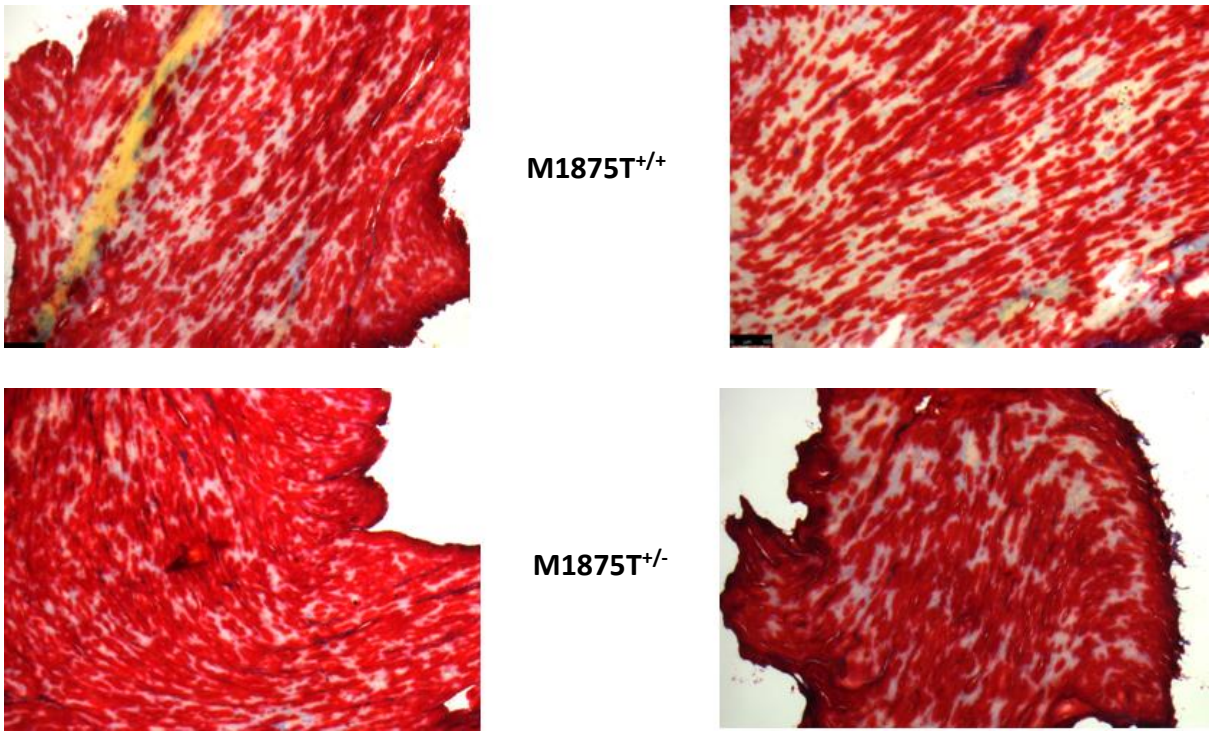

Figure 4-18 Right ventricular gross histology for wild(M1875T+/+) and mutant M1875T+/- on Masson Trichome stain using light microscope Leica DM6000 under 10x Magnification. (Scalebar =100micron).

M1875T$^{+/+}$ Mouse ID 398758(L), 402135(R) ; M1875T$^{+/-}$ ID 402126(L), 402120(R)

5 Discussion

5.1 Previous work

Extensive work has been carried out to study the pathogenesis, progression and response to treatment for various cardiomyopathies in mouse models.[9-13] Echocardiography has been a cornerstone in such work to assess for understanding of phenotypic presentation of such defects and response to treatments and disease modifying factors like exercise. For instance, echocardiography was used to assess preload reducing therapy with nitrates and loop diuretics in genetically altered mice to prevent the phenotypic appearance of Arrhythmogenic Right Ventricular Cardiomyopathy (ARVC).[11] They assessed RV area and volumes in systole and diastole and found that treated heterozygous plakoglobulin-deficient mice did not developed RV dilation.

Similarly other genetic defects like SCN5A mutation are also widely studied for their link with various arrythmias and cardiomyopathies.[14-18] Almost 10 different genetic variations of SCN5A gene are related to cardiac diseases.[19] These mutations may affect the structure, function or both of the Nav1.5 protein in the cell membrane of the cardiomyocytes. So far, various cardiac channelopathies (Brugada syndrome, long QT syndrome, atrial stand still) and cardiomyopathies (dilated cardiomyopathy, arrhythmogenic right ventricular cardiomyopathy) can be related to mutations in this gene.[19] A previous study observed the effect of a heterozygous $Scn5a^{+/-}$ mutation related to Lenegre's disease in aged SV-129 mouse models. These mice had reduced Sodium channel density. However, the channel-gating characteristics were identical. Phenotypically, mice showed ventricular myocardial fibrosis alongside age related

progressive conduction system abnormality. Interestingly this study did not show any effect on LV or RV morphology and systolic or diastolic function.[80] Another study was carried out on a mouse model to assess the effect of heterozygous overexpression of N1325S mutation in Scn5a gene related to long QT syndrome. This also showed extensive myocardial fibsosis on histology and interestingly increased LV end systolic dimension, reduced IVS and LVPW thickness.[81] There was also reduced fractional shortening. Additionally, the histological changes were seen in younger mice before they showed any echocardiographical evidence of impaired cardiac function.

5.2 Significance of echocardiographic findings

There is a previous case series in humans of a family with SCN5A gene mutations but not at the M1875T location showing echocardiographic and cardiac MRI features consistent with cardiomyopathy.[82] As far as we are aware, this is the first work of its kind for echocardiographic assessment of gross morphological changes in mouse heart with the gain of function Scn5agene mutation at the M1875T location as this is a newly designed genetically modified murine model.[55, 83] Previous work has been based on assessment of electrophysiological parameters in the family of patients.[55]

This work highlights that in mice with the Scn5a M1875T gain of function gene defect, there is no significant difference in the whole cohort including mice from all age groups (8-40 weeks). However for mature mice (≥25 to 40 week) there was a significantly higher LV systolic and diastolic dimension and volume for the mice with M1875T+/- mutation. Moreover, these mice had lesser fractional shortening and ejection fraction. This indicates there may be some chronic effect on LV internal dimension and volumes by the M1875T+/- gene defect. Interestingly, prior work on a different Scn5a

overexpression mutation at the N1325S location also showed increased LV dimensions and reduced LV fractional shortening in older mice.[81] It has also been shown in another study that in mouse models the extent of arrhythmogenicity and myocardial fibrosis is dependant upon age.[80] In a case study in humans with a proband and 3 carriers, SCN5A mutation leading to LQT3 syndrome associated with an A1180V cardiac sodium channel showed no effect on cardiac structure on function in echocardiography.[84] Finally, analysis of the left atrium and right ventricular size did not reveal any significant differences between the two group in our work.

Broadly the effect of Scn5a mutation on cardiac function is not consistent and in some case there is no effect. Our study shows that there may be an association between this mutation and LV size and function. This effect was seen in older mice ≥25 weeks. Although the mouse numbers were small for this age group but a definite trend was observed and this needs to be verified in larger studies.

In summary, our studies of structure and function effects of this familial M1875T+/- mutation in a newly designed M1875T knock-in murine disease model suggest chronic effects of the mutations on left ventricular size and function and therefore suggest further phenotyping at mature age, including electrophysiological phenotyping and arrhythmia testing.

5.3 Strengths

5.3.1 Inter-observer Reproducibility

A strength of this work is the inter-observer reproducibility of its findings. This was assessed by comparing the measurements obtained during experiments (SA) by those from an expert operator (LF).

5.3.2 Novelty of work

As mentioned previously, this work is the first of its kind assessing the effect on cardiac structure and function for the M1875T+/- Scn5 gene defect in newly designed murine model. The current work needs to be followed up with higher sample size in mature mice to confirm or refute this hypothesis of this gene defect associated with any echocardiographic change in mouse heart.

5.4 Limitations

5.4.1 Chamber size quantification and histology:

The highest precision and statistical power was reached for LV measurements. Any LA dilation might not be evenly distributed because of its asymmetrical shape. It may not dilate in the anteroposterior dimension as easily as it does in other dimensions. For this work, our measurements based on the long and short parasternal axis views. We set up the methodology for 3D echocardiography for this model, but future experiments will gather data from sufficient numbers for analysis.

In the time available, it was possible to establish histological and 3D echo methods for this model, but due to time and access restrictions in 2020, further histological quantitative analysis was not possible. We expect to see myocardial fibrosis and elongation of cardiomyocytes based on the evidence from other experiments.[80] We suggest that this alongside 3D echo experiments should be concidered for future work.

5.4.2 Specialised Doppler-echocardiography measurements:

There are other specialised features of cardiac ultrasound, some recent use of speckle tracking and strain measurements to assess LV systolic and diastolic function in patients

that have shown good promise but are quite specialised and require advanced echocardiography equipment, relevant software modules and expertise for the operator.[26, 27] They have not been validated in murine models and this is beyond the scope of this work.

5.4.3 Sample size:

Although a total sample size of 79 is reasonable for such an experiment, a higher sample size between subgroups in the future will give more power to e.g. discern between different background strains, sex and to investigate subtle differences in atrial size and function.

Statistics were not adapted for multiple measurements as some measurements were mostly assessed to confirm controlled conditions and reproducibility of the investigation like heart rate, weight, aortic size etc.

Experiments could have focussed on a specific strain of mice, like FVB or SV-129 which would have provided more consistency in the results and removed variations seen due to mice strain. In future, with prospective planning, experiments could be planned to mitigate this issue.

5.4.4 Effect of disease modifying factors:

Various disease modifying factors can have a small but relevant affect on the observations. [47]These include:

a. **Variation of phenotype expression:**

Subjects with the same genetic defect may show different variations in the disease presentation which depends on a complex bio-physical interaction with the animal's

phenotype. It is seen that family member's with the same genetic defect may have different expression of the disease process.[85] This phenomenon could have an effect on these results, although this is less likely in an inbred murine strain. Differences between the two background strains could however lead to changes in phenotypic expression.[86]

b. Age and Sex

Kyndt *et al* previously showed that sex can lead to differences in the variation of phenotype with the same genetic defect.[87] Probst *et al* later showed modulation of phenotype with age.[74] This could have an effect on the findings in our work. For this reason the analysis was separately done in mice ≥25 weeks. In order to investigate effects of sex, more n are needed in the future.

5.4.5 Differences in physiology of mouse and human heart

Previous work has shown that there are certain physiological differences between mouse and human heart, like differences in heart rate, electrical conduction and composition of the key proteins of cardiomyocytes. All of these factors can contribute to the pathophysiological variation or difference in the expression of phenotype due to of seemingly similar gene alterations between mouse and human hearts.[88, 89]

Moreover, sedentary life style of laboratory mice can not be ignored as a distinctive factor from humans.[88]

5.5 Future work

5.5.1 Advanced echocardiography techniques

Future work could involve assessment of cardiac chamber size and functional assessment using advanced modialites like 3D echo and strain. This would alse give an

opportunity to compare results obtained from current methods. Feasibility of 3D echo was done during this study. It was found that for a trained echo operator, 3D echo requires minimal further training and the time for experiments was kept within an hour.

5.5.2 Combining echocardiographic findings with histology, molecular analysis and patch clamping

With increased numbers, further experiments can be designed to link echocardiographic findings with any histolical variations across the genotypes. This would help understand the microscopic phenotype that leads to gross macroscopic findings as per the echocardiography. Furthermore, experiments like protein characterization and patch clamping can provide additional proof to relate the phenotypic changes brought by certain genetic alterations.

5.5.3 Experiments on a single background strain

It is suggested that further similar work is done on more mice from same background strain, either FVB or SV129 to reduce the phenotypic variations on the same genetic mutation. This will also lead to less variation in the size and weight of the mice and any effects of the background on Nav1.5 function.

6 References

1. Girolami F, Frisso G, Benelli M, et al. Contemporary genetic testing in inherited cardiac disease: tools, ethical issues, and clinical applications. J Cardiovasc Med (Hagerstown) 2018;19:1-11.
2. Cecchi F, Tomberli B, Olivotto I. Clinical and molecular classification of cardiomyopathies. Glob Cardiol Sci Pract 2012;2012:4.
3. Behere SP, Weindling SN. Inherited arrhythmias: The cardiac channelopathies. Ann Pediatr Cardiol 2015;8:210-20.
4. Recchia FA, Lionetti V. Animal models of dilated cardiomyopathy for translational research. Vet Res Commun 2007;31 Suppl 1:35-41.
5. Milani-Nejad N, Janssen PM. Small and large animal models in cardiac contraction research: advantages and disadvantages. Pharmacol Ther 2014;141:235-49.
6. Camacho P, Fan H, Liu Z, et al. Small mammalian animal models of heart disease. Am J Cardiovasc Dis 2016;6:70-80.
7. Rai V, Sharma P, Agrawal S, et al. Relevance of mouse models of cardiac fibrosis and hypertrophy in cardiac research. Mol Cell Biochem 2017;424:123-145.
8. Papadimitriou D, Xanthos T, Dontas I, et al. The use of mice and rats as animal models for cardiopulmonary resuscitation research. Lab Anim 2008;42:265-76.
9. Ellawindy A, Satoh K, Sunamura S, et al. Rho-Kinase Inhibition During Early Cardiac Development Causes Arrhythmogenic Right Ventricular Cardiomyopathy in Mice. Arterioscler Thromb Vasc Biol 2015;35:2172-84.
10. Moreth K, Afonso LC, Fuchs H, et al. High throughput phenotyping of left and right ventricular cardiomyopathy in calcineurin transgene mice. Int J Cardiovasc Imaging 2015;31:669-79.
11. Fabritz L, Hoogendijk MG, Scicluna BP, et al. Load-reducing therapy prevents development of arrhythmogenic right ventricular cardiomyopathy in plakoglobin-deficient mice. J Am Coll Cardiol 2011;57:740-50.
12. Kirchhof P, Fabritz L, Zwiener M, et al. Age- and training-dependent development of arrhythmogenic right ventricular cardiomyopathy in heterozygous plakoglobin-deficient mice. Circulation 2006;114:1799-806.
13. Pashmforoush M, Pomies P, Peterson KL, et al. Adult mice deficient in actinin-associated LIM-domain protein reveal a developmental pathway for right ventricular cardiomyopathy. Nat Med 2001;7:591-7.
14. Brugada J, Campuzano O, Arbelo E, et al. Present Status of Brugada Syndrome: JACC State-of-the-Art Review. J Am Coll Cardiol 2018;72:1046-1059.
15. Crotti L, Spazzolini C, Schwartz PJ, et al. The common long-QT syndrome mutation KCNQ1/A341V causes unusually severe clinical manifestations in patients with different ethnic backgrounds: toward a mutation-specific risk stratification. Circulation 2007;116:2366-75.
16. Hermida J-S, Lemoine J-L, Aoun FB, et al. Prevalence of the brugada syndrome in an apparently healthy population. The American journal of cardiology 2000;86:91-94.
17. Martin CA, Zhang Y, Grace AA, et al. In vivo studies of Scn5a+/- mice modeling Brugada syndrome demonstrate both conduction and repolarization abnormalities. J Electrocardiol 2010;43:433-9.
18. Moreau A, Chahine M. A New Cardiac Channelopathy: From Clinical Phenotypes to Molecular Mechanisms Associated With Nav1.5 Gating Pores. Front Cardiovasc Med 2018;5:139.

19. Zaklyazminskaya E, Dzemeshkevich S. The role of mutations in the SCN5A gene in cardiomyopathies. Biochim Biophys Acta 2016;1863:1799-805.
20. Liu X, Francis R, Kim AJ, et al. Interrogating congenital heart defects with noninvasive fetal echocardiography in a mouse forward genetic screen. Circ Cardiovasc Imaging 2014;7:31-42.
21. Channer K, Robertson E. Echocardiography or cardiac catheterisation--a comparison of risks, benefits and costs. Health Trends 1991;23:141-4.
22. Youn HJ, Rokosh G, Lester SJ, et al. Two-dimensional echocardiography with a 15-MHz transducer is a promising alternative for in vivo measurement of left ventricular mass in mice. J Am Soc Echocardiogr 1999;12:70-5.
23. Suehiro K, Takuma S, Cardinale C, et al. Assessment of segmental wall motion abnormalities using contrast two-dimensional echocardiography in awake mice. Am J Physiol Heart Circ Physiol 2001;280:H1729-35.
24. Kiatchoosakun S, Restivo J, Kirkpatrick D, et al. Assessment of left ventricular mass in mice: comparison between two-dimensional and m-mode echocardiography. Echocardiography 2002;19:199-205.
25. Nakamura Y, Yoshiyama M, Omura T, et al. Transmitral inflow pattern assessed by Doppler echocardiography in angiotensin II type 1A receptor knockout mice with myocardial infarction. Circ J 2002;66:192-6.
26. Wang G, Zhang L, Ruan L, et al. Speckle tracking echocardiography assessment of global and regional contraction dysfunction in the mice model of pressure overload. J Huazhong Univ Sci Technolog Med Sci 2015;35:271-277.
27. Li Z, Li Y, Zhang L, et al. Reduced Myocardial Reserve in Young X-Linked Muscular Dystrophy Mice Diagnosed by Two-Dimensional Strain Analysis Combined with Stress Echocardiography. J Am Soc Echocardiogr 2017;30:815-827 e9.
28. Brigden W. Uncommon myocardial diseases: the non-coronary cardiomyopathies. Lancet 1957;273:1243-9.
29. Goodwin JF, Gordon H, Hollman A, et al. Clinical aspects of cardiomyopathy. Br Med J 1961;1:69-79.
30. Report of the WHO/ISFC task force on the definition and classification of cardiomyopathies. Br Heart J 1980;44:672-3.
31. Elliott P, Andersson B, Arbustini E, et al. Classification of the cardiomyopathies: a position statement from the European Society Of Cardiology Working Group on Myocardial and Pericardial Diseases. Eur Heart J 2008;29:270-6.
32. Pinto YM, Elliott PM, Arbustini E, et al. Proposal for a revised definition of dilated cardiomyopathy, hypokinetic non-dilated cardiomyopathy, and its implications for clinical practice: a position statement of the ESC working group on myocardial and pericardial diseases. Eur Heart J 2016;37:1850-8.
33. Marcus FI, McKenna WJ, Sherrill D, et al. Diagnosis of arrhythmogenic right ventricular cardiomyopathy/dysplasia: proposed modification of the Task Force Criteria. Eur Heart J 2010;31:806-14.
34. Orie JE, Liedtke AJ. Cardiomyopathy. 2. Hypertrophic and restrictive/obliterative types. Postgrad Med 1986;79:95-106.
35. Mamedova FA. [Characteristics of cardiac hemodynamics and right ventricular function in patients with various types of cardiomyopathy and ischemic heart disease]. Kardiologiia 1989;29:70-3.
36. Jonkaitiene R, Mizariene V. [Arrhythmogenic dilated cardiomyopathy]. Medicina (Kaunas) 2003;39:673-6.
37. Luk A, Ahn E, Soor GS, et al. Dilated cardiomyopathy: a review. J Clin Pathol 2009;62:219-25.

38. Afonso LC, Bernal J, Bax JJ, et al. Echocardiography in hypertrophic cardiomyopathy: the role of conventional and emerging technologies. JACC Cardiovasc Imaging 2008;1:787-800.
39. Geske JB, Ommen SR, Gersh BJ. Hypertrophic Cardiomyopathy: Clinical Update. JACC Heart Fail 2018;6:364-375.
40. Muchtar E, Blauwet LA, Gertz MA. Restrictive Cardiomyopathy: Genetics, Pathogenesis, Clinical Manifestations, Diagnosis, and Therapy. Circ Res 2017;121:819-837.
41. Kaski JP, Syrris P, Burch M, et al. Idiopathic restrictive cardiomyopathy in children is caused by mutations in cardiac sarcomere protein genes. Heart 2008;94:1478-84.
42. Duru F, Hauer RNW. Multiple facets of arrhythmogenic cardiomyopathy: the Fuwai classification of a unique disease based on clinical features, histopathology, and genotype. Eur Heart J 2019;40:1704-1706.
43. Wu L, Bao J, Liang E, et al. Atrial involvement in arrhythmogenic right ventricular cardiomyopathy patients referred for ventricular arrhythmias ablation. J Cardiovasc Electrophysiol 2018;29:1388-1395.
44. Sen-Chowdhry S, Syrris P, Ward D, et al. Clinical and genetic characterization of families with arrhythmogenic right ventricular dysplasia/cardiomyopathy provides novel insights into patterns of disease expression. Circulation 2007;115:1710-20.
45. Abriel H, Zaklyazminskaya EV. A modern approach to classify missense mutations in cardiac channelopathy genes. Circ Cardiovasc Genet 2012;5:487-9.
46. Wilde AAM, Amin AS. Clinical Spectrum of SCN5A Mutations: Long QT Syndrome, Brugada Syndrome, and Cardiomyopathy. JACC Clin Electrophysiol 2018;4:569-579.
47. Remme CA. Cardiac sodium channelopathy associated with SCN5A mutations: electrophysiological, molecular and genetic aspects. J Physiol 2013;591:4099-116.
48. Steiner R, Makarovic S, Makarovic Z, et al. Brugada syndrome and right ventricle morphofunctional abnormalities on echocardiography in young male with family anamnesis of sudden cardiac death. Coll Antropol 2014;38:363-6.
49. Wilde AA, Antzelevitch C, Borggrefe M, et al. Proposed diagnostic criteria for the Brugada syndrome: consensus report. Circulation 2002;106:2514-9.
50. Medeiros-Domingo A, Kaku T, Tester DJ, et al. SCN4B-encoded sodium channel beta4 subunit in congenital long-QT syndrome. Circulation 2007;116:134-42.
51. Schwartz PJ, Crotti L, Insolia R. Long-QT syndrome: from genetics to management. Circ Arrhythm Electrophysiol 2012;5:868-77.
52. Zareba W. Genotype-specific ECG patterns in long QT syndrome. J Electrocardiol 2006;39:S101-6.
53. Goldenberg I, Moss AJ. Long QT Syndrome. Journal of the American College of Cardiology 2008;51:2291-2300.
54. Perez-Riera AR, Barbosa-Barros R, Daminello Raimundo R, et al. The congenital long QT syndrome Type 3: An update. Indian Pacing Electrophysiol J 2018;18:25-35.
55. Makiyama T, Akao M, Shizuta S, et al. A novel SCN5A gain-of-function mutation M1875T associated with familial atrial fibrillation. J Am Coll Cardiol 2008;52:1326-34.
56. Lang RM, Badano LP, Mor-Avi V, et al. Recommendations for cardiac chamber quantification by echocardiography in adults: an update from the American Society of Echocardiography and the European Association of Cardiovascular Imaging. Eur Heart J Cardiovasc Imaging 2015;16:233-70.
57. Vinhas M, Araujo AC, Ribeiro S, et al. Transthoracic echocardiography reference values in juvenile and adult 129/Sv mice. Cardiovasc Ultrasound 2013;11:12.
58. Tanaka N, Dalton N, Mao L, et al. Transthoracic echocardiography in models of cardiac disease in the mouse. Circulation 1996;94:1109-17.

59. Cheng HW, Fisch S, Cheng S, et al. Assessment of right ventricular structure and function in mouse model of pulmonary artery constriction by transthoracic echocardiography. J Vis Exp 2014:e51041.
60. Kohut A, Patel N, Singh H. Comprehensive Echocardiographic Assessment of the Right Ventricle in Murine Models. J Cardiovasc Ultrasound 2016;24:229-238.
61. Abhayaratna WP, Seward JB, Appleton CP, et al. Left atrial size: physiologic determinants and clinical applications. J Am Coll Cardiol 2006;47:2357-63.
62. Tsang TS, Abhayaratna WP, Barnes ME, et al. Prediction of cardiovascular outcomes with left atrial size: is volume superior to area or diameter? J Am Coll Cardiol 2006;47:1018-23.
63. Fabritz L, Kirchhof P, Fortmuller L, et al. Gene dose-dependent atrial arrhythmias, heart block, and brady-cardiomyopathy in mice overexpressing A(3) adenosine receptors. Cardiovasc Res 2004;62:500-8.
64. Ujino K, Barnes ME, Cha SS, et al. Two-dimensional echocardiographic methods for assessment of left atrial volume. Am J Cardiol 2006;98:1185-8.
65. Badano LP, Miglioranza MH, Mihaila S, et al. Left Atrial Volumes and Function by Three-Dimensional Echocardiography: Reference Values, Accuracy, Reproducibility, and Comparison With Two-Dimensional Echocardiographic Measurements. Circ Cardiovasc Imaging 2016;9.
66. Schneider M, Binder T. Echocardiographic evaluation of the right heart. Wien Klin Wochenschr 2018;130:413-420.
67. Ling LF, Obuchowski NA, Rodriguez L, et al. Accuracy and interobserver concordance of echocardiographic assessment of right ventricular size and systolic function: a quality control exercise. J Am Soc Echocardiogr 2012;25:709-13.
68. Forfia PR, Fisher MR, Mathai SC, et al. Tricuspid annular displacement predicts survival in pulmonary hypertension. Am J Respir Crit Care Med 2006;174:1034-41.
69. McLeod CJ, Bos JM, Theis JL, et al. Histologic characterization of hypertrophic cardiomyopathy with and without myofilament mutations. Am Heart J 2009;158:799-805.
70. Rakowski H, Carasso S. Diastolic dysfunction and histopathology in hypertrophic cardiomyopathy: is relaxation in disarray? J Am Soc Echocardiogr 2009;22:1335-7.
71. Radu RI, Bold A, Pop OT, et al. Histological and immunohistochemical changes of the myocardium in dilated cardiomyopathy. Rom J Morphol Embryol 2012;53:269-75.
72. Mali P, Yang L, Esvelt KM, et al. RNA-guided human genome engineering via Cas9. Science 2013;339:823-6.
73. Thomas KR, Capecchi MR. Site-directed mutagenesis by gene targeting in mouse embryo-derived stem cells. Cell 1987;51:503-12.
74. Probst V, Kyndt F, Potet F, et al. Haploinsufficiency in combination with aging causes SCN5A-linked hereditary Lenègre disease. J Am Coll Cardiol 2003;41:643-52.
75. Harkness A, Ring L, Augustine DX, et al. Normal reference intervals for cardiac dimensions and function for use in echocardiographic practice: a guideline from the British Society of Echocardiography. Echo Res Pract 2020;7:X1.
76. Lang RM, Badano LP, Mor-Avi V, et al. Recommendations for cardiac chamber quantification by echocardiography in adults: an update from the American Society of Echocardiography and the European Association of Cardiovascular Imaging. J Am Soc Echocardiogr 2015;28:1-39 e14.
77. Chen G, Li Y, Tian J, et al. Application of echocardiography on transgenic mice with cardiomyopathies. Biochem Res Int 2012;2012:715197.
78. Gao S, Ho D, Vatner DE, et al. Echocardiography in Mice. Curr Protoc Mouse Biol 2011;1:71-83.

79. Gratz D, Winkle AJ, Dalic A, et al. Computational tools for automated histological image analysis and quantification in cardiac tissue. MethodsX 2020;7:22-34.
80. Royer A, van Veen TA, Le Bouter S, et al. Mouse model of SCN5A-linked hereditary Lenegre's disease: age-related conduction slowing and myocardial fibrosis. Circulation 2005;111:1738-46.
81. Zhang T, Yong SL, Drinko JK, et al. LQTS mutation N1325S in cardiac sodium channel gene SCN5A causes cardiomyocyte apoptosis, cardiac fibrosis and contractile dysfunction in mice. Int J Cardiol 2011;147:239-45.
82. Cronin H, Kerins D, Fahy G, et al. 20 The role of SCN5A mutations in hypertrophic cardiomyopathy. Heart 2018;104:A15-A16.
83. Wang Q, Shen J, Splawski I, et al. SCN5A mutations associated with an inherited cardiac arrhythmia, long QT syndrome. Cell 1995;80:805-11.
84. Zhang Y, Wang J, Chang S, et al. The SCN5A mutation A1180V is associated with electrocardiographic features of LQT3. Pediatr Cardiol 2014;35:295-300.
85. Bezzina C, Veldkamp MW, van Den Berg MP, et al. A single Na(+) channel mutation causing both long-QT and Brugada syndromes. Circ Res 1999;85:1206-13.
86. Remme CA, Wilde AA, Bezzina CR. Cardiac sodium channel overlap syndromes: different faces of SCN5A mutations. Trends Cardiovasc Med 2008;18:78-87.
87. Kyndt F, Probst V, Potet F, et al. Novel SCN5A mutation leading either to isolated cardiac conduction defect or Brugada syndrome in a large French family. Circulation 2001;104:3081-6.
88. Ehsan M, Kelly M, Hooper C, et al. Mutant Muscle LIM Protein C58G causes cardiomyopathy through protein depletion. J Mol Cell Cardiol 2018;121:287-296.
89. Carrier L, Mearini G, Stathopoulou K, et al. Cardiac myosin-binding protein C (MYBPC3) in cardiac pathophysiology. Gene 2015;573:188-97.